

**OPTICS DESIGN AND OPTIMIZATION OF ELECTRON BUNCH  
COMPRESSOR TRANSFER LINE  
(WITH A CASE STUDY OF CTF3 BUNCH COMPRESSOR)**

*By*

**AMALENDU SHARMA**

Enrolment No. PHYS03200804003

Raja Ramanna Centre for Advanced Technology, Indore

*A thesis submitted to  
Board of Studies in Physical Sciences  
In partial fulfilment of requirements  
For the degree of*

**DOCTOR OF PHILOSOPHY**

*of*

**HOMI BHABHA NATIONAL INSTITUTE**



**December, 2013**

## Homi Bhabha National Institute

### Recommendations of the Viva Voce Committee

As members of the Viva Voce Committee, we certify that we have read the dissertation prepared by **Amalendu Sharma** entitled "**Optics design and optimization of electron bunch compressor transfer line (with a case study of CTF3 bunch compressor)**" and recommend that it may be accepted as fulfilling the thesis requirement for the award of Degree of Doctor of Philosophy.

Chairman - Prof. S. B. Roy

Date: 7-8-2014

Guide/ Convener - Prof. Pitamber Singh

Date: 7/8/2014

The Technology Advisor - Shri Gurnam Singh

Date: 7/8/2014

Member 1 - Prof. G. S. Lodha

Date: 7/8/14

Member 2 - Prof. V. S. Pandit

Date: 07/08/2014

Final approval and acceptance of this thesis is contingent upon the candidate's submission of the final copies of the thesis to HBNI.

I hereby certify that I have read this thesis prepared under my direction and I recommend that it may be accepted as fulfilling the thesis requirement.

Date: August 07, 2014

Place: RRCAT, Indore.

Pitamber Singh  
Guide

## **STATEMENT BY AUTHOR**

This dissertation has been submitted in partial fulfilment of requirements for an advanced degree at Homi Bhabha National Institute (HBNI) and is deposited in the Library to be made available to borrowers under rules of the HBNI.

Brief quotations from this dissertation are allowable without special permission, provided that accurate acknowledgement of source is made. Requests for permission for extended quotation from or reproduction of this manuscript in whole or in part may be granted by the Competent Authority of HBNI when in his or her judgment the proposed use of the material is in the interests of scholarship. In all other instances, however, permission must be obtained from the author.



Amalendu Sharma

## **DECLARATION**

I, hereby declare that the investigation presented in thesis is carried out by me. The work is original and has not been submitted earlier as a whole or in a part for degree / diploma at this or any other Institution / university.



Amalendu Sharma

## List of Publications arising from the thesis

### Journal

1. "Optics design and second order longitudinal dispersion minimization in a bunch compressor transfer line for CTF3", **Amalendu Sharma**, Abdurrahim, A.D.Ghodke and Gurnam Singh. Nuclear Instruments and Methods in Physics Research A, 602, Issue 2, (2009), p. 342-351.
2. "Analytical expressions of transfer functions for a hard edge dipole magnet using a basic geometrical approach", **Amalendu Sharma**, P. Singh, Abdurrahim, A. D. Ghodke and Gurnam Singh. Physical Review Special Topics- Accelerators and Beams, 16, 014001 (2013), p. 014001-1 to 014001-12.

### Conferences

1. "Design of the Transfer Line-2 for the CTF-3 at CERN", **Amalendu Sharma**, A. Rahim, A.D.Ghodke and Gurnam Singh, APAC Proceedings, APAC-2007, pp 71-73.
2. "Optimization strategy for Transfer Line-2 for CTF3", Abdurrahim, **Amalendu Sharma**, A.D.Ghodke and Gurnam Singh, InPAC Proceedings, InPAC-2009, Indore, India.
3. "CSR studies of Transfer Line-2 Bunch Compressor at CTF3, CERN", **Amalendu Sharma**, P. Singh, Gurnam Singh and A. D. Ghodke. InPAC Proceedings, InPAC-2013, Kolkata, India, p676-678.

## Others

"Optics design for Transfer Line -2 for CTF3", **Amalendu Sharma**, A.D.Ghodke, Gurnam Singh and Abdurrahim. CTF3 Note -091, CERN (May 2008).



Amalendu Sharma

## **DEDICATIONS**

*I dedicate this dissertation to my doting parents,*

***Late Smt. Latika Sharma***

**&**

***Shri Anant Sharma***

*I take this opportunity to acknowledge their unwavering faith, persistence and instilling in me  
the essence of free thinking and quest for knowledge.*

## **ACKNOWLEDGEMENT**

I still remember the day, when Shri Gurnam Singh (then Head, Indus Operation and Accelerator Physics Design Division) called me and asked if I can do the beam optics design of a bunch compressor transfer line for the CTF3 under DAE-CERN collaboration. I had no experience in the beam dynamics of a bunch compressor. After discussion with Shri Gurnam Singh, I found the work to be interesting and took up this assignment. At that time, I had not imagined that I would pursue my doctoral thesis on this work.

On one day, Shri Gurnam Singh called me and asked why I should not register myself for pursuing PhD programme. I thought over it for few days and asked him, if it was possible for me to do the thesis on the CTF3 bunch compressor work. Till that time, some work on the design had been done. He readily agreed and encouraged me to do the thesis on this work. Dr. Pitamber Singh (Head, Ion Accelerator Development Division, BARC) also kindly agreed to be my guide for the PhD work. Today I take this opportunity to express my gratitude to Dr. Pitamber Singh, who provided me valuable guidance and active support at each stage of the work. I am also deeply thankful to Shri Gurnam Singh (presently DAE Raja Ramanna Fellow) without whom, this work would not have been possible. He minutely examined and reviewed my each contribution and gave guidance and very useful advice during the entire course of my PhD work.

It is a pleasure to thank Dr. P. D. Gupta, Director, RRCAT, who not only granted me permission to pursue the PhD programme but has been a continuous source of encouragement. I would also like to thank Shri P. R. Hannurkar, Head, Indus Operation and Accelerator Physics Design Division for continuing to provide full support to this work.

I am also thankful to Dr. S. B. Roy, Dr. G. S. Lodha, Dr. V. S. Pandit, Shri A. D. Ghodke, Dr. K. K. Pant and Dr. Vinit Kumar, the members / co-opted members of my Doctoral Committee for critically reviewing the progress of my work, which helped me to put more efforts in this task. It is a pleasure to gratefully acknowledge the valuable suggestions received from Dr. H. H. Braun (CERN) and Dr. F. Tecker (CERN) during the design of the transfer line.

I am very thankful to Shri Abdurrahim, my colleague and my friend in Beam Dynamics Laboratory, who has been involved in this work with me since the beginning. I had never used MATLAB earlier, but whenever I had to use MATLAB for my work, he was available for me. He also helped me verifying various results from time to time.

I thank to Shri Pradeep Kumar with whom I always discussed various aspects related to thesis work. I thank all my colleagues and friends in Beam Dynamics Laboratory, who have helped me without hesitation, whenever required.

Last but not least, I am thankful to my family, which has continuously provided every possible support during the entire course of PhD work.

## CONTENTS

	Page No.
<b>SYNOPSIS</b>	<b>1</b>
<b>LIST OF FIGURES</b>	<b>7</b>
<b>LIST OF TABLES</b>	<b>12</b>
<b>CHAPTER 1 INTRODUCTION</b>	<b>13</b>
1.1    Equation of motion	14
1.2    Solution of Hill's equation: Transfer matrix	19
1.3    Off momentum particle	23
1.4    Motion in longitudinal plane	26
1.5    Transfer matrix for a combination of elements (Optical section)	31
1.6    Parameterization of charged particle optics	32
1.6.1 Twiss parameters	32
1.6.2 Beam emittance	34
1.6.3 Twiss parameters and transfer matrix	36
1.7    Second order map	37
1.8    Bunch compression	39
1.8.1 Bunch length control	39
1.8.2 General optics for bunch compressors	42

<b>CHAPTER 2 CTF and CLIC at CERN</b>	<b>55</b>
2.1 CLIC (Compact Linear Collider)	56
2.2 Brief introduction to CTF	58
2.2.1 CTF1	58
2.2.2 CTF2	59
2.2.3 CTF3	59
<b>CHAPTER 3 LINEAR OPTICS OF TRANSFER LINE-2 BUNCH COMPRESSOR</b>	<b>63</b>
3.1 Geometrical layout of TL-2	66
3.2 Modules and optics of TL-2	67
3.2.1 Module-1	67
3.2.2 Module-2	69
3.2.3 Module-3	70
3.3 Twiss parameters	77
3.4 Alternative optics	95
<b>CHAPTER 4 SEXTUPOLE OPTIMIZATION FOR TRANSFER LINE-2</b>	<b>101</b>
4.1 Sextupole scheme for TL2	103
4.2 Sextupole errors in dipole magnets	118

<b>CHAPTER 5 CSR STUDIES FOR TRANSFER LINE-2</b>	<b>120</b>
5.1    General overview of Synchrotron Radiation (SR)	120
5.2    Effects of CSR on beam dynamics	124
5.3    CSR simulation studies and results for TL-2	127
<b>CHAPTER 6 ANALYTICAL MAP FOR DIPOLE MAGNET AND APPLICATION TO BUNCH COMPRESSOR</b>	<b>132</b>
6.1    Map for sector dipole magnet	133
6.2    Validation of the derived analytical map	143
6.2.1    Linear terms	143
6.2.2    Higher order terms	145
6.3    Example of a bunch compressor	147
6.4    Analytical map for wedge magnet	151
<b>SUMMARY AND CONCLUSIONS</b>	<b>157</b>
<b>APPENDIX A</b>	<b>160</b>
<b>APPENDIX B</b>	<b>163</b>
<b>APPENDIX C</b>	<b>176</b>
<b>REFERENCES</b>	<b>180</b>

## SYNOPSIS

Recently various charged particle accelerator projects, related to linear colliders for leptons and FELs are being pursued. All of them are designed to deliver electron pulses with a very short bunch length either for high power, high frequency RF generation or for luminosity enhancement or to achieve high intensity in emitted radiation. For obtaining a very short bunch length, all these facilities at one or another stage include bunch compressors. Therefore in last one or two decades the beam dynamics studies and optimization for the bunch compressors has been an active area of research.

Electron beam bunch compressors are used to compress the electron bunch using RF manipulation followed by a magnetic optics. This compression is therefore a two step process. In the first step, a correlation is established between the momentum spread and longitudinal position through the RF system (RF system changes momentum of an electron as a function of its longitudinal position) and the second step is passing this bunch through a magnetic optics, which generates a correlation between the longitudinal position and momentum spread via dependency of path length on momentum deviation. The thesis work is related to second step i.e. in the thesis I have carried out magnetic optics studies and its optimization for the bunch compressors with a case study of CTF3 (CLIC Test Facility 3) transfer line (TL-2) bunch compressor at CERN.

In a co-ordinate system, which is used for studying the beam dynamics in an accelerator or a beam transport system, the beam propagation direction is known as the longitudinal direction. The plane in perpendicular direction to the beam propagation axis is known as transverse plane. The origin of this co-ordinate system moves in a fashion that a particle with correct momentum, which lies initially on the design trajectory i.e. no transverse displacement and angle with respect to design trajectory, always remains on the origin. This reference particle is known as a synchronous particle. Any other particle's state at a given instant is designated

by six parameters in this co-ordinate system. Transverse displacement ( $x, y$ ) and angles with design orbit ( $x', y'$ ) are four transverse co-ordinates out of these six co-ordinates. Along the longitudinal direction, the parameters describing particle's state are distance (or time) from the origin (reference particle) and fractional change in momentum with respect to design momentum (generally known as momentum offset). In beam dynamics, each magnetic element is represented by a map, which relates the co-ordinates of a particle at exit of this element from the particle's co-ordinate at the entry of this element. This map can be represented by matrices (known as transfer matrix). A charged particle optics is governed by a suitable arrangements of different types of magnets and the overall map of this optics is a composition of maps of individual magnets. In designing and in optimization of a bunch compressor, the elements of a map (transfer matrix), related to longitudinal plane become very important. These matrix elements provide a relation for path length (hence time of flight) of a particle traversing the element in terms of its initial co-ordinates and momentum offset. Among these elements, pure chromatic elements i.e. elements which relate path length to momentum offset play the most significant role. These elements are termed as  $R_{56}$ ,  $T_{566}$ ,  $U_{5666}$  etc for the linear, second order and third order maps, respectively. The path length relation with momentum for a particle in dipole magnet including higher orders (above mentioned matrix elements) provides the actual achievable bunch length in magnetic optics. The basic beam dynamics useful in understanding the magnetic optics with emphasis on bunch compression is provided in **Chapter 1**. This chapter also includes a brief introduction of different types of optics usually employed for the bunch compressor.

The main focus among the bunch compressors in this thesis is on the CTF3 Transfer Line-2 (TL-2) bunch compressor, which has a very wide tuning range of  $R_{56}$ . The compressed bunch is used to generate a high frequency, high power RF for the CTF3 project at CERN. CTF3 is a test facility for the upcoming CLIC (Compact Linear Collider) at CERN. This test facility is

used to demonstrate the high frequency, high power RF generation using a drive beam as well as to test RF components of CLIC. **Chapter 2** contains some information on the CLIC and CTF3 projects of CERN.

In CTF3, bunches of an electron beam, extracted from Combiner Ring is transferred to CLEX area (CLIC Experimental Area) through Transfer Line-2 (TL-2), where these bunches generate high frequency RF power in the PETS (Power Exchange Test Structure). In this transfer of bunches, TL-2 compresses the bunch length and matches the optical parameters at the entry of optics just before the PETS. TL-2 bunch compressor is designed in a modular structure in which there are three modules. First module is an achromatic arc formed by two extraction septa of CR and one dipole magnet. Second module provides proper matching between first and last modules as well as accommodates a vertical achromat, required to overcome the building constraint. The last module is a  $R_{56}$  tuning arc and is the most important module of this line. Tuning of  $R_{56}$  is carried out by shaping the dispersion curve in this achromatic module. Three quadrupole triplets and four dipole magnets form the  $R_{56}$  arc. After this arc, in this module, there is a quadrupole doublet to match the Twiss parameters at the exit. This transfer line bunch compressor was to be installed in the already available building. Some of the magnets were also available. Thus there were magnetic and geometric constraints in designing the beam optics for this line. Under these constraints a symmetric optics design is not possible i.e. Twiss parameters are not symmetric in  $R_{56}$  arc and therefore optical optimization poses a challenge. Being a test facility, the tuning range is also very wide i.e from -0.30 m to +0.30 m. Therefore bunch length can be compressed from 8.3 ps to 1.5 ps for a wide range of initial distribution of electrons in the longitudinal phase space. **Chapter 3** summarizes the geometry, modules and optics optimization for wide range of  $R_{56}$  in this line. At a very short bunch length of 1.5 ps, the higher order optics also becomes important and second order longitudinal dispersion term  $T_{566}$  plays effective role in deciding the bunch

length. Thus, in the entire range of  $R_{56}$  tuning, second order term  $T_{566}$  has to be suppressed. For suppressing this term, sextupole magnets are included in the line. Due to optically asymmetric beam line, second order correction with sextupoles brings detrimental effects on the transverse phase space and transverse emittance blows up. Due to asymmetry in optical functions and very wide tuning range of  $R_{56}$ , standard sextupole correction scheme, like identity transformer in which two sextupole magnets are kept at  $\pi$  betatron phase apart, is not suitable. Therefore a new technique for optimizing the sextupole magnets is evolved and applied successfully in this line, in which  $T_{566}$  is controlled and there is very small emittance growth in the transverse plane. This is described in **Chapter 4**.

When relativistic electron bunch passes through a dipole magnet, it emits synchrotron radiation due to curvature in the path. When the bunch length becomes very small, the emitted radiation has significant coherent synchrotron radiation (CSR). This CSR generally has significantly adverse effects (sometimes larger than higher order effects, described in chapter 4 and 5) on the transverse emittance and on the momentum spread (which changes the bunch length in dispersive section). In last one decade this problem drew significant interest in beam dynamics. Although, the bunch length in TL-2 of CTF3 is not compressed to a very short length (i.e. sub-ps or shorter), nevertheless it is always essential to quantify the effects of CSR in a bunch compressor. Using computer code ELEGANT, we have carried out studies of CSR and its effect on CTF3 bunch compressor, which is summarized in **Chapter 5**.

For compressing a bunch to a very short length in a magnetic optics with a reasonable values of  $R_{56}$ , the RF system has to generate a large momentum spread. At a very short bunch length with large momentum spread even the higher order terms (more than 2<sup>nd</sup> order) can have detrimental effects in longitudinal plane. Control on bunch length depends mainly on the dipole magnets, employed in an optics through the path length variation as a function of

momentum in dipole magnets. Thus there is a need to make a higher order model of a dipole magnet. Presently the available models are based on the Hamiltonian methods by making Lie operators up to higher orders and also using perturbation techniques in the equation of motion, in which the Green's function for driving terms for higher orders are used to solve the problems. But these techniques are complex in nature and increasing order one by one in computation may be a tedious job. Computer codes for obtaining results up to higher orders are also available, but numerical integration does not provide a good insight into the problem as well as increasing order of computation also pays a cost of computation time. On the basis of geometrical arguments, in this thesis, we obtained analytical expression of maps for hard edge dipole magnets which are exact. The single analytical term encompasses all the orders and thus is useful in quick analysis. Approximation used in numerical computation (i.e. truncation of map up to 2<sup>nd</sup> or 3<sup>rd</sup> order in computer codes) brings deviation mainly in longitudinal plane from the accurate results, obtained using the analytical map derived in the thesis. Therefore this analytical formulation has more importance for bunch compressors, where higher order effects on bunch length can be estimated accurately. The analytical results for a single magnet as well as for a bunch compressor are compared with code MAD8 and ELEGANT. The model and results are presented in **Chapter 6**.

At the end, the work carried out is summarized in this paragraph. Transfer Line-2 (TL-2) has been designed for a very wide tuning range of longitudinal dispersion  $R_{56}$ , satisfying all the requirements which include utilization of available magnets and installation of the line in an already existing building with several geometrical constraints. Second order longitudinal dispersion  $T_{566}$  is corrected in the entire range of  $R_{56}$ . A new sextupole scheme is evolved for this correction with minimum dilution of transverse emittance and applied successfully on this bunch compressor transfer line. Effects of CSR on the beam in TL-2 is quantified and found that there are no significant detrimental effects on the bunch length and transverse

emittance in the operating domain of this line. An exact map for hard edge dipole magnets is obtained analytically and it is applied on a chicane type bunch compressor to estimate the bunch length and emittance accurately. A comparison of analytical results with tracking codes is presented, which shows the deviation in the results of longitudinal plane obtained using tracking codes due to approximations of truncation of maps up to third order in these codes.

## LIST OF FIGURES

<b>Fig.</b>	<b>Caption of the figure</b>	<b>Page</b>
<b>No.</b>		<b>No.</b>
1.1	Co-ordinate system in accelerator physics	15
1.2	Co-ordinate system defined locally according to bend in the design trajectory	16
1.3	A quadrupole magnet	17
1.4	Effective length and hard edge model of a magnet	19
1.5	Trajectories in dipole magnet due to momentum spread	24
1.6	Trajectories in a small section of a dipole magnet	27
1.7	Phase space ellipse in $x-x'$ plane	33
1.8	Ellipse encompassing ~67% and ~95% particles from a beam, distributed in phase space	35
1.9	Longitudinal phase space, showing a bunch	40
1.10	Schematic of incoming and exit beam in two cases of bunch compressors	43
1.11	Layout of a C-chicane optics	44
1.12	Chicane geometry including quadrupole magnets	46
1.13	Different plots, showing the behaviour of a chicane optics	48
1.14	Layout of a dog-leg optics	51
1.15	Two dog-leg optics in succession with a quadrupole doublet in between	52
1.16	Different plots, showing behaviour of an arc formed by two dog-leg optics	53
1.17	Wiggler based optics for bunch length manipulation	54
2.1	RF power generation efficiency with RMS bunch length	57
2.2	Schematic layout of CLIC	58
2.3	Schematic layout of CTF3	61
3.1	Layout of the building, where TL-2 is installed (measurements are in m)	67

3.2	Schematic layout of Module-1	68
3.3	Combination of first two quadrupole strengths (magnitude) for making the module as an achromat for a fixed strength of third quadrupole magnet	69
3.4	Schematic layout of Module-2	70
3.5	Layout of an S-arc with possibility to tune the $R_{56}$	71
3.6	Layout of an S-arc with possibility to achieve a value of $R_{56}$ with different combination of strengths of Q1 and Q2 quadrupole magnets	72
3.7	Different plots, showing behaviour of an S-arc	74
3.8	Layout of the optics of an S-arc, on which tuning $R_{56}$ arc of Module-3 is based	75
3.9	Schematic layout of Module-3 of TL-2	76
3.10A	Dispersion and beta functions @ $R_{56} = +0.30$ m	81
3.10B	Dispersion and beta functions @ $R_{56} = +0.25$ m	82
3.10C	Dispersion and beta functions @ $R_{56} = +0.20$ m	83
3.10D	Dispersion and beta functions @ $R_{56} = +0.15$ m	84
3.10E	Dispersion and beta functions @ $R_{56} = +0.10$ m	85
3.10F	Dispersion and beta functions @ $R_{56} = +0.05$ m	86
3.10G	Dispersion and beta functions @ $R_{56} = 0.00$ m	87
3.10H	Dispersion and beta functions @ $R_{56} = -0.05$ m	88
3.10I	Dispersion and beta functions @ $R_{56} = -0.10$ m	89
3.10J	Dispersion and beta functions @ $R_{56} = -0.15$ m	90
3.10K	Dispersion and beta functions @ $R_{56} = -0.20$ m	91
3.10L	Dispersion and beta functions @ $R_{56} = -0.25$ m	92
3.10M	Dispersion and beta functions @ $R_{56} = -0.30$ m	93
3.11A	Beam size (considering 1% momentum spread) for $R_{56} = +0.30$ m	94
3.11B	Beam size (considering 1% momentum spread) for $R_{56} = 0.00$ m	94

3.11C	Beam size (considering 1% momentum spread) for $R_{56} = -0.30$ m	95
3.12A	Dispersion and beta functions @ $R_{56} = +0.30$ m	97
3.12B	Dispersion and beta functions @ $R_{56} = +0.25$ m (proposed nominal operating point)	98
3.12C	Dispersion and beta functions @ $R_{56} = 0.00$ m	99
3.12D	Dispersion and beta functions @ $R_{56} = -0.30$ m	100
4.1A	Variation in kick angles generated by sextupole magnets [Eq. 4.10 and 4.11] for $R_{56} = +0.30$ m optics	106
4.1B	Variation in kick angles generated by sextupole magnets [Eq. 4.10 and 4.11] for $R_{56} = -0.30$ m optics	107
4.2A	Tracking results, showing phase space distortion in both the planes ( $1\sigma$ and $2\sigma$ ) at different initial horizontal $\beta$ function (-35%, -10%, +10% and +35%) at Module-3 for $R_{56} = +0.30$ m. Horizontal scale is in mm and vertical is in mrad	109
4.2B	Tracking results, showing phase space distortion in both the planes ( $1\sigma$ and $2\sigma$ ) at different initial horizontal $\beta$ function (-35%, -10%, +10% and +35%) at Module-3 for $R_{56} = +0.30$ m. Horizontal scale is in mm and vertical is in mrad	111
4.3	Variation in kick angles generated by sextupole magnets [Eq. 4.10 and 4.11] for $R_{56} = +0.25$ m optics	112
4.4A	Distortion in horizontal and vertical phase space in both the planes ( $1\sigma$ and $2\sigma$ ) at negative $R_{56}$ (0.30, 0.25, 0.20, 0.15, 0.10, and 0.05m) due to $T_{566}$ correcting sextupoles in normalized phase space. Horizontal scale is in mm and vertical is in mrad	114
4.4B	Distortion in horizontal and vertical phase space in both the planes ( $1\sigma$ and $2\sigma$ ) at positive $R_{56}$ (-0.05, -0.10, -0.15, -0.20, -0.25 and -0.30m) due to $T_{566}$	

correcting sextupoles in normalized phase space. Horizontal scale is in mm and vertical is in mrad	116
4.4C Distortion in horizontal and vertical phase space in both the planes ( $1\sigma$ and $2\sigma$ ) at zero $R_{56}$ (isochronous mode) due to $T_{566}$ correcting sextupoles in normalized phase space. Horizontal scale is in mm and vertical is in mrad	117
5.1 Spectrum of synchrotron radiation for four different electron beam energies (150 MeV, 300 MeV, 450 MeV and 600 MeV). Bending radius $\rho$ is taken 1 m	121
5.2 Emitted power (normalized) with bunch length (normalized)	123
5.3 Tail-head interaction of an electron bunch due to emitted CSR	125
5.4 Variation in beam parameters at exit from TL-2 for different number of electrons in the simulation	129
5.5 Initial electron distribution in bunch	130
5.6 Electron density distribution in bunch along the longitudinal direction at different $R_{56}$ settings without and with CSR effects	130
5.7 Horizontal and vertical phase space for extreme tuning of $R_{56}$ with and without CSR effects	131
6.1 Geometry of the sector dipole magnet with co-ordinate system and particle trajectory	134
6.2 Trajectory of a particle having vertical inclination ( $\beta_i$ ) from the median plane	137
6.3 Procedure for obtaining final co-ordinates of a particle travelled through a sector dipole magnet as a function of initial co-ordinates	139
6.4 Variation in final bunch length with initial transverse emittance	140
6.5 Variation in difference in final bunch length obtained from analytical expression and MAD as a function of initial bunch length	141
6.6 Longitudinal phase space after passing through magnet (obtained from MAD	

6.7A Variation in  $P$  and  $Q$  with bending radius for fixed bending angle of  $30.75^\circ$ .

The  $x_i$  and  $\alpha_i$  are taken as 100 mm and 20 mrad respectively

145

6.7B Variation in  $P$  and  $Q$  with bending angle for fixed bending radius of 0.96 m.

The  $x_i$  and  $\alpha_i$  are taken as 100 mm and 20 mrad respectively

146

6.8 Geometry of C-chicane optics

148

6.9 Initial beam distribution in horizontal and vertical phase space

150

6.10 Phase space distribution of beam after bunch compressor (analytical and numerical model)

151

6.11 Geometry of the wedge magnet in fixed  $u-v$  co-ordinate system

152

6.12 Deviation in emittance from numerical computation using analytical results as a function of initial horizontal emittance

156

B.1 Rectangular magnet as used in chicane geometry

163

B.2 First half geometry of a chicane optics

166

## LIST OF TABLES

Table No.	Title of the table	Page No.
1.1	Parameters of the example optics for chicane	47
2.1	Main parameters of drive beam in CTF3 and CLIC	62
3.1	Parameters for the Transfer Line-2 (TL-2) bunch compressor	65
3.2	Parameters of the available magnets	66
3.3	Parameters of the example optics for S-arc	73
3.4	Vacuum chamber aperture of the line	78
3.5A	Quadrupole strength ( $g/B\rho$ in $\text{m}^{-2}$ ) for different $R_{56}$ settings of TL-2	79
3.5B	Quadrupole strength ( $g/B\rho$ in $\text{m}^{-2}$ ) for different $R_{56}$ settings of TL-2	80
3.6	Quadrupole strength ( $g/B\rho$ in $\text{m}^{-2}$ ) for different settings of $R_{56}$ of alternative optics for TL-2	96
4.1A	Sextupole strength ( $\text{m}^{-3}$ ) for $T_{566}$ correction for positive and zero $R_{56}$	117
4.1B	Sextupole strength ( $\text{m}^{-3}$ ) for $T_{566}$ correction for negative $R_{56}$	118
4.2	Tolerable integrated sextupole component in dipole magnets for different $R_{56}$ settings	119
5.1	CSR related parameters for TL-2 dipole magnets	124
6.1	Parameters of the chicane optics	148

# **CHAPTER 1**

## **INTRODUCTION**

The electron beam bunch compressors, which are charged particle beam optical systems for compressing the electron bunch length, are nowadays an integral part of various accelerator programmes, such as high power high frequency RF generation (CLIC, CERN), linear colliders (CLIC, ILC) and FEL projects [1-8]. The interest in short bunches emanates from the requirement of achieving high efficiency of RF power generation in RF structures, high luminosity in colliders and increasing peak intensity of the emitted radiation in FELs. In last one or two decades, there is a vast advancement in understanding and optimization of such bunch compressors and it became an active area of studies. The goal of a bunch compressor is to bring the head and tail of a bunch closer to each other. This bunch compression process comprises of two steps. First is the establishment of correlation between the momentum of an electron in a bunch and its position (time) with respect to the bunch centre. This is achieved by a suitable RF system, which changes the momentum of an electron in a bunch depending on its position from the bunch centre. The second part is the utilization of this correlation to compress the bunch length by passing this bunch through a magnetic optics, in which the path length of an electron is correlated to its momentum [9-11] i.e. path length changes according to momentum of an electron in a bunch. In this thesis, we have focused on the second part i.e. optical design and optimization of a magnetic optics for the bunch compression. The optical design of CTF3 (CLIC Test Facility 3) Transfer Line-2 (TL2) bunch compressor is presented with details.

It is essential to know the effects of a magnetic field on the motion of a charged particle and to obtain a suitable arrangement of magnetic elements to achieve the goal of a controlled

transfer of charged particles i.e. designing a charged particle optical system for beam transport. Therefore in this first chapter, the basics of beam dynamics under different magnetic field configurations, which are useful for understanding the charged particle optical systems are reviewed. In Section 1.1, accelerator co-ordinate system, equation of motion in this co-ordinate system and different magnetic field configurations (dipole and quadrupole magnets) are provided. The solution for an off momentum particle is discussed in next section. Then the parameterization of charged particle optics and beam is described in brief. Next section is focused on how to utilize this charged particle magnetic optics for the bunch compression. In last section, some commonly employed optics for bunch compressors are summarized.

## 1.1 Equation of motion

Any charged particle, passing through a magnetic field, experiences Lorentz force, given by

$$\vec{F} = q(\vec{v} \times \vec{B}) \quad [1.1]$$

Here  $\vec{v}$  is the velocity of the charged particle,  $q$  is its charge,  $\vec{B}$  is the applied magnetic field and  $\vec{F}$  is the force on the charged particle. In any accelerator or beam transport system, there is a design path i.e. a particle of correct energy with initial positions and angles exactly on this path, will follow this trajectory under the design magnetic fields. It is always convenient to make this design trajectory as a reference for defining the charged particle's co-ordinates. Therefore, in accelerator physics, a local co-ordinate system is chosen in a way, so that its origin moves and moving origin defines the design trajectory. A reference particle is also defined such that it has precisely the desired momentum (in accelerator jargon it is known as on-momentum particle), lies exactly on the design trajectory or path or orbit (i.e. neither

displaced nor having any angle with this trajectory). This particle, which also moves with the origin of co-ordinate system, is also known as synchronous particle. Fig. 1.1 depicts such curvilinear co-ordinate system.

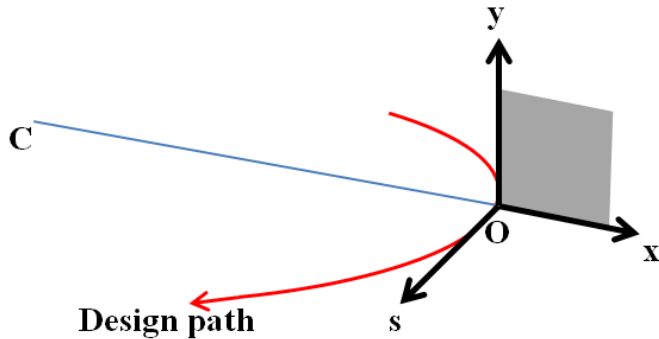


**Fig. 1.1 Co-ordinate system in accelerator physics**

The direction of design trajectory (beam propagation direction) is designated by  $s$ , the direction opposite to the centre of radius of curvature (locally) is designated by  $x$  and third direction is in the vertical direction to the plane formed by  $x-s$  in right hand sense. Generally in accelerators or beam transport systems, the bending takes place horizontally and therefore  $x-s$  plane is known as horizontal plane (also known as median plane) and  $y-s$  plane is known as vertical plane. Plane  $x-y$  is known as transverse plane. This co-ordinate system is a well known "Frenet-Serret co-ordinate system" [12, 13].

Fig. 1.2 shows such co-ordinate system for a more complex design trajectory which is bent by two separate magnetic fields. In this figure, the co-ordinate system is shown at four different locations **A**, **B**, **C** and **D**. As shown in this figure, both the magnets bend beam trajectory in opposite sense, thus if one magnet is assigned positive bending angle, the other one is assigned negative bending angle.

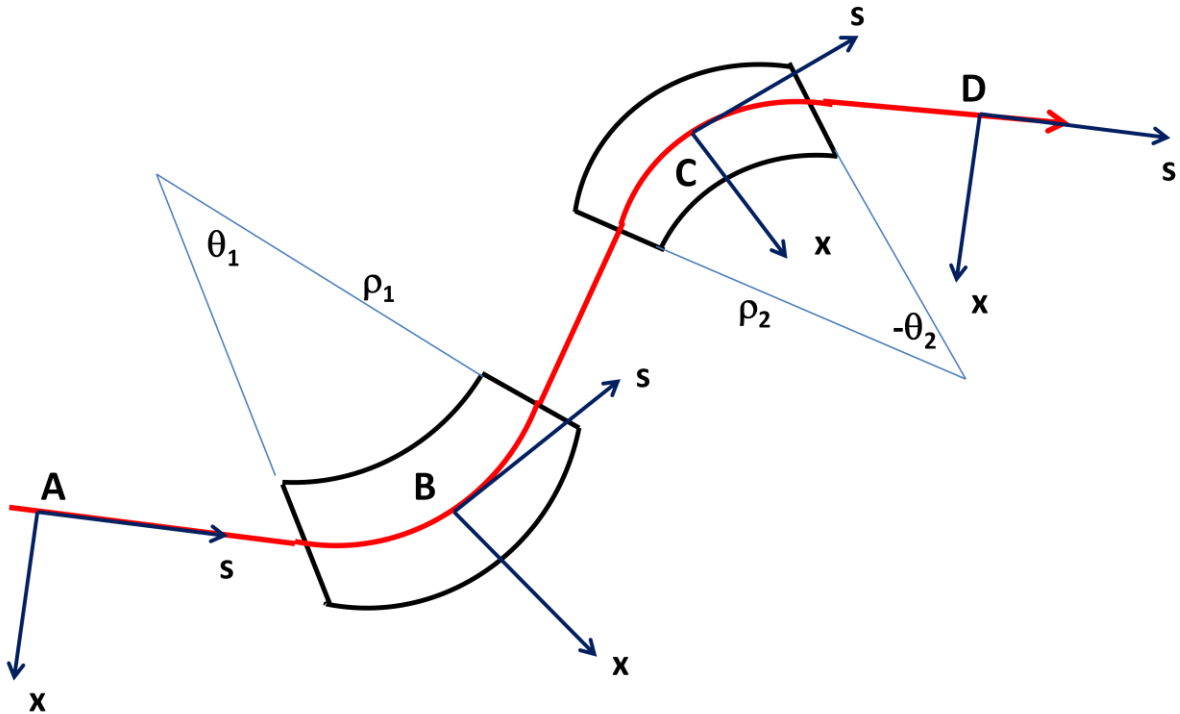


**Fig. 1.2 Co-ordinate system defined locally according to bend in the design trajectory**

In synchrotrons or cyclic accelerators, in general a closed path is formed by only one type of magnets and chosen sign of bending is positive. However in a beam transport system including bunch compressors, both types of magnets may be present. In Fig. 1.2, it is shown that a constant magnetic field (region bounded with black bold lines in Fig. 1.2) perpendicular to the plane of trajectory and curvature defines the desired design path. Therefore, a dipole magnet is used to define a desired design trajectory in accelerators or beam transport systems. For a horizontal dipole magnet (which bends beam horizontally), the horizontal and vertical components of field are  $B_x = 0$  and  $B_y = B_0$ , respectively. Here  $B_0$  is the desired constant magnetic field.

Charged particle beam is an ensemble of particles, which has finite extent in space and time. Here in the above figure, only design trajectory is displayed, while in a beam, many particles may deviate from the design trajectory and may also have some angles with respect to this

trajectory. For confining this beam along and near to beam propagation axis, there is a need for a focusing force, which would try to bring back the deviated particles towards the design trajectory. This focusing action is obtained using a quadrupole magnet. Fig. 1.3 shows a quadrupole magnet.

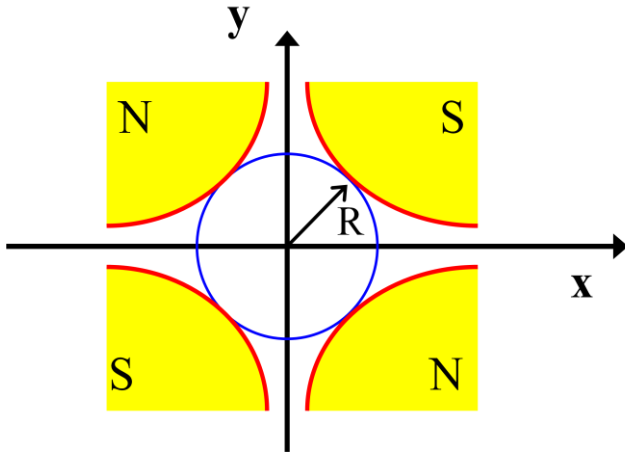


**Fig. 1.3 A quadrupole magnet**

The field of a quadrupole magnet is zero at the centre ( $x=0, y=0$ ) and increases as distance increases from the centre in the transverse plane. The horizontal and vertical components of the quadrupole field are  $B_x = gy$  and  $B_y = gx$ , respectively. Here  $g$  is the field gradient ( $g = \partial B_y / \partial x$ ) of the quadrupole magnet and is a constant parameter for a given quadrupole magnet at some defined pole tip field.

Therefore the minimum requirement for making a beam transport system is to have dipole magnets (if desired design trajectory is curved) and quadrupole magnets. There will be some space between these magnets, known as drift space. Using Eq. 1.1 in accelerator co-ordinate system, retaining only linear terms for an on-momentum particle, one gets Hill's equation for the motion of the charged particle under the dipole and quadrupole magnetic field (field has only vertical component in the median plane) [13-16] i.e.

$$\frac{d^2x(s)}{ds^2} + K(s)x(s) = 0 \quad [1.2]$$

Here independent variable is 's' instead of time 't' and  $K(s)$  is the strength (magnetic strength or normalized strength) of the magnet and is a function of  $s$ . If we define  $k = g/B\rho$  then in the case of a dipole magnet,  $K(s)$  is  $k - 1/\rho^2$  and for a quadrupole magnet,  $K(s)=k$ . For a dipole magnet,  $k$  is non-zero only if magnet has some gradient in the field along transverse direction i.e. it has a quadrupole component and  $1/\rho^2$  represents the geometrical focusing term of a dipole magnet. Term  $B\rho$  is known as the magnetic rigidity and is directly proportional to momentum ( $p$ ) of the beam i.e.  $B\rho=p/q$ . Normalizing the strength with beam rigidity allows the description of an optics independent of beam momentum.  $K(s)$  is different for different magnets along 's' and is zero in a magnet free region i.e. drift space. Within a magnet also, it varies along 's' due to fringing of the magnetic field at edges of a magnet. For a single magnet, using concept of 'effective length', the strength can be made constant inside this magnet and the parameter  $K$  becomes a step function at edges of this magnet. This model in accelerator physics is known as 'hard edge model' and solution of the equation obtained using this approximation is known as 'piece-wise solution'. In each piece, Hill's equation becomes similar to that of a simple harmonic oscillator. The effective length of a magnet is chosen in such a way, that the integration of strength parameter along 's' considering fringing for a magnet becomes equal to  $KL_{eff}$ . The concept of effective length is shown in Fig. 1.4.

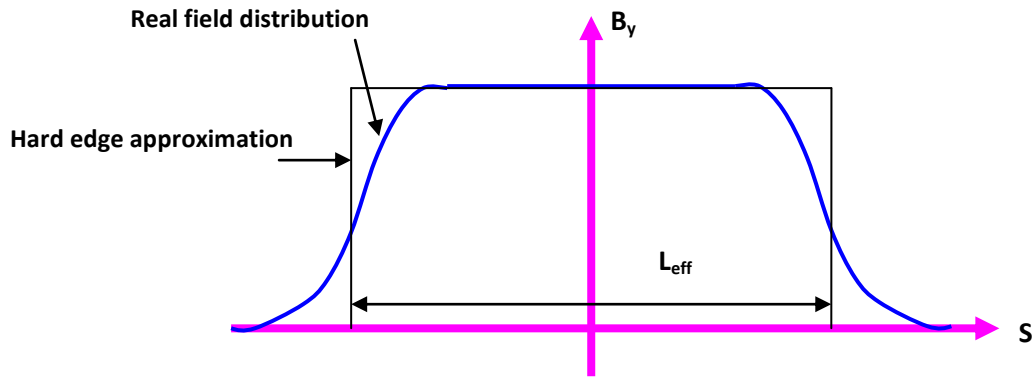


**Fig. 1.4 Effective length and hard edge model of a magnet**

## 1.2 Solution of Hill's equation: Transfer matrix

Discussion of the previous section reveals that the motion of a charged particle in a field of a particular magnet is characterized by its magnetic strength and effective length. A particle trajectory in one plane can be described by  $x$  and  $dx/ds$  ( $=x'$ ) i.e. displacement from the design path and the angle of motion with the design path. Here, the prime denotes the differentiation of  $x$  with respect to  $s$  and a dot over symbol will be used for differentiation with respect to time. Each magnet is characterized by a map (represented by a matrix in linear dynamics), which transforms the input co-ordinates of a particle  $(x_{in}, x'_{in})$  to the co-ordinates at the exit of a magnet  $(x_{out}, x'_{out})$ . The elements of this matrix (this matrix is known as transfer matrix) are the principle solutions of Hill's equation. The theory is general in nature i.e.  $x_{in}$  and  $x_{out}$  need not be exactly entry and exit point of a magnet, even these points can be located within the magnet itself, only one has to consider the matrix between these two points. A similar matrix can be defined for the other plane i.e.  $y-s$  plane considering the co-ordinates  $(y_{in}, y'_{in})$  and  $(y_{out}, y'_{out})$ .

The transfer matrices for commonly used magnets are given below. The complete and detailed derivation can be found in Refs [13-18].

### **1. Drift space (i.e. magnetic field free region) of length $L$**

Here the transfer matrix for horizontal plane is given below. The same matrix is valid for the vertical plane also.

$$\tilde{\mathbf{R}}_{x-drift} = \begin{bmatrix} 1 & L \\ 0 & 1 \end{bmatrix} \quad [1.3]$$

### **2. Quadrupole magnet**

In the focusing plane, a quadrupole magnet of strength  $k$  and effective length  $L$  has trigonometric functions in the solution of Hill's equation, which shows a bounded oscillatory motion. Using the principle solution of Hill's equation, transfer matrix of a focusing quadrupole (focusing in horizontal plane, also known as F-quadrupole) is constructed as follows

$$\tilde{\mathbf{R}}_{x-quadrupole-F} = \begin{bmatrix} \cos\sqrt{|k|}L & \frac{\sin\sqrt{|k|}L}{\sqrt{|k|}} \\ -\sqrt{|k|}\sin\sqrt{|k|}L & \cos\sqrt{|k|}L \end{bmatrix} \quad [1.4]$$

In defocusing plane (vertical plane), the particle goes away from the design trajectory and instead of trigonometric functions, matrix elements contain hyperbolic functions. This gives an unbounded motion i.e. defocusing.

$$\tilde{\mathbf{R}}_{y-quadrupole-F} = \begin{bmatrix} \cosh\sqrt{|k|}L & \frac{\sinh\sqrt{|k|}L}{\sqrt{|k|}} \\ \sqrt{|k|}\sinh\sqrt{|k|}L & \cosh\sqrt{|k|}L \end{bmatrix} \quad [1.5]$$

If the focal length of a quadrupole magnet is much larger than the thickness of the magnet, then magnet can be approximated as a thin lens, which changes only the angle of a particle ( $x'$ ) but leaving displacement from the design trajectory unchanged ( $x$ ). Thus a magnet in thin lens approximation, changes the particle trajectory with some angle. This approximation is often valid in practical situations and provides a powerful tool for initial handy calculations.

In this approximation, the matrix of a quadrupole magnet becomes

$$\tilde{\mathbf{R}}_{x\text{-}quadrupole} = \begin{bmatrix} 1 & 0 \\ -\frac{1}{f} & 1 \end{bmatrix} \quad [1.6]$$

Here  $f$  is the focal length, given by  $f=1/k/L$ . In defocusing plane,  $1/f$  appears in matrix instead of  $-1/f$ . The change in angle of the direction of motion by a magnet (known as kick) under thin lens approximation is given by

$$\theta_x = \frac{B_y L_{eff}}{B\rho}$$

In case of a quadrupole magnet, this kick becomes

$$\theta_x = \frac{KL_{eff}x}{B\rho}$$

Here  $KL_{eff}$  is the integrated strength of the quadrupole magnet. Now onwards, the subscript 'eff' with  $L$  will be omitted and in case of a magnet,  $L$  will always refer to the effective length.

### **3. Sector type dipole magnet**

The geometry of this type of magnet is a sector of a circle, in which the design trajectory enters and exits perpendicular to the edges of the magnet. In a bending plane, the matrix is given by

$$\tilde{\mathbf{R}}_{x-dipole} = \begin{bmatrix} \cos\theta & \rho\sin\theta \\ -\frac{\sin\theta}{\rho} & \cos\theta \end{bmatrix} \quad [1.7]$$

Here  $\rho$  is the design bending radius and  $\theta$  is the bending angle. In the other plane, this dipole magnet acts as a drift space of length  $L=\rho\theta$ .

#### **4. Parallel edge dipole magnet (rectangular dipole magnet)**

In this type of dipole magnets, design trajectory enters and exits at the half of bending angle with respect to centre axis of the magnet along the length (angle of  $\pi/2-\theta$  with edges) and both the magnet edges are parallel. Due to this geometry, the dipole magnet acts as a drift space in bending plane and acts as a focusing quadrupole in other plane (due to virtue of coordinate system). For bending in horizontal plane, the matrices are given by

$$\tilde{\mathbf{R}}_{x-dipole} = \begin{bmatrix} 1 & \rho\sin\theta \\ 0 & 1 \end{bmatrix} \quad [1.8]$$

$$\tilde{\mathbf{R}}_{y-dipole} = \begin{bmatrix} \cos\theta & \rho\sin\theta \\ -\frac{\sin\theta}{\rho} & \cos\theta \end{bmatrix} \quad [1.9]$$

Here horizontal and vertical matrices are shown separately. Combining both the matrices and ignoring horizontal to vertical coupling of motion, a  $4\times 4$  matrix of the following form can be constructed

$$\tilde{\mathbf{R}}_{4\times 4} = \begin{bmatrix} \tilde{\mathbf{R}}_{x-2\times 2} & \tilde{\mathbf{0}}_{2\times 2} \\ \tilde{\mathbf{0}}_{2\times 2} & \tilde{\mathbf{R}}_{y-2\times 2} \end{bmatrix} \quad [1.10]$$

Here  $\tilde{\mathbf{0}}_{2\times 2}$  is a null matrix that shows the horizontal motion is not coupled with the vertical motion. It is not always true. If a magnetic field of a quadrupole magnet has a non-vanishing component of magnetic field in the median plane (i.e. field is not exactly perpendicular to the

median plane due to rotation of the quadrupole magnet around the beam propagation direction), then horizontal and vertical motion are coupled and instead of having null matrices in above equation, some non-zero element will be present and above matrix in this case will show a coupled transverse matrix [19].

A beam is a large collection of charged particles having a certain momentum spread around the central momentum. Effect of magnet on motion of a charged particle also depends on the momentum, therefore with the co-ordinates  $(x_{in}, x'_{in}, y_{in}, y'_{in})$ , one more co-ordinate has to be introduced i.e.  $\Delta p/p$  ( $=\delta$ ) which is a fractional offset in momentum from the central momentum  $p$ . In next section, the dependence of co-ordinate on momentum offset is discussed.

### 1.3 Off momentum particle

Particles with different momenta experience different forces under the magnetic field of a dipole magnet. A dipole magnet therefore generates different trajectories for particles with different momenta. In Fig. 1.5, trajectories of three particles, having different momenta are shown, which are on the same trajectory before entering the magnet. The magnet bends less (smaller bending angle) a higher momentum particle and bends more (larger bending angle) a particle with a lower momentum.

Considering momentum deviation in Hill's equation, the transfer matrices for dipole magnets are given by following expressions [15-18]

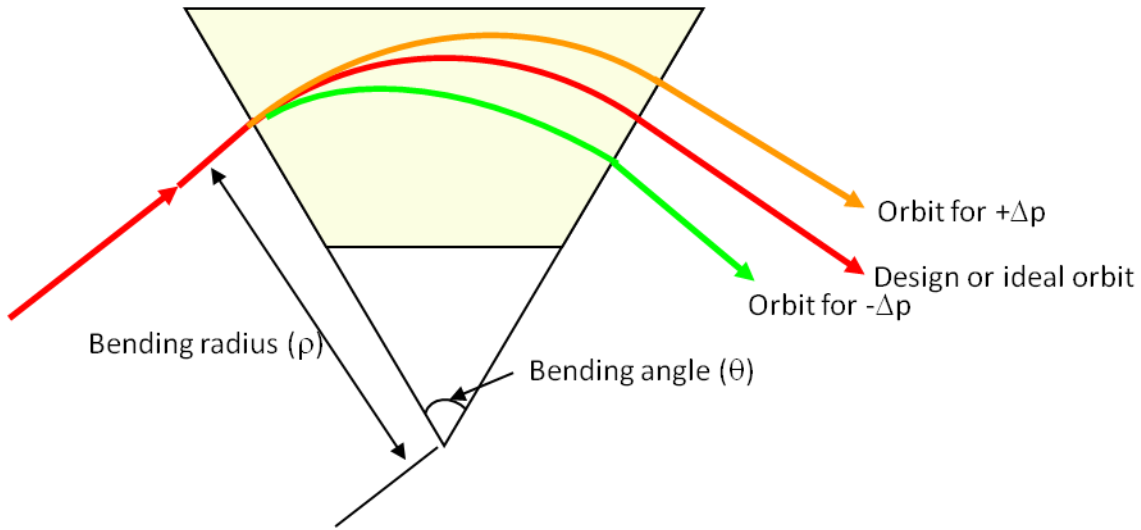


**Fig. 1.5 Trajectories in dipole magnet due to momentum spread**

### 1. Sector type dipole magnet (horizontal bending)

$$\begin{bmatrix} x \\ x' \\ \delta \end{bmatrix}_{out} = \begin{bmatrix} \cos\theta & \rho\sin\theta & \rho(1 - \cos\theta) \\ -\frac{\sin\theta}{\rho} & \cos\theta & \sin\theta \\ 0 & 0 & 1 \end{bmatrix} \begin{bmatrix} x \\ x' \\ \delta \end{bmatrix}_{in} \quad [1.11]$$

The last row ensures that  $\delta$  does not change in a dipole magnet.

### 2. Rectangular type dipole magnet (horizontal bending):

$$\begin{bmatrix} x \\ x' \\ \delta \end{bmatrix}_{out} = \begin{bmatrix} 1 & \rho\sin\theta & \rho(1 - \cos\theta) \\ 0 & 1 & 2\tan\frac{\theta}{2} \\ 0 & 0 & 1 \end{bmatrix} \begin{bmatrix} x \\ x' \\ \delta \end{bmatrix}_{in} \quad [1.12]$$

The deviation in a trajectory with respect to the design trajectory due to a momentum offset, is quantified as 'dispersion' and can be written as (in first order of  $\delta$ )

$$x_d(s) = D(s)\delta \quad [1.13]$$

Here  $x_d$  is the deviation in an off momentum trajectory from the design trajectory and  $D(s)$  is the dispersion. This is first order dispersion. The angle of this deviated trajectory can be written as

$$x'_d(s) = D'(s)\delta \quad [1.14]$$

Here  $D'$  is the derivative of  $D$  with respect to  $s$ . Above two equations reveal that the dispersion follows same transfer matrices as followed by transverse co-ordinates  $x$  and  $x'$ . Therefore, the transfer matrix for dispersion vector for a sector type dipole magnet is given by

$$\begin{bmatrix} D \\ D' \\ 1 \end{bmatrix}_{out} = \begin{bmatrix} \cos\theta & \rho\sin\theta & \rho(1 - \cos\theta) \\ -\frac{\sin\theta}{\rho} & \cos\theta & \sin\theta \\ 0 & 0 & 1 \end{bmatrix} \begin{bmatrix} D \\ D' \\ 1 \end{bmatrix}_{in} \quad [1.15]$$

Similarly matrix for a rectangular dipole magnet is following

$$\begin{bmatrix} D \\ D' \\ 1 \end{bmatrix}_{out} = \begin{bmatrix} 1 & \rho\sin\theta & \rho(1 - \cos\theta) \\ 0 & 1 & 2\tan\frac{\theta}{2} \\ 0 & 0 & 1 \end{bmatrix} \begin{bmatrix} D \\ D' \\ 1 \end{bmatrix}_{in} \quad [1.16]$$

The dipole magnet generates a dispersion in the plane of bending i.e. horizontal bending magnet generates a horizontal dispersion, which is mostly the cases with all accelerators. A vertical dipole magnet generates a vertical dispersion.

This deviation in trajectory also brings a change in total path length travelled by an off-momentum particle as compared to length of the design trajectory. This path length dependence on momentum is the key parameter used in designing a bunch compressor.

Similar to a dipole magnet, an off-momentum particle experiences a different kick from a quadrupole magnet and therefore, focal length of a quadrupole magnet becomes momentum dependent. Considering first order in momentum deviation, this chromatic effect of a thin quadrupole magnet can be expressed as follows

$$k_\delta = k(1 + \delta)^{-1} \approx k(1 - \delta)$$

Here  $k_\delta$  is the effective quadrupole strength for an off-momentum particle.

## 1.4 Motion in longitudinal plane

A particle may also lead or lag behind the synchronous particle (origin of moving co-ordinate system) and therefore time (or distance along  $s$ ) from the origin (or synchronous or reference particle) is also needed to specify the particle's state. By introduction of this time co-ordinate, now there are six co-ordinates. Using these 6 co-ordinates, complete state of a particle for accelerator optics is described. In full 6-D, mapping (matrix equation) of the co-ordinates looks like the following

$$\tilde{\mathbf{X}}_{out} = \tilde{\mathbf{R}}_{6 \times 6} \tilde{\mathbf{X}}_{in} \quad [1.17]$$

Here, subscripts '*in*' and '*out*' refers to co-ordinates of the particle at the entry and exit of the optical element (or an optical section). Matrix  $\tilde{\mathbf{R}}_{6 \times 6}$  is the transfer matrix of the magnet (or optical element), describing a 6-D linear map. Here  $\tilde{\mathbf{X}}_{in}$  and  $\tilde{\mathbf{X}}_{out}$  is the column vector ( $6 \times 1$ ) of co-ordinates for a particle.

$$\tilde{\mathbf{X}}_{in/out} = \begin{bmatrix} x \\ x' \\ y \\ y' \\ \Delta t \\ \delta \end{bmatrix}_{in/out} = \begin{bmatrix} x_1 \\ x_2 \\ x_3 \\ x_4 \\ x_5 \\ x_6 \end{bmatrix}_{in/out} \quad [1.18]$$

Here new symbols  $x_i$ 's are introduced for co-ordinates. Note here that time is the fifth co-ordinate and momentum offset is the sixth co-ordinate, although we introduced these two co-ordinates in reverse order. Sometimes 'z' (distance from synchronous particle along  $s$ ) is taken as the fifth co-ordinate, instead of time difference from synchronous particle ( $\Delta t$ ). An element of the transfer matrix  $R_{ij}$  gives the dependence of  $i^{th}$  co-ordinate of the particle at the exit on the  $j^{th}$  co-ordinate of the particle at the entrance of the optical element.

The dynamics of longitudinal co-ordinates  $\Delta t$  and  $\delta$  decides the bunch length and therefore the evolution of these co-ordinates in a given optics is very important in designing and analysing the bunch compressors. Magnets do not change momentum offset ( $\delta$ ) of a particle

(if we ignore radiation emission during bending of a charge particle). In accelerators, for energy manipulation of the beam, RF cavities are used, which changes this momentum offset. When a charge particle passes through this cavity, the electric field manipulates the energy of this charge particle, hence its momentum offset changes. In magnetic optics, path length, hence time of flight of a particle depends on momentum offset. In this way, RF cavity changes momentum offset  $\delta$  on the basis of particle's position in a bunch and magnetic optics changes  $\Delta t$  on the basis of its momentum offset. Combination of RF cavity with magnetic optics can change both the longitudinal parameters and bunch length can be controlled. Now in following sub-section, we obtain the longitudinal map of a dipole magnet and an RF cavity.

### **1. Longitudinal map of a dipole magnet**

A dipole magnet does not change the momentum offset of a particle and therefore  $R_{65}$  and  $R_{66}$  is zero and one respectively. These two elements  $R_{65}$  and  $R_{66}$  establish a relation of  $\delta_{out}$  with  $\Delta t_{in}$  and  $\delta_{in}$ , respectively. Now we compute the path length dependence on momentum offset in a dipole magnet. Fig. 1.6 shows two trajectories inside a small section of a dipole magnet.

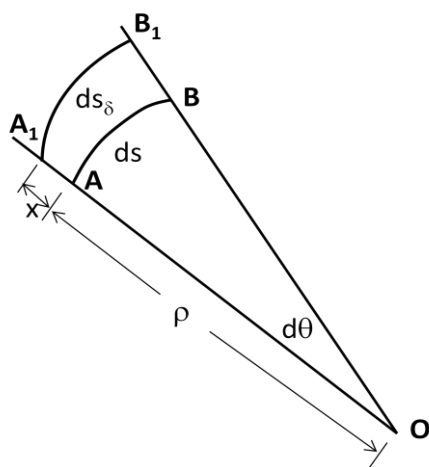


**Fig. 1.6 Trajectories in a small section of a dipole magnet**

In this figure curve **AB** depicts the design trajectory and another deviated trajectory (due to momentum offset) at a distance of  $x$ , is shown by the curve **A<sub>1</sub>B<sub>1</sub>**. The length of these trajectories are ' $ds$ ' and ' $ds_\delta$ ', respectively and  $\rho$  is the design bending radius. In first order approximation, the length of the deviated trajectory can be written as [15]

$$ds_\delta = (x + \rho)d\theta = \left(1 + \frac{x}{\rho}\right)\rho d\theta = \left(1 + \frac{D\delta}{\rho}\right)ds \quad [1.19]$$

Thus change in path length between these two trajectories over this small arc section is

$$\Delta s = ds_\delta - ds = \frac{Dds}{\rho} \delta \quad [1.20]$$

Integration of this quantity over the complete optics of length  $L$ , gives a total change in path length. Change in path length for unit momentum offset is the  $R_{56}$  element of the transfer matrix. Using the above equation,  $R_{56}$  is given by

$$R_{56} = \frac{\Delta L}{\delta} = \int_0^L \frac{D(s)}{\rho} ds \quad [1.21]$$

This change in path length is translated in a change in time of flight for an off-momentum particle and thus total travel time of a particle in optics becomes a function of its momentum. In general the higher momentum particle (positive momentum offset) follows a longer path, hence a general optics has a positive  $R_{56}$  and in the thesis, this sign convention is followed. Computer program MAD8 [20], which has been extensively used in design and optimization of CTF3 Transfer Line-2 (TL-2) bunch compressor, has opposite sign convention i.e. in the above case it gives a negative  $R_{56}$ . Evaluating the integration of Eq. 1.21 for a particular type of magnet provides the explicit expression of  $R_{56}$  for that magnet.

If an on-momentum particle enters a dipole magnet with non-zero  $x$  or  $x'$ , this changes the path length even for an on-momentum particle also. But for beam with smaller size and divergence, these effects are negligible. These contributions in path length gives non-zero

element  $R_{51}$  and  $R_{52}$ . Now we can write full  $6 \times 6$  linear map (matrix) for a horizontal dipole magnet as following [21-23]

$$\tilde{\mathbf{R}}_{6 \times 6} = \begin{bmatrix} R_{11} & R_{12} & 0 & 0 & 0 & R_{16} \\ R_{21} & R_{22} & 0 & 0 & 0 & R_{26} \\ 0 & 0 & R_{33} & R_{34} & 0 & 0 \\ 0 & 0 & R_{43} & R_{44} & 0 & 0 \\ R_{51} & R_{52} & 0 & 0 & 1 & R_{56} \\ 0 & 0 & 0 & 0 & 0 & 1 \end{bmatrix} \quad [1.22]$$

## 2. Longitudinal map of an RF cavity

Let a sinusoidal RF variation of voltage at a frequency  $f$  with a peak value of  $V$  in a cavity. Synchronous phase be  $\phi_s$  i.e. RF phase at which synchronous particle arrives in an RF cavity. A particle enters the cavity at a phase  $\phi$  (i.e. a phase deviation of  $\Delta\phi$  from the synchronous phase) with a momentum offset  $\delta_{in}$ . The energy of this particle at time of entering in the cavity is [9-11]

$$E_{in} = E_{s,in}(1 + \delta_{in}) \quad [1.23]$$

Here ' $E_{s,in}$ ' is the energy of the synchronous particle at the time of entering the cavity. Similarly, after exit from this cavity, the energy of the synchronous and off momentum particle become

$$E_{s,out} = E_{s,in} + qVs \sin \phi_s \quad [1.24]$$

$$E_{out} = E_{s,out}(1 + \delta_{out}) = E_{in} + qVs \sin(\phi_s - \Delta\phi) \quad [1.25]$$

Combining above three equations (1.23, 1.24 and 1.25), yield

$$E_{s,out}(1 + \delta_{out}) = E_{s,in}(1 + \delta_{in}) + qVs \sin(\phi_s - \Delta\phi) \quad [1.26]$$

This gives

$$\delta_{out} = \frac{E_{s,in}(1 + \delta_{in}) + qVs \sin(\phi_s - \Delta\phi)}{E_{s,in} + qVs \sin \phi_s} - 1 \quad [1.27]$$

$$\begin{aligned}
&= (1 + \delta_{in}) \left( 1 + \frac{qV}{E_{s,in}} \sin \phi_s \right)^{-1} \\
&\quad + \frac{qV}{E_{s,in}} \sin(\phi_s - \Delta\phi) \left( 1 + \frac{qV}{E_{s,in}} \sin \phi_s \right)^{-1} - 1
\end{aligned} \tag{1.28}$$

For a high energy beam, the ratio  $\frac{qV}{E_{s,in}} \ll 1$  and thus retaining only linear terms of this ratio,

we get

$$\delta_{out} = \delta_{in} \left( 1 - \frac{qV}{E_{s,in}} \sin \phi_s \right) - \frac{qV}{E_{s,in}} \sin \phi_s + \frac{qV}{E_{s,in}} \sin(\phi_s - \Delta\phi) \tag{1.29}$$

The phase deviation  $\Delta\phi$  is  $k_{rf}z_{in}$ , where  $k_{rf}$  is the magnitude of RF wave vector and  $z_{in}$  is the distance of the particle from the synchronous particle. Using this value of  $\Delta\phi$ , above expression reduces to

$$\delta_{out} = \delta_{in} \left( 1 - \frac{qV}{E_{s,in}} \sin \phi_s \right) + \frac{qV}{E_{s,in}} (\sin(\phi_s - k_{rf}z_{in}) - \sin \phi_s) \tag{1.30}$$

If particle's deviation from the synchronous phase is small, then keeping linear terms in the above equations, provides us the following expression

$$\delta_{out} = \delta_{in} \left( 1 - \frac{qV}{E_{s,in}} \sin \phi_s \right) - z_{in} \frac{qV k_{rf}}{E_{s,in}} \cos \phi_s \tag{1.31}$$

Considering cavity as a thin lens, it does not change relative distance ( $z_{in}$ ) of a particle from the synchronous particle. Thus transfer matrix of a cavity for the longitudinal plane can be written as

$$\begin{bmatrix} x_{5,out} \\ x_{6,out} \end{bmatrix} = \begin{bmatrix} z_{out} \\ \delta_{out} \end{bmatrix} = \begin{bmatrix} 1 & 0 \\ R_{65} & R_{66} \end{bmatrix} \begin{bmatrix} x_{5,in} \\ x_{6,in} \end{bmatrix} \tag{1.32}$$

Under thin lens approximation,  $R_{55}=1$  and  $R_{56}=0$ . The other elements of above matrix are as following

$$R_{65} = -\frac{qV k_{rf}}{E_{s,in}} \cos\phi_s \quad [1.33]$$

and

$$R_{66} = 1 - \frac{qV}{E_{s,in}} \sin\phi_s \quad [1.34]$$

Above transfer matrix of an RF cavity provides a quantified information of the change in momentum offset of a particle, passing through a cavity, as a function of its position.

## 1.5 Transfer matrix for a combination of elements (optical section)

In the above sections, expressions of linear map for different types of elements used in beam optics are presented. After an optical element, we can write

$$x_{i,out} = \sum_{j=1}^6 R_{ij} x_{j,in} \quad [1.35]$$

In a beam transfer line or an accelerator, there is a series of elements, through which a particle passes during its course of motion. The overall map of the optics is a composition of maps of individual elements i.e. the overall transfer matrix for this transfer line or accelerator can be obtained by successive multiplication of individual transfer matrices of elements. For a transfer line or cell of  $n$ -elements, this complete transfer matrix can be written as following

$$\tilde{\mathbf{R}}_{complete} = \tilde{\mathbf{R}}_n \tilde{\mathbf{R}}_{n-1} \tilde{\mathbf{R}}_{n-2} \dots \tilde{\mathbf{R}}_2 \tilde{\mathbf{R}}_1 \quad [1.36]$$

## 1.6 Parameterization of charged particle optics

### 1.6.1 Twiss parameters

A map provides a way to obtain the trajectory of a particle which passes through the optics with certain initial conditions. The optics (in linear domain) can be characterized by another equivalent method and this method is more comprehensive for understanding the optical system and behaviour of the complete beam rather than the individual particle. This method is presented in this section in brief. Details are provided in various books and reports on accelerator physics [13-18].

The solution of Hill's equation (Eq. 1.2) can be written as [13-18]

$$x(s) = A\sqrt{\beta(s)}\cos(\mu(s) - \mu_0) \quad [1.37]$$

Here amplitude  $A\sqrt{\beta(s)}$  is  $s$ -dependent and  $A$  is a constant. The function  $\beta(s)$  is called 'beta function' and  $\mu(s)$  is the 'betatron phase'. This solution shows that particle exhibits a kind of oscillatory motion, known as 'betatron oscillation'. Similar oscillation occurs in  $y$ -direction also. Distribution of beta function depends on the magnetic (mainly focusing-defocusing elements) arrangement (location and strength) in the optics i.e. distribution of  $K(s)$  of Hill's equation. Differentiating twice the Eq. 1.37 with respect to  $s$  and then putting these values in Hill's equation, gives

$$\gamma(s)x(s)^2 + 2\alpha(s)x(s)x'(s) + \beta(s)x'(s)^2 = A^2 \quad [1.38]$$

This expression gives the invariant of motion. Here two more parameters are introduced, which are the following

$$\alpha(s) = -\frac{1}{2}\frac{d\beta(s)}{ds} \quad [1.39]$$

$$\gamma(s) = \frac{1 + \alpha(s)^2}{\beta(s)} \quad [1.40]$$

The expression for a constant of motion is the equation of an ellipse with an area of  $\pi A^2$  and therefore area of the ellipse is invariant of motion, also known as 'Courant-Synder invariant'. These three parameters ( $\beta(s)$ ,  $\alpha(s)$  and  $\gamma(s)$ ) are known as Twiss parameters. Solution of Hill's equation gives the maximum displacement at any location  $s$  for a particle as following

$$x_{max}(s) = A\sqrt{\beta(s)} \quad [1.41]$$

Similarly, maximum angle of a particle trajectory with the design trajectory at any location is given by

$$x'_{max}(s) = A\sqrt{\gamma(s)} \quad [1.42]$$

These relations show that Twiss parameters  $\beta(s)$  and  $\gamma(s)$  provide an information of the beam size and beam divergence at any location ( $s$ ) in a magnetic optics. The parameter  $\alpha(s)$  provides a correlation between displacement and angle. Fig. 1.7 shows an ellipse at a particular location. Similar ellipse will be formed in the vertical plane ( $y-y'$ ) and parameters of this ellipse will be defined by  $\alpha(s)$ ,  $\beta(s)$  and  $\gamma(s)$  in vertical plane at that location.

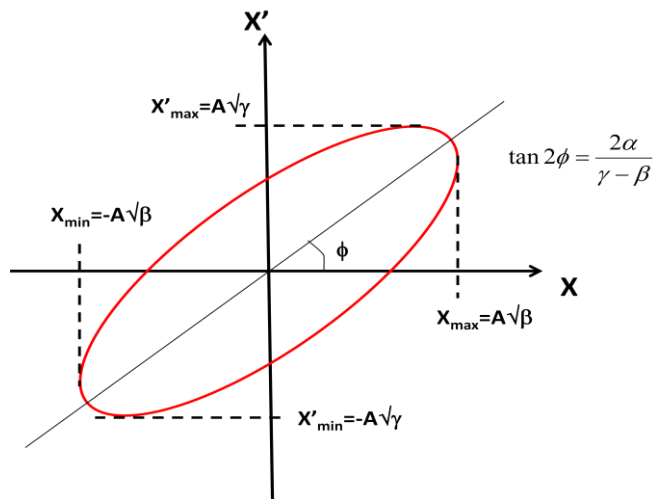


**Fig. 1.7 Phase space ellipse in  $x-x'$  plane**

The plane formed by  $x$  and  $x'$  (similarly  $y$ ,  $y'$  and another plane by  $t$ ,  $\delta$ ) is the plane in phase space. At different locations, due to change in Twiss parameters, the size of major, minor axes and rotation of this ellipse may change, but area remains constant.

In presence of dispersion, the displacement of betatron oscillation becomes

$$x(s) = A\sqrt{\beta(s)}\cos(\mu(s) - \mu_0) + D(s)\delta \quad [1.43]$$

At high dispersion point, displacement of a particle increases as well as displacement for a particle with momentum offset is larger as compared to on-momentum particle.

It is evident that the dipole magnet generates the dispersion, but at various downstream locations in a transfer line, there may be a requirement for a dispersion free region, especially placing some subsystem etc. To suppress the dispersion downstream, there is a need to enforce dispersion and its derivative ( $D'(s)$ ) to vanish at some location, from where, in downstream there will be availability of a dispersion free region, at least in linear theory. Using a second dipole magnet and quadrupole magnet, we can achieve the goal. The section of charged particle optics, in which there is finite dispersion and outside of it (before entrance and after exit), there is no dispersion, is known as 'achromat'.

### 1.6.2 Beam emittance

A beam is a large collection of particles, distributed in phase space. For each initial  $x$ ,  $x'$  there is an associated ellipse with constant area. Now the beam size can be defined either by standard deviation of positions of particles or choosing particle whose ellipse encompasses 90% particles or 95% particles etc as shown in Fig. 1.8. Such an ellipse defines the beam size and beam divergence.

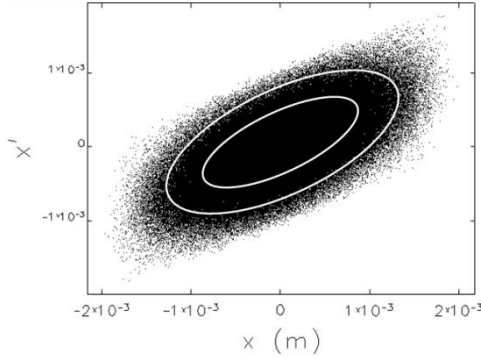


**Fig. 1.8 Ellipses encompassing ~67% and ~95% particles from a beam, distributed in phase space**

The area of the ellipse, which is the invariant of motion is known as 'beam emittance'. It is one of the most important parameters to describe the quality of the beam. Beam emittance, beta function, dispersion and momentum spread of a beam decide the beam size in a beam transport system or in an accelerator. Due to  $s$ -dependence of beta function and dispersion, beam size is also a function of ' $s$ '. Beam size and divergence are defined by

$$\sigma(s) = \sqrt{\epsilon\beta(s)} \quad [1.44]$$

$$\sigma'(s) = \sqrt{\epsilon\gamma(s)} \quad [1.45]$$

Here  $\epsilon$  is the beam emittance and  $A^2=\epsilon$ . Larger emittance means larger beam sizes and divergence and vice versa. In case of a linear system, the propagation of beam size, divergence and emittance through a magnetic optics can be described by another approach using 'beam matrix'. Beam matrix is provided in Appendix A.

Beam transfer lines and accelerators are not perfectly linear dynamical system. Instead of this, there are sextupole magnets, incorporated in optics to compensate the chromatic aberrations generated by quadrupole magnets and also there are higher order multipole errors

in the dipole and quadrupole magnets. These make the system nonlinear. In this case, problem becomes difficult to find out the invariant of motion and the distribution of beam cannot be characterized by an ellipse. In this case, the beam emittance is defined by considering the second moments of beam distribution in positions and angle. This definition of emittance is statistical emittance, also known as RMS emittance [24].

$$\epsilon_{RMS} = f(\langle x \rangle^2 \langle x' \rangle^2 - \langle xx' \rangle^2) \quad [1.46]$$

Similar expression exists for other two planes also. Here  $f$  is a factor, which depends on the distribution. For Gaussian distribution, it is 1/4. The physical significance of this factor is to match the RMS emittance definition for a well defined distribution with emittnace defined geometrically (i.e. area of ellipse). In most of the literature, this factor is often omitted, as the RMS emittance is generally used to quantify the relative change, rather than an absolute value.

Often emittance is normalized by relativistic parameters  $\beta (=v/c)$  and  $\gamma (= \frac{1}{\sqrt{1-\beta^2}})$  to make emittance energy independent. This is known as normalized emittance.

A bunch of charged particles has certain finite length along  $s$ -axis (i.e. in time). If we pick the particles from a bunch for a very short time slice, we can define the transverse emittance of that slice. In this way, we separate the bunch in short slices and projection of all the slice emittances provide the emittance, measured by a detector. The slice emittance has importance when one looks the effect of wake field induced by one part of the bunch on the other part of this bunch.

### **1.6.3 Twiss parameters and transfer matrix**

Twiss parameters and map (transfer matrix in linear theory), both describe the same optical system. Therefore, these two descriptions are connected. We can define a matrix of a magnet

or a section of an optical system, which maps the Twiss parameters at entry to exit and element of this matrix are the function of elements of the transfer matrix of that magnet or optical section. The matrix for mapping the Twiss parameters in horizontal is given below

$$\begin{bmatrix} \beta \\ \alpha \\ \gamma \end{bmatrix}_{x,out} = \begin{bmatrix} R_{11}^2 & -2R_{11}R_{12} & R_{12}^2 \\ -R_{11}R_{21} & R_{11}R_{22} + R_{12}R_{21} & -R_{21}R_{22} \\ R_{21}^2 & -2R_{21}R_{22} & R_{22}^2 \end{bmatrix} \begin{bmatrix} \beta \\ \alpha \\ \gamma \end{bmatrix}_{x,in} \quad [1.47]$$

For vertical plane,  $R_{11}$ ,  $R_{12}$ ,  $R_{21}$  and  $R_{22}$  will be replaced by  $R_{31}$ ,  $R_{32}$ ,  $R_{41}$  and  $R_{42}$  respectively in above relation.

Similarly a transfer matrix based on Twiss parameters and betatron phase advance can be made and this matrix transforms, co-ordinates of the particle from one location (say 1) to another location (say 2). This matrix relation is given by [15-17]

$$\begin{bmatrix} x \\ x' \end{bmatrix}_2 = \begin{bmatrix} \sqrt{\frac{\beta_2}{\beta_1}}(\cos\Delta\mu + \alpha_1 \sin\Delta\mu) & \sqrt{\beta_1\beta_2}\sin\Delta\mu \\ -\frac{1 + \alpha_1\alpha_2}{\sqrt{\beta_1\beta_2}}\sin\Delta\mu + (\alpha_1 - \alpha_2)\cos\Delta\mu & \sqrt{\frac{\beta_1}{\beta_2}}(\cos\Delta\mu - \alpha_2 \sin\Delta\mu) \end{bmatrix} \begin{bmatrix} x \\ x' \end{bmatrix}_1 \quad [1.48]$$

Similar relation holds for vertical plane too.

## 1.7 Second order map

Above theory is based on the linearization of the equation of motion, hence  $\tilde{\mathbf{R}}$  matrix maps co-ordinates of a particle at the exit of an element (or optical section) from co-ordinates at the entry point in a linear fashion. If the equation of motion is expanded up to second order, the solution (i.e. co-ordinates of particle) can be written down using perturbation techniques as follows

$$x_{i,out} = \sum_{j=1}^6 R_{ij} x_{j,in} + \sum_{j=1, k=1}^6 T_{ijk} x_{j,in} x_{k,in} \quad [1.49]$$

Here  $T_{ijk}$  represents the second order transfer map. It shows a dependence of co-ordinates at the exit on a combination of two initial co-ordinates. Detailed expressions for second order transfer map for a dipole magnet, quadrupole magnet and sextupole magnet are derived in an elegant way using perturbation technique in the classic work of Brown [23]. Element  $T_{655}$  of RF cavity, which provides a functional relationship between momentum offset ( $x_6$ ) and position squared of particle within the bunch ( $x_5^2$ ) and element  $T_{566}$  of magnetic optics that relates the path length ( $x_5$ ) with square of momentum offset ( $x_6^2$ ) are important second order parameters for a bunch compressor.

Here, we obtain the second order element  $T_{655}$  of an RF cavity. We extend Eq. 1.29 up to second order [9] as follows.

$$\delta_{out} = \delta_{in} \left( 1 - \frac{qV}{E_{s,in}} \sin \phi_s \right) + \frac{qV}{E_{s,in}} \left( -k_{rf} \cos \phi_s z_{in} - \frac{1}{2} k_{rf}^2 \sin \phi_s z_{in}^2 \right) \quad [1.50]$$

This gives

$$T_{655} = -\frac{1}{2} \frac{qV}{E_{s,in}} k_{rf}^2 \sin \phi_s \quad [1.51]$$

This element of second order map shows how the momentum deviation depends on the square of distance of a particle from the synchronous phase in an RF cavity. Generating correlation in momentum and position (i.e. chirping) using an RF cavity, the nonlinear term  $T_{655}$  brings a curvature in momentum spread curve with respect to the position. In case of the synchronous phase of 0 or  $\pi$ , second order term  $T_{655}$  becomes zero. Another transverse elements of second order map, which are important in the present study will be discussed in Chapter 4.

## 1.8 Bunch compression

In the following sub section, it will be shown that using above theory, presented so far, how a bunch of electrons can be compressed. Next sub-section discusses the different types of magnetic optics usually employed for the bunch compression.

### 1.8.1 Bunch length control

An electron bunch, generated from a thermionic electron source, has a distribution in longitudinal phase space as depicted in Fig. 1.9A. In this distribution, higher and lower momentum particles are almost uniformly distributed throughout the bunch length. The spread in momentum is un-correlated. For compressing the bunch length, head and tail of the bunch must be brought closer to each other for which time of flight for the particles, which are ahead (head of bunch) of the bunch centre (synchronous particle), must be longer and similarly, time of flight must be shorter for the particles which are lagging behind (tail of bunch) the synchronous particle. In case, where electron beam is highly relativistic (this is the case studied in this thesis, where electron beam energy is 300 MeV), the velocity of electrons remains almost constant and is nearly equal to the speed of light (therefore in this thesis effects of velocity will always be ignored). Therefore, time of flight depends on the path length only, i.e. if the path length is longer, time of flight will also be longer and vice versa. If a magnetic optics is tuned to a certain value of  $R_{56}$  (say positive  $R_{56}$ ), then path length for higher momentum particles will be longer. In above mentioned bunch (Fig. 1.9A) higher momentum particles are in the head as well as in the tail of the bunch. Thus higher momentum particles, which are in head will reach closer to bunch centre, while which are in tail, will become farther from bunch centre. Similar will be the case for lower momentum particles. For this type of bunch, optics only redistributes the particles within the bunch, but

bunch length is not changed. So  $R_{56}$  setting (control of path length due to momentum) alone cannot compress such bunch. But if there is some correlation in momentum and time in the particles of a bunch, such as depicted in Fig. 1.9B, then particular  $R_{56}$  setting of a magnetic optics can be used to compress the bunch. Now in this correlated bunch, higher momentum particles are almost in tail and lower momentum particles are almost in head. An optics with certain  $R_{56}$ , in which higher momentum particles take shorter path can be used to compress this type of bunch. Therefore, before passing a bunch through a magnetic optics for compression, a correlation in momentum and position is generated using  $R_{65}$  element of an RF cavity.

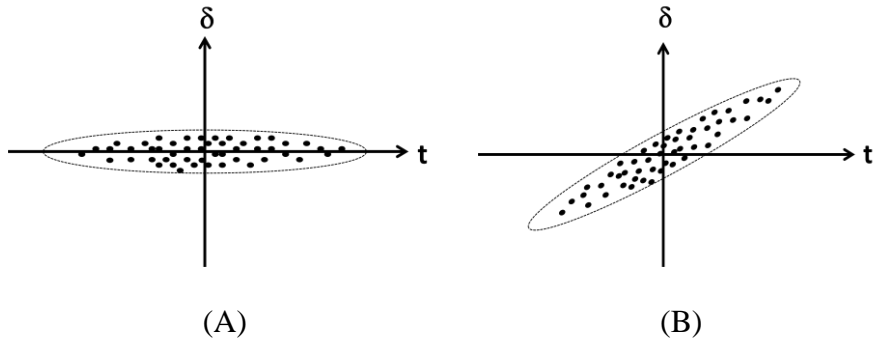


**Fig. 1.9 Longitudinal phase space, showing a bunch**

Now we see the effects on the longitudinal co-ordinates of an electron, when it passes through an RF cavity and then through a magnetic optics.

$$\begin{bmatrix} z_{out} \\ \delta_{out} \end{bmatrix} = \begin{bmatrix} 1 & R_{56} \\ 0 & 1 \end{bmatrix}_{optics} \begin{bmatrix} 1 & 0 \\ R_{65} & R_{66} \end{bmatrix}_{cavity} \begin{bmatrix} z_{in} \\ \delta_{in} \end{bmatrix} \quad [1.52]$$

$$\begin{bmatrix} z_{out} \\ \delta_{out} \end{bmatrix} = \begin{bmatrix} 1 + R_{56}R_{65} & R_{56}R_{66} \\ R_{65} & R_{66} \end{bmatrix} \begin{bmatrix} z_{in} \\ \delta_{in} \end{bmatrix} \quad [1.53]$$

If cavity is not intended to change the central energy of the beam, but only to generate a correlation between momentum and position i.e. for chirping, the synchronous phase  $\phi_s$  is either zero or  $\pi$ . In this case  $R_{66}$  becomes 1. Thus we have [9-11]

$$z_{out} = (1 + R_{56}R_{65})z_{in} + R_{56}\delta_{in} \quad [1.54]$$

With this expression, we get overall bunch length (RMS averaged on all electrons)

$$\sigma_{out} = \sqrt{(1 + R_{56}R_{65})^2\sigma_{in}^2 + R_{56}^2\delta_{in}^2} \quad [1.55]$$

Thus for a given uncorrelated momentum spread  $\delta_{in}$ , the minimum bunch length is possible when  $R_{56}=-1/R_{65}$ . In this case, the final bunch length is given by  $\sigma_{out,min}=R_{56}\delta_{in}$ . If optics is designed for very small  $R_{56}$ , then for achieving shorter bunch, the magnitude of  $R_{65}$  will be very large and the correlated momentum spread becomes larger. For smaller values of  $R_{65}$  i.e. lower correlated momentum spread, the required  $R_{56}$  is large in the optics for producing shorter bunches, hence very large dispersion is needed to be generated in magnetic optics. Thus  $R_{56}$  and  $R_{65}$  should be chosen judiciously for designing a bunch compressor. The same conclusion is arrived using another approach (beam matrix in longitudinal plane) and is discussed in Appendix A.

This discussion can be extended up to second order in a straight forward way. Let the electron passes through an RF cavity. After passing through a cavity, the momentum offset of the electron is modified as follows

$$\delta_{out,rf} = R_{65}z_{in} + R_{66}\delta_{in} + T_{655}z_{in}^2 \quad [1.56]$$

Now this electron passes through a magnetic optics. Thus final position of the electron after the magnetic optics is given by

$$z_{out} = z_{in} + R_{56}\delta_{out,rf} + \sum_{j,k=1}^6 T_{5jk}x_{j,out,rf}x_{k,out,rf} \quad [1.57]$$

In most of the practical cases of bunch compressors, the transverse emittances are small and thus pure transverse geometric effects and chromatic added with transverse geometric effects can be neglected as compared to pure chromatic effects. Under this approximation, above equation reduces to

$$z_{out} = z_{in} + R_{56}\delta_{out,rf} + T_{556}z_{in}\delta_{out,rf} + T_{566}\delta_{out,rf}^2 \quad [1.58]$$

Using  $\delta_{out,rf}$  from Eq. 1.56 in the above expression, we get

$$\begin{aligned} z_{out} = & (1 + R_{56}R_{65})z_{in} + R_{56}R_{66}\delta_{in} + R_{56}T_{655}z_{in}^2 + R_{66}T_{566}\delta_{in}^2 \\ & + T_{566}(R_{65} + R_{66})z_{in}\delta_{in} \end{aligned} \quad [1.59]$$

Using two RF systems (one fundamental and one higher harmonic),  $R_{65}$  and  $T_{655}$ , both can be controlled. In a magnetic optics,  $T_{566}$  can be controlled using sextupole magnets. When synchronous phase is 0 or  $\pi$ ,  $R_{66}$ , becomes 1 and  $T_{655}$  vanishes. In this case, the above equation reduces to

$$z_{out} = (1 + R_{56}R_{65})z_{in} + R_{56}\delta_{in} + T_{566}\delta_{in}^2 + T_{566}(R_{65} + 1)z_{in}\delta_{in} \quad [1.60]$$

Thus a finite  $T_{566}$  generates a curvature in longitudinal phase space distribution as well as an unwanted correlation in  $z$  and  $\delta$ . The electron density shows a sharp peak and using sextupole magnets,  $T_{566}$  is suppressed in bunch compressors. However instead of zero, obtaining different values of  $T_{566}$  with sextupole magnets can shape the density distribution of electrons in a bunch along the propagation direction [25].

### 1.8.2 General optics for bunch compressors

In this section, a discussion on some commonly employed optics for bunch compressors is presented. We will discuss only those achromatic optics in which the beam at the exit of optics is either parallel to incoming beam or is on the same axis as of incoming beam i.e. exit beam with some lateral displacement or without displacement from the incoming beam (Fig 1.10).

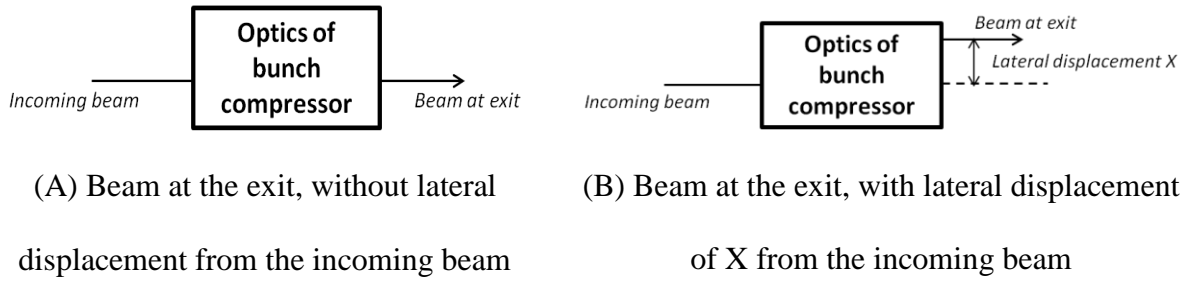


**Fig. 1.10 Schematic of incoming and exit beam in two cases of bunch compressors**

Therefore, in all the optics, which are discussed in this thesis, dipole magnets with opposite nature of bending angles will be present. The type of optics in which beam at the exit is on the same axis as of incoming beam, is formed by a chicane and its variants or a wiggler based bunch compressor. Another type of optics, in which there is a finite lateral displacement in beam at the exit, is formed either by a dog-leg optics or an arc and their different variants. In following sub-sections, we discuss these types of optics.

### 1. Chicane

This is the simplest optics for bunch compression, in which the exit beam and incoming beam are on the same axis. A chicane is formed using four dipole magnets, in which two dipole magnets bend the beam in positive direction, while other two dipole magnets bend the beam in negative direction keeping the overall resultant bending angle zero. This chicane generally known as C-chicane, is shown in Fig. 1.11. It consists of four rectangular dipole magnets of equal length ( $L_{bm}$ ). The separation between first and second dipole magnets and that between third and fourth dipole magnets is  $L_{12}$ .

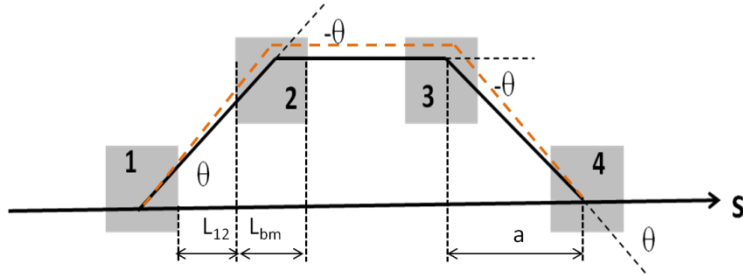


**Fig. 1.11 Layout of a C-Chicane optics**

In this optics, in the first dipole magnet, beam enters at the right angle to the edge of the magnet and therefore, the magnet behaves as the sector magnet at the entry. The exit beam makes an angle of  $\theta$  (bending angle) with the edge. In this orientation the higher momentum electron in this magnet has a shorter path length, which gives negative  $R_{56}$  for this magnet. The matrix of this magnet can be obtained by the matrix of a sector magnet and the matrix for edge focusing. Second magnet is just the reverse of this first magnet i.e. edge and then sector magnet. In Fig. 1.11, dashed line shows a trajectory for the lower momentum electron and bold continuous line shows design trajectory. The trajectory of an off-momentum electron meets the design trajectory at the exit i.e. optics is achromatic. Symmetry in an optics helps in suppressing the higher order aberrations [26, 27] and the chicane optics is achromatic up to all orders. Using simple geometry, approximate value of  $R_{56}$  for this optics can be obtained and is given by the following expression [28]

$$R_{56} \approx -2\theta^2 \left( L_{12} + \frac{2}{3}L_{bm} \right) \quad [1.61]$$

and

$$T_{566} \approx 3\theta^2 \left( L_{12} + \frac{2}{3}L_{bm} \right) = -\frac{3}{2}R_{56} \quad [1.62]$$

$R_{56}$  can be obtained using two methods or approaches namely geometrical approach and matrix approach. In the geometrical approach, the path lengths taken are the lengths of the

trajectory in actual length of the magnets. Thus path lengths of the trajectory of an off-momentum electron with a positive momentum deviation in a C-chicane are shorter than the design trajectory and equal to each other in all dipole magnets, giving negative  $R_{56}$  for the chicane optics (see appendix-B for details). In the matrix approach, the dipole magnets are considered as sector magnets and edge angle effects are taken care of with thin lenses at their edges. Due to this assumption, the second and third dipole magnet contribute larger and negative  $R_{56}$ , while first and last dipole magnet contribute smaller and positive  $R_{56}$ , making overall a negative  $R_{56}$  for the chicane. The final value of  $R_{56}$  for the chicane is same from both the approaches.

For very small magnets ( $L_{bm} \ll L_{12}$ ), the approximate values of  $R_{56}$  and  $T_{566}$  are  $-2a\theta^2$  and  $3a\theta^2$ , respectively (here ' $a$ ' is the distance from the first magnet centre to the second magnet centre). More accurate expression of  $R_{56}$  for a chicane geometry, based on actual transfer matrices of all the elements (including drifts) is given in Ref [29]. There may be different variations in this geometry which include asymmetric chicane, in which first and second dipole magnets are different from the third and fourth dipole magnets and distance between first and second dipole magnets may be different from the distance between third and fourth dipole magnets. By removing fourth dipole magnet, a mirror optics is added to the chicane to form an S-chicane, which is another variant of this geometry. These variants are discussed in Ref [30]. One interesting variant, in which beam at the exit is in opposite direction to the incoming beam by inclusion of a  $\pi$ -bend ("Bates bend") is discussed in Ref [29].

All these variants of optics provide a fixed value of  $R_{56}$ . Inclusion of quadrupole magnets in chicane can make the tuning of  $R_{56}$  possible. In general, a chicane is used to describe the optics, without quadrupole magnets, but in this section we also analyze the chicane optics

with quadrupole magnets. Fig. 1.12 shows such an optics, in which tuning of  $R_{56}$  is possible while fulfilling the first order achromatic condition also.

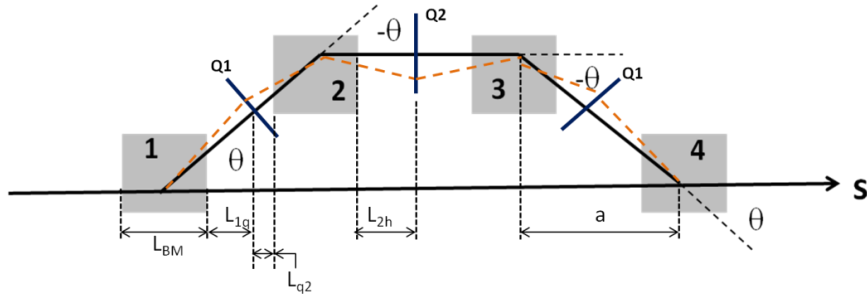


**Fig. 1.12 Chicane geometry including quadrupole magnets**

In all the cases of optics considered, we will discuss only the bending plane, which decides the value of  $R_{56}$ . In an actual beam transport system design, one has to take care of another plane also, that is the plane vertical to this bending plane. In the present discussion, ignoring dynamics in vertical plane is justified, because here, the purpose is only to discuss using approximate results, the general behaviour (i.e.  $R_{56}$  tuning,  $R_{56}$  variation with momentum offset etc.) of these optics not the detailed studies of Twiss parameters, beam distribution etc. Nevertheless, this discussion is useful to understand the optical behaviour from the bunch compression point of view as the  $R_{56}$  is decided by the motion in bending plane. In the optics, shown in Fig. 1.12, quadrupole Q1 is used to vary the dispersion or its derivative at the entrance of the second dipole magnet, which tunes the optics at the desired value of  $R_{56}$ . Second quadrupole magnet Q2, placed at mirror symmetry location, ensures the achromatic condition of this optics. Using simple geometry and considering quadrupole magnet as thin lens, approximate value of  $R_{56}$  for this optics can be obtained and is given by

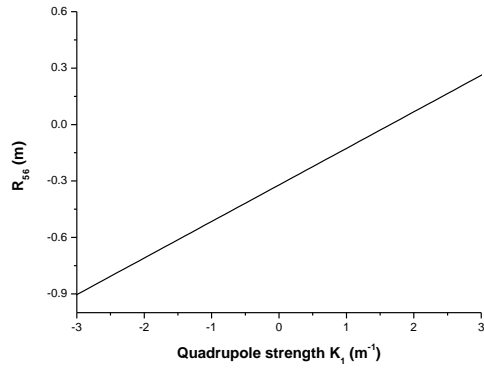
$$R_{56} = -2 \left( L_{12} + \frac{2L_{bm}}{3} \right) \theta^2 - L_{bm} \theta^2 - 2K_1 \left( L_{1q} + \frac{L_{bm}}{2} \right) \left( L_{q2} + \frac{L_{bm}}{2} \right) \theta^2 \quad [1.63]$$

Here  $K_1$  is the integrated strength of the quadrupole magnet Q1.  $L_{1q}$  is the distances from the first dipole exit to the first quadrupole magnet and  $L_{q2}$  is the distance between first quadrupole magnet and entrance of second dipole magnet (see Fig. 1.12, these distances are along the direction of incoming beam). Complete derivation of this expression is provided in Appendix B. This expression reveals that even the positive  $R_{56}$  can be obtained for this optics after inclusion of the quadrupole magnet ( $K_1$  is negative for a focusing quadrupole magnet in the above expression). For a particular optics (Table 1.1 provides parameters of the chosen example optics), this tuning in  $R_{56}$  with quadrupole strength is shown in Fig. 1.13A. In Fig. 1.13B and 1.13C, dispersion distribution for positive and negative  $R_{56}$  is shown. For making large positive  $R_{56}$ , required excursion in dispersion becomes larger in order to produce a large positive dispersion at the second dipole magnet.

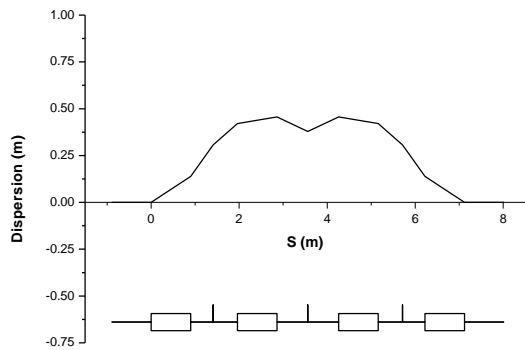
**Table 1.1: Parameters of the example optics for chicane**

Dipole magnet length	0.90 m
Bending angle of dipole magnet	$17.25^\circ$
First dipole end to first quadrupole distance ( $L_{1q}$ )	0.51 m
First quadrupole magnet to second dipole start ( $L_{q2}$ )	0.55 m
Total distance between first dipole end to start of second dipole ( $L_{12}$ )*	1.06 m
Second dipole magnet end to second quadrupole magnet ( $L_{2h}$ )	0.7 m

\*The distance  $L_{12}$  is chosen for  $R_{56}=-0.30$  m without quadrupole magnets and dipole length and angles are chosen from one of the types of dipole magnet, used in the optics of TL-2

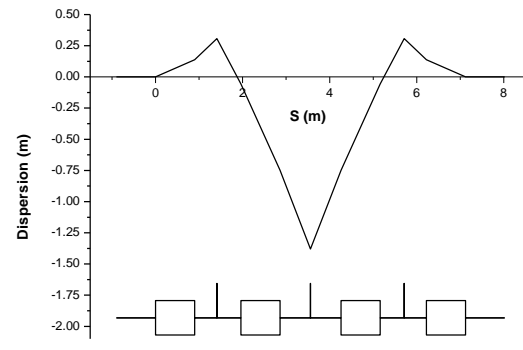


(A) Tuning of  $R_{56}$  with quadrupole strength  $K_1$



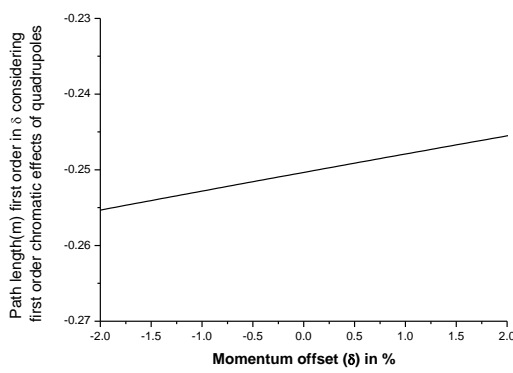
(B) Dispersion for tuning at  $R_{56}=0.25$  m ( $K_1 = 0.364$   $m^{-1}$ ).

Rectangles (boxes) represent dipole magnets and vertical line segments show focusing quadrupole magnets.

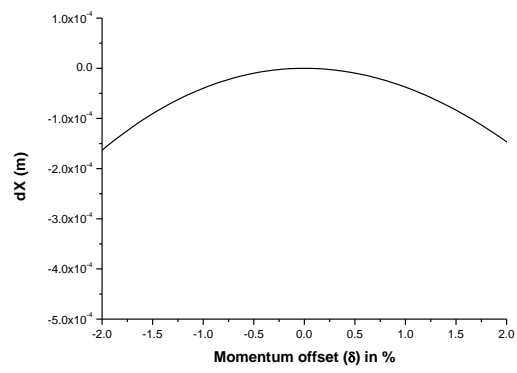


(C) Dispersion for tuning at  $R_{56}=-0.25$  m ( $K_1 = 2.945$   $m^{-1}$ ).

Rectangles (boxes) represent dipole magnets and vertical line segments show focusing quadrupole magnets.



(D) Path length with momentum offset for  $R_{56} = -0.25$  m



(E) Displacement from design trajectory with momentum offset at the exit for first order chromatic effect of quadrupoles at  $R_{56} = -0.25$  m

**Fig. 1.13 Different plots, showing the behaviour of a chicane optics**

To ensure the achromatic condition of the optics, the required integrated strength of the second quadrupole magnet Q2 can also be obtained and is given by

$$K_2 = \frac{2\theta_{q1}}{\Delta x_{q2}}(1 + \delta) \quad [1.64]$$

Here  $\theta_{q1}$  is the kick by the first quadrupole magnet and  $\Delta x_{q2}$  is the deviation of the off-momentum trajectory from the design trajectory at the location of second quadrupole magnet. These parameters are given by the following expressions

$$\begin{aligned} \theta_{q1} &= K_1 \frac{\Delta x_{q1}}{1 + \delta} \\ &= \frac{K_1}{1 + \delta} \left[ L_{1q} \left( \tan \frac{\theta}{1 + \delta} - \tan \theta \right) \right. \\ &\quad \left. + L_{bm} \left( \tan \frac{\theta}{2(1 + \delta)} - \tan \frac{\theta}{2} \right) \right] \end{aligned} \quad [1.65]$$

$$\begin{aligned} \Delta x_{q2} &= L_{bm} \tan \frac{\theta}{2(1 + \delta)} + L_{1q} \tan \frac{\theta}{1 + \delta} + L_{q2} \tan \frac{\theta + \theta_{q1}}{1 + \delta} \\ &\quad + L_{bm} \tan \left( \frac{\theta/2 + \theta_{q1}}{(1 + \delta)} \right) + L_{2h} \tan \frac{\theta_{q1}}{1 + \delta} - L_{12} \tan \theta \\ &\quad - 2L_{bm} \tan \frac{\theta}{2} \end{aligned} \quad [1.66]$$

A quadrupole magnet kick depends on the momentum offset i.e. a quadrupole magnet generates chromatic effect, which leads to a non-zero second order dispersion. Considering this chromatic effect of quadrupole magnets, the path length obtained for a particular value of  $K_1$  also depends on the chosen momentum offset. This variation in path length deviation from the design path length with momentum offset is plotted for the optics (after last dipole magnet) under consideration in Fig. 1.13D. For obtaining this curve, the displacement of electrons from the design trajectory for different momentum offset is obtained at the entrance

of second dipole magnet under the first order chromatic effect of quadrupole magnet. Initially, all these electrons were launched on the design trajectory. The parameter  $\Delta x'_{bm2}/\delta$  is quantified as the derivative of the dispersion and path length is computed considering the derivative of the dispersion for each electron. The final lateral displacement of an off-momentum trajectory should vanish for an achromatic condition. However, above mentioned chromatic effect of all the quadrupole magnets (two magnets of Q1 type and one magnet of Q2 type) makes the lateral displacement non zero and it becomes a function of the momentum offset i.e. optics is only first order achromatic. The variation in lateral displacement with momentum offset is depicted in Fig. 1.13E. In drifts and dipole magnets, second order dispersion approximately follows the first order dispersion with opposite sign, however quadrupole magnet brings an extra term in second order dispersion due to above chromatic effect [7]. Due to different focusing for first and second order dispersion, optics remains only first order achromatic. In order to tune the optics for large positive  $R_{56}$ , required strength of quadrupole magnets also becomes higher (for  $R_{56} = -0.25$  m and  $+0.25$  m, it is  $0.36 \text{ m}^{-1}$  and  $2.94 \text{ m}^{-1}$  respectively). The stronger quadrupole magnets produce larger chromatic effects in optics, making second order achromatic condition worse in the case of positive  $R_{56}$ . The ratio of  $T_{566}$  to  $R_{56}$  in this optics also depends on the quadrupole strength.

## ***2. Dog-leg optics***

This optics uses two dipole magnets with opposite bending angles and is the simplest optics for providing a lateral displacement ( $X$ ) in the beam with a particular value of  $R_{56}$ . Fig. 1.14 shows this type of optics.

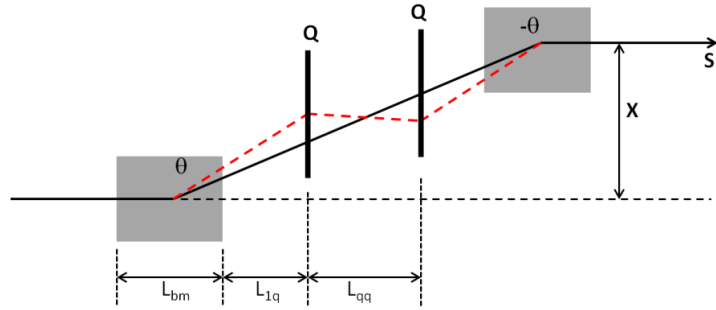


**Fig. 1.14 Layout of a dog-leg optics**

Inclusion of quadrupole magnets are essential to make the optics achromatic for a dog-leg beam transport system, made by rectangular dipole magnets. The one complete wave of dispersion ( $2\pi$  phase advance) is needed to form the achromat due to opposite nature of bending magnets and hence, requires at least two quadrupole magnets. Both the dipole magnets provide same sign of  $R_{56}$  and in a symmetric optics, the value is also same. The  $R_{56}$  up to second order of bending angle is given by

$$R_{56} \approx \frac{L_{bm}}{3} \theta^2 \quad [1.67]$$

The advantage of this optics is its simplicity, less number of magnetic elements and its compactness. A discussion on dog-leg optics can be found in Ref [31] with correction of second order longitudinal dispersion. If two dog-leg optics are joined in succession with a quadrupole doublet in between and considering complete optics as a single achromat, tuning in  $R_{56}$  can be obtained similar to that of chicane with quadrupole magnets. The quadrupole doublet in between these two dog-leg optics will assure achromatic condition. Such possible variation in this optics is shown in Fig. 1.15.

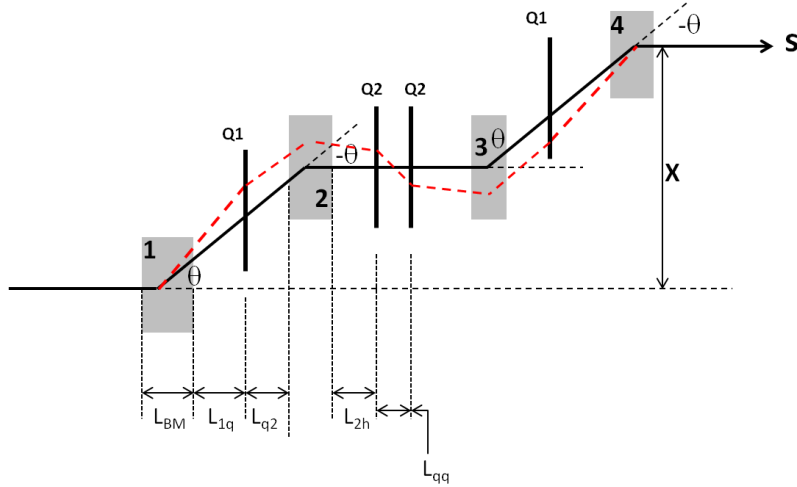
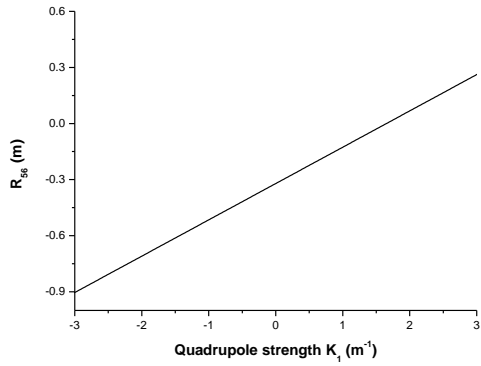
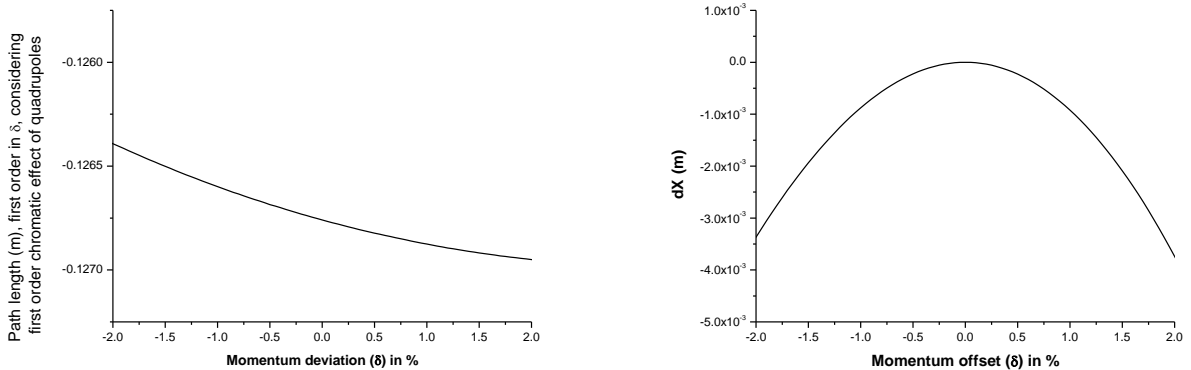


**Fig. 1.15 Two dog-leg optics in succession with a quadrupole doublet in between**

Here quadrupole magnet Q1 is used to tune the value of  $R_{56}$ . Again this optics can be tuned for positive to negative  $R_{56}$ . Tuning in  $R_{56}$  with quadrupole strength  $K_1$  (integrated strength of quadrupole Q1) is shown in Fig. 1.16A. Here the parameters (dipole magnets and distances) are chosen the same as in the example of the chicane optics. Similar to the chicane, in this optics, quadrupole magnets bring chromatic effects. The change in path length deviation with momentum offset due to chromatic effect is depicted in Fig. 1.16B and Fig. 1.16C shows a deviation in the orbit from the design orbit as a function of momentum offset at the exit of this optics. Due to strong quadrupole  $K_2$  (integrated strength of quadrupole Q2) to make the achromat and absence of leaver arm made by opposing dipole magnets, the chromatic effects are more prominent in this optics than the chicane.



(A) Tuning of  $R_{56}$  with quadrupole strength  $K_1$



(B) Path length with momentum offset for  $R_{56} = -0.25$  m

(C) Displacement at the exit from design trajectory with momentum offset for first order chromatic effect of quadrupoles at  $R_{56} = -0.25$  m

**Fig. 1.16 Different plots, showing behaviour of an arc formed by two dog-leg optics**

### 3. Wiggler based optics

This is another optics for bunch compressors, in which orbit wiggles around design trajectory and final beam at the exit is on the same trajectory as of incoming beam i.e. without lateral displacement [28]. This optics is generally employed when large  $R_{56}$  is required. The wiggler based optics is shown schematically in Fig. 1.17.

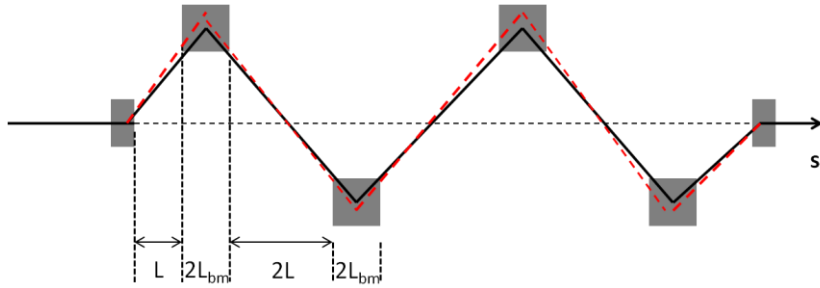


**Fig. 1.17 Wiggler based optics for bunch length manipulation**

In this optics, if there are  $N$  periods (each period consists of two dipole magnets), the  $R_{56}$  is given by [28]

$$R_{56} \approx 4N\theta^2 \left( L + \frac{L_{BM}}{2} \right) - (2N + 1)\theta^2 \frac{L_{BM}}{3} \quad [1.68]$$

Here each dipole magnet in the wiggler has a length of  $2L_{bm}$  with a bending angle of  $2\theta$ , separated from each other by a distance of  $2L$ . This optics is an achromatic optics.

#### 4. S-arc

In this optics, for making a symmetric optics, four dipole magnets are used and TL-2 tuning arc is a variant of this type of optics. Here, first two dipole magnets bend the beam in positive direction and last two dipole magnets bend the beam in negative direction. This type of optics is discussed in Section 3.2.3, where optics for tuning arc of TL-2 is also presented.

## CHAPTER 2

### CTF AND CLIC AT CERN

In this thesis, the focus is the study of optics design for Transfer Line-2 (TL-2) bunch compressor of CTF3 (CLIC Test Facility) at CERN. It is appropriate to discuss briefly about the CTF and the CLIC before presenting the work on Transfer Line-2. CLIC is an upcoming Lepton collider at CERN. Presently, at CERN, LHC is operational, which is a Hadron collider. Hadrons have composite structure of quarks, hence hadron collision is a complex phenomenon. Therefore, LHC is known as discovery machine. Leptons are fundamental particles and do not have composite structure. So in future, to quantify precisely the parameters of physics, lepton colliders are needed. To reach a very high energy for electrons in a circular accelerator is practically unfeasible due to a huge loss of energy in form of synchrotron radiation on the bending of electrons on a curved path. Synchrotron radiation loss for a given bending radius increases with beam energy in fourth order [32]. Therefore as the energy is increased, the loss increases many folds. Due to this reason, future lepton colliders are planned to be based on linear accelerators, such as TESLA, CLIC and ILC, in which synchrotron radiation loss is insignificant. In linear accelerators, reaching higher energy means increase in accelerator length. To make length shorter, one needs a very high frequency, high gradient field in cavities (RF structures). CLIC will be a collider with a 3 TeV centre of mass energy [33]. CLIC is adopting the path of normal conducting RF structures, working at very high frequency (12 GHz) with very high gradient (100 MV/m) to make the accelerator length shorter. To generate, such a high frequency, high gradient field, the concept of drive beam is used [34]. In this method, a very high current beam is passed through an RF structure to generating EM field (and thus power) in this structure. The

generated power is transferred to the main accelerating structure, in which by utilizing this field, low current main colliding beam is accelerated to a high energy. This is known as two-beam acceleration scheme. In following section, we outline briefly about CLIC and in next section an introduction to CTF is presented.

## **2.1 CLIC (Compact LInear Collider)**

The future project of CERN, namely CLIC, will be an electron-positron linear collider with a centre of mass energy 3 TeV. The CLIC study of two beam acceleration begun in 1996 [35]. The original idea of two beam acceleration was proposed by A. Sessler. Later, this idea for CLIC was proposed by W. Schnell using superconducting cavities and single bunch operation. Going further to enhance the luminosity, multi bunch operation was proposed and thus instead of superconducting cavities, normal conducting cavities were proposed. This approach seems feasible and also cost effective.

The scheme proposed can be summarized as follows:

1. Using a 973 MHz RF system, accelerate high current electron drive beam, in which bunches are separated by 64 cm (bunch repetition frequency is half of the RF Frequency). A pulse of 130 ns, consists of bunches separated by 64 cm can be accelerated using the available linac technology.
2. The goal in this acceleration is to utilize the linac RF power with very high efficiency ( $> 95\%$ ), employing a travelling wave structure and the operation with full beam loading must be achieved [36].
3. Then bunch spacing is reduced in steps, first spacing reduced by two fold in a Delay Loop (DL) and then it is reduced by four fold in first Combiner Ring (CR) and again four

fold in next Combiner Ring, making final bunch separation of 2 cm. This separation corresponds to a frequency of 30 GHz. This process is known as 'frequency multiplication' [37].

4. Length of the individual bunch is also compressed in bunch compressors to increase the peak intensity and to obtain a better bunch form factor for generating RF power. Ideally a delta pulse have bunch form factor of 1 and increasing the bunch length reduces bunch form factor continuously [38]. Fig. 2.1 shows the RF power generation efficiency with RMS bunch length. This generated RF power can be transferred to the main linac of collider.

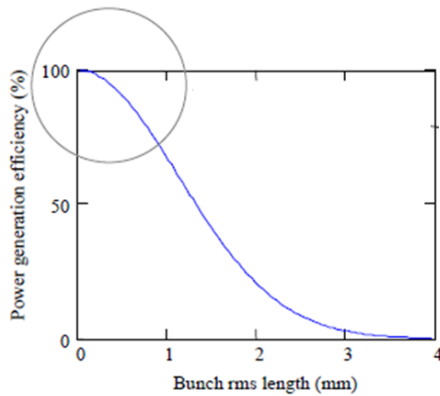


**Fig. 2.1 RF power generation efficiency with RMS bunch length (taken from Ref [39])**

In nutshell the input RF power at 973 MHz is converted into RF power at 30 GHz which is used for beam acceleration. In the process of frequency multiplication, the pulse train separation becomes  $\sim 4.2 \mu\text{s}$  (i.e.  $130 \text{ ns} \times 2 \times 4 \times 4$ ). Fig. 2.2 shows a schematic of the CLIC. Later on after some test on 30 GHz components, a decision was taken to change the frequency to 12 GHz. Now CTF3 studies are focused on 12 GHz RF power production.

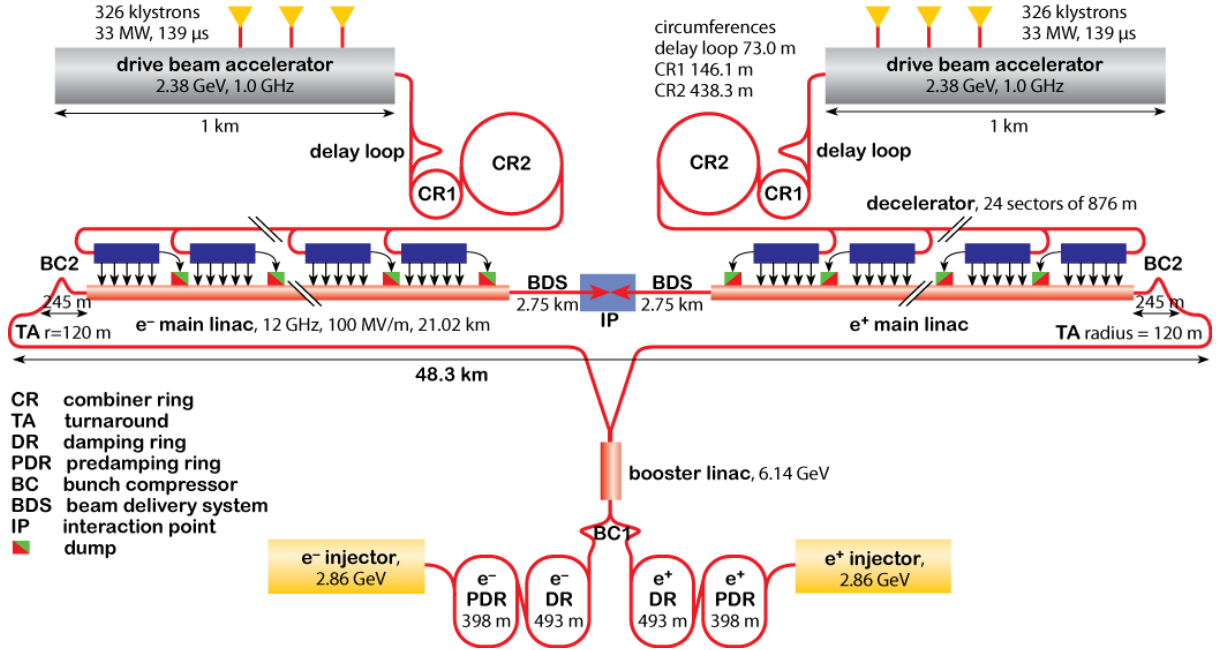


*Fig. 2.2 Schematic layout of CLIC*

## 2.2 Brief introduction to CTF (CLIC Test Facility)

The CTF was conceptualized to demonstrate the idea of two beam acceleration. Here, a high charge electron beam is to be generated and after that frequency multiplication and bunch compression has to be achieved. This beam will pass through PETS (Power Exchange Transfer System) and will generate the desired RF power. This facility will also be used for testing the RF components of CLIC. This test facility has three different phases of development i.e. CTF1, CTF2 and CTF3. In following sections, we briefly outline different phases of CTF with an emphasize on 3<sup>rd</sup> phase i.e. CTF3.

### 2.2.1 CTF1

The construction of CTF1 launched in 1988 [39, 40]. The main aim of this phase was to develop an RF photocathode gun to produce a very high charge for generating 30 GHz RF power and to test the beam position monitors. In a single bunch, 35 nC charge is produced

and in a train of 48 bunches total charge of 450 nC is generated. At the beam energy of 92 MeV, 76 MW RF power was generated by de-accelerating the beam in the PETS [41].

### **2.2.2 CTF2**

In CTF2, with generated RF power, a low charge probe beam was accelerated i.e. CTF2 achieved two beam acceleration, but without frequency multiplication. A pre-accelerated probe beam of 45 MeV was accelerated to 55 MeV in two RF structures. Drive beam generated a very high gradient of 290 MV/m in structures. All the results of measurements agreed remarkably with the expected values.

### **2.2.3 CTF3**

CTF3 is a complete test facility based on the concept of two beam acceleration, including frequency multiplication and bunch compression. Therefore, CTF3 can be considered as a small scale CLIC. CTF3 has been completed through an international collaboration. This thesis has a central theme of TL-2 optics design, which was carried out under DAE-CERN collaboration (Indian collaboration with CERN).

The schematic layout of CTF3 is given in Fig. 2.3. A drive electron beam is first generated and accelerated to a maximum energy of 300 MeV (nominal energy of 120 MeV) in a 70 m long linac. For reducing the cost of project, the acceleration is done in a 3 GHz linear accelerator rather than in 973 MHz accelerator as the various components of 3 GHz RF were available.

A train of 187.5 ns length is filled with even buckets of the linac and next adjacent train has bunches in odd bucket of linac [37]. Thus two successive bunches in a train is separated by 1.5 GHz (i.e. 666.67 ps). All the bunches of one train passes through a 42 m long Delay Loop and next train bypasses the Delay Loop. Thus two trains each of 187.5 ns are interleaved and

total length remains 187.5 ns (with an extra bunch separated with 3 GHz, so more accurate bunch length is 187.8 ns) with a bunch separation of 3 GHz. Thus a frequency multiplication of 2 occurs. Now such four trains are combined in a 84 m long Combiner Ring through injection using RF deflectors. Thus after the Combiner Ring, the frequency is multiplied by 4. So total frequency is multiplied by 8 and thus bunch separation becomes 83.3 ps, which corresponds to a frequency of 12 GHz. Thus in CTF3, only two stage frequency multiplication is achieved while in CLIC three stage multiplication is planned. Initial pulse current of 3.7 A increases to 30 A through this process. In a train of 187.5 ns, there are ~281 bunches and after interleaving total bunches in a train becomes 2250. Each of these bunches have a bunch length of ~8.3 ps (accelerated by 3 GHz structure). After compressing this bunch length to ~1.5 ps in TL-2 transfer line, this beam generates a gradient of ~100 MV/m at 12 GHz in PETS structures. Main parameters of the drive beam in CTF3 and CLIC are given in Table 2.1.

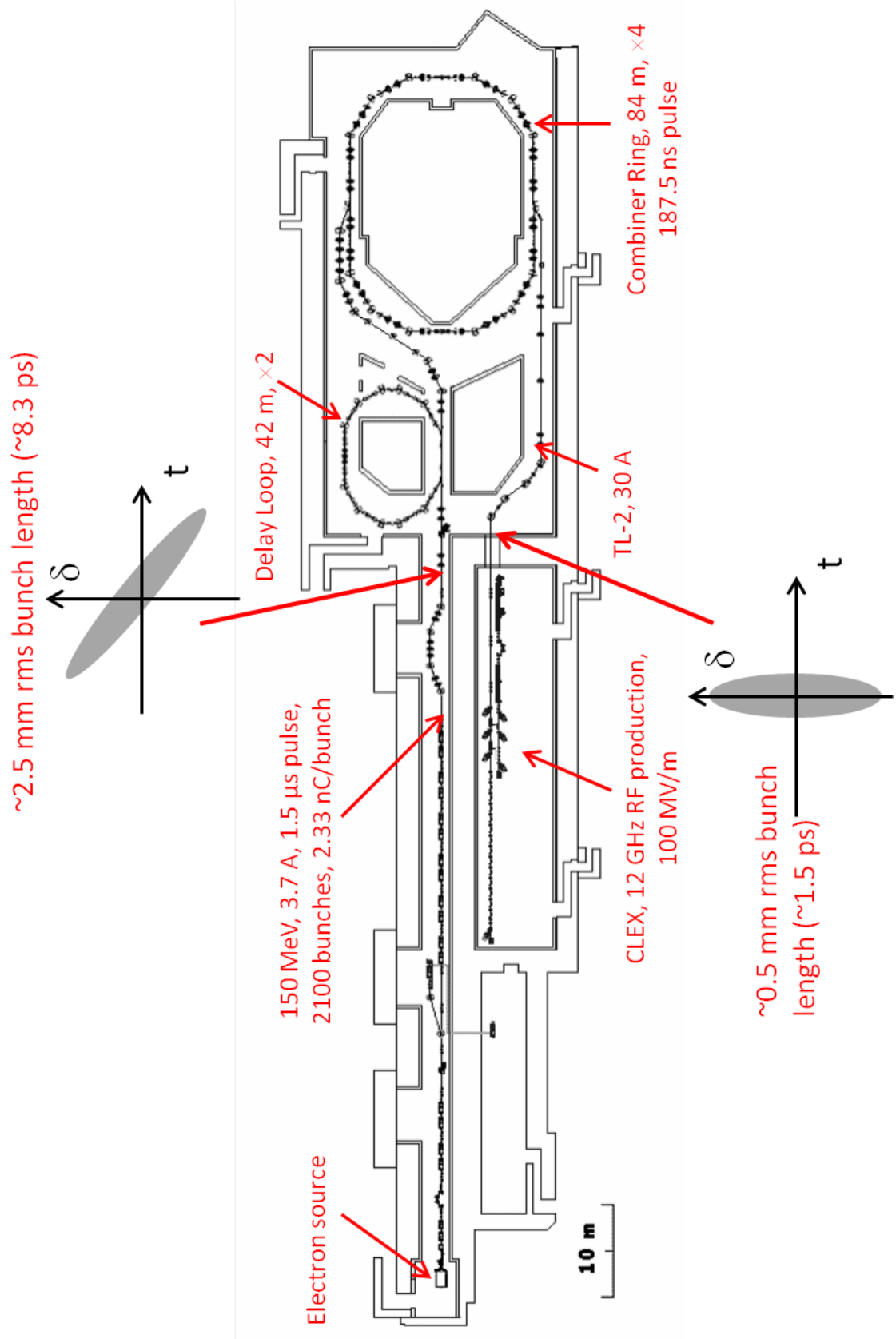


Fig. 2.3 Schematic layout of CTF3

**Table 2.1: Main parameters of drive beam in CTF3 and CLIC**

Parameter	CTF3 [42]	CLIC [33]
Drive beam energy	300 MeV maximum, nominal 150 MeV	2.371 GeV
Pulse length from Linac	1.5 $\mu$ s	140 $\mu$ s
Pulse current	3.7 A	4.2 A
Bunch separation	666.67 ps	2 ns
Charge per bunch	2.33 nC	8.4 nC
Delay Loop multiplication	$\times 2$	$\times 2$
Combiner Ring-1 multiplication	$\times 4$	$\times 4$
Combiner Ring-2 multiplication	No	$\times 3$
Pulse length after multiplication	187.5 ns	240 ns
Pulse current after multiplication	30 A	101 A
Bunch separation after multiplication	83.3 ps	83.3 ps
Repetition rate	5 Hz	50 Hz
Main RF frequency generated	12 GHz	12 GHz

## CHAPTER 3

### LINEAR OPTICS FOR TRANSFER LINE-2 BUNCH COMPRESSOR

In Transfer Line-2 (TL-2), a drive electron beam with a maximum energy of 300 MeV is transferred from the extraction point of the Combiner Ring (CR) to CLEX area (Fig. 2.3). This transfer line constitutes the last stage, where bunch length can be manipulated. After this transfer line, the beam is delivered to the experimental area via a very short optical section of quadrupole magnets, known as TL-2'. In this experimental area, the electron beam generates RF power of the required high frequency and a high gradient. In CTF3, being a test facility, there is a requirement to control the bunch length over a wide range and also there may be a change in parameters of upstream linac and therefore, this line must be able to compress the bunch length with different chirping, provided by the upstream RF system of linac, i.e. for a wide range of initial parameters, the line should be able to control the bunch length. So most important requirement of the optics design of this line is the possible tuning for a wide range of  $R_{56}$  parameter. The bunch length from the Combiner Ring is 8.3 ps and it should be compressed to lower than 1.5 ps. The required  $R_{56}$  tuning range is -0.30 m to +0.30 m.

CTF3 is installed in already available building of LEP pre-injector and thus geometry of TL-2 is constrained by the building layout. Some of the magnets were also available at CERN and this poses a second constraint of using the available magnets for designing this line. Optics design for a wide range of  $R_{56}$  under these constraints is a challenge. Table 3.1 and Table 3.2 show the important parameters to be achieved by design and parameters of the already available magnets, respectively.

In this chapter, the design philosophy of the line, basic geometry and linear optics studies are presented. The subsequent chapter describes the sextupole scheme for this line and nonlinear studies.

The pre-existing building of LEP injector and CLEX area have different floor height and therefore there is a requirement to send the beam vertically upside also. Thus the functions of this line can be summarized as follows [43]:

1. Tuning of  $R_{56}$  in a wide range i.e. from -0.30 m to +0.30 m.
  2. Matching of Twiss parameters at the entry point of TL-2' in CLEX area.
  3. Sending the beam vertically upside due to floor height mismatch between two building floors.
  4. In the entire range of  $R_{56}$  tuning, second order aberration  $T_{566}$  has to be corrected.
  5. Transverse emittance growth should be less than 10% due to this  $T_{566}$  correction.
  6. Accommodating the line within the building and using the available magnets.
- For easy handling of  $R_{56}$  tuning, an achromatic arc for tuning the  $R_{56}$  seems a better choice. For avoiding coupling, vertical dispersion should be zero except the point where the beam has to be shifted vertically up. In this section, horizontal dispersion must be zero. After the tuning arc, there must be a provision of required matching of Twiss parameters at the exit. In this chapter the linear optical design of this line is presented.

**Table 3.1: Parameters for the Transfer Line-2 (TL-2) bunch compressor [43]**

	<b>CR extraction</b>	<b>CLEX injection</b>
	Reference point in CR as provided by CERN (center quadrupole Q540)	Reference point half way in wall separating CR and CLEX buildings
Maximum beam energy	300 MeV	300 MeV
Nominal beam energy	150 MeV	150 MeV
Nominal bunch charge	2.33 nC	2.33 nC
Bunch spacing	83.4 ps	83.4 ps
Train duration	140 ns	140 ns
$\beta_H$	4.23 m	<20 m in entire separation wall
$\alpha_H$	2.76	not specified
$\varepsilon_H$ (normalised, $1\sigma$ )	$100 \pi$ mm mrad	<110 $\pi$ mm mrad
$\beta_V$	7.79 m	<20 m in entire separation wall
$\alpha_V$	-2.47	not specified
$\varepsilon_V$ (normalised, $1\sigma$ )	$100 \pi$ mm mrad	<110 $\pi$ mm mrad
$D$	0 m	0 m
$D'$	0	0
$\Delta P/P$ ( $1\sigma$ )	1%	1%
Height of beam-line above ground	1.35 m	0.85 m

In section 3.1 a geometrical layout of the line is described and in next section, beam optical design is presented. In section 3.3, alternative optical solutions of some selected  $R_{56}$  are presented, in which the horizontal dispersion is kept at very lower magnitude. This mode of optics is suitable from commissioning point of view, but due to a low dispersion, second order aberration  $T_{566}$  cannot be corrected with the available strength of sextupole magnets.

*Table 3.2: Parameters of the available magnets [43]*

Magnet	Type	Strength/ Bending angle	Effective Length (mm)	Mechanical Length (with coils) (mm)	Mechanical width (mm)	Aperture (full) (mm)
<b>Dipole</b>	Short	6°-17.5°	268	520	794	100×45
	Long	12°-35°	518	770	794	100×45
	Sector	6°	470	597	276	70
<b>Quadrupole</b>	Slim	8.0 T/m	300	384	340	100
	Standard	5.4 T/m	380	592	819	184
	TSL	10.6 T/m	295	430	650	101
	Q3L	11.2 T/m	226	287	282	58
<b>Sextupole</b>	Short	180 T/m <sup>2</sup>	100	160	420	108
	Long	44 T/m <sup>2</sup>	246	350	420	167

### 3.1 Geometrical layout of TL-2

In Fig. 3.1 the building of LEP pre-injector is shown in which TL-2 has to be installed (see Fig. 2.3 also). The extraction septum (point **E** in the figure) of Combiner Ring sends the beam horizontally towards the wall **AB** and the exit point of TL-2 is the point **D** on the wall **BC**.

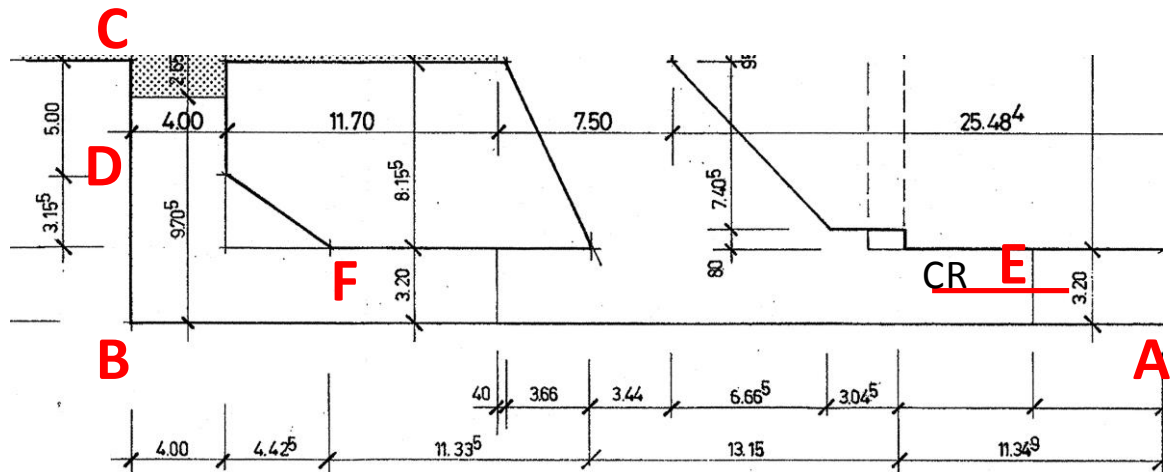


**Fig. 3.1 Layout of the building, where TL-2 is installed (measurements are in m)**

There is a requirement to steer (and transfer parallel to the wall **AB**) the extracted beam from the CR, which is coming towards the wall **AB**. In order to reach the exit point **D**, again there is a requirement to steer that beam in the direction away from the wall **AB** after (or near) the point **F**. Thus this line design can be broken in three modules. The first module is from the extraction point to the point where line becomes parallel to wall **AB**. This is a small horizontal achromat. The second module is from point **E** to **F**, where line runs parallel to wall and third module again bends the beam trajectory and sends the beam to the exit point **D**.

Now we present the design details of each optical module of this line in the following section.

### 3.2 Modules and optics of TL-2

#### 3.2.1 Module-1

Module-1 of the line begins from the extraction septum of CR and this module is upto the first dipole magnet of TL-2. Extraction septum (two in number) and dipole magnet bend the beam horizontally in opposite direction with an angle of  $\pm 11^\circ$ . This module is achromatic. Due to opposite nature of bending, in order to make an achromat there is a necessity of a full

wave of dispersion and therefore there is a requirement of minimum two focusing quadrupole magnets to match the dispersion and its derivative. This achromat has a dog-leg optics, discussed in Section 1.8.2. For controlling the vertical motion of electrons, one more quadrupole magnet, focusing in vertical plane is needed. Therefore a quadrupole triplet, consisting of two focusing and one defocusing quadrupoles, is used to form an achromat. The schematic layout (not to scale) of this module is shown in Fig. 3.2.

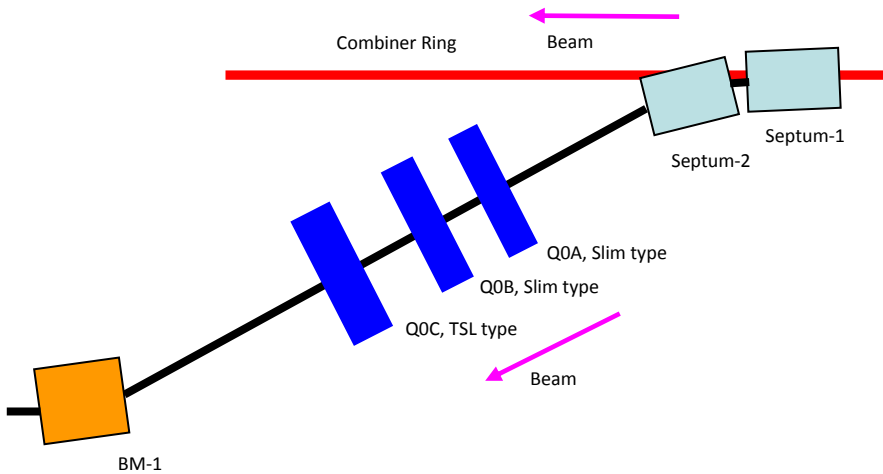


**Fig. 3.2 Schematic layout of Module-1**

There is a requirement to keep a minimum distance between Septum-2 and first quadrupole magnet (Q0A), so that there is no any mechanical interference of this magnet from the Combiner Ring components as well as there is a sufficient space to install this magnet. In a similar fashion, the last quadrupole magnet cannot be moved nearer to first dipole magnet. The third quadrupole magnet between these two quadrupole magnets, is placed at a optimum distance, so that for matching the Twiss parameters, the required strength do not reach a very high magnitude. By considering the geometry, two slim type quadrupole magnets (Table 3.2) are used in this modules. The strength of first two quadrupole magnets to form the achromat for a fixed maximum strength of TSL type quadrupole magnet varies with the distance of the second quadrupole magnet from the Septum-2 magnet as shown in Fig. 3.3.

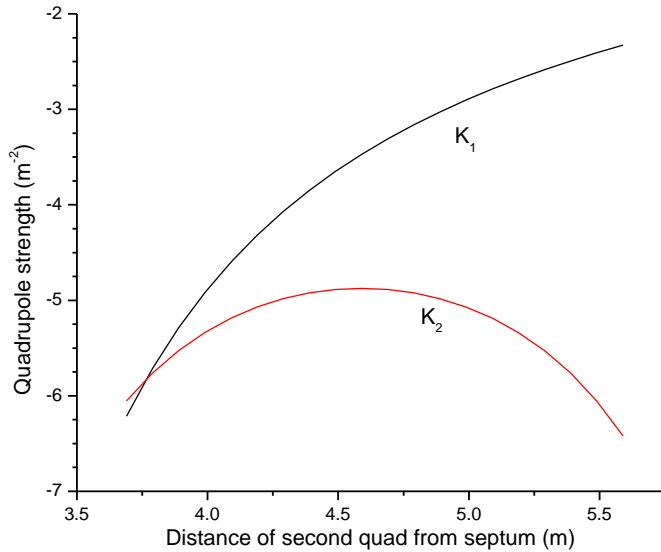


**Fig. 3.3 Combination of first two quadrupole strengths (magnitude) for making the module as an achromat for a fixed strength of third quadrupole magnet**

### 3.2.2 Module-2

Module-2 is from the end edge of the first horizontal dipole magnet (end of Module-1) to the beginning of the second horizontal dipole magnet. It is horizontally a straight module i.e. no horizontal dipole magnet is there. Fig. 3.4 shows a schematic diagram (not to scale) of this module. Module-2 of the line is designed by keeping various points in view. As stated earlier that the floor of CLEX area is higher than the LPI building, this module consists of a vertical achromatic dog-leg, formed by two sector type dipole magnets, each of  $6^\circ$  bending angle. To match the vertical dispersion, this achromat has a quadrupole triplet. In LPI building, there is an emergency exit. As per safety requirement, there should not be any magnetic element in front of this emergency exit. There is also a requirement of nearly 4 m clear space in line to place a tail clipper. Therefore, in this line a clear space of nearly 6 m is available in the design to serve both of these purposes. This module also serves as a matching optics between Module-1 and Module-2.

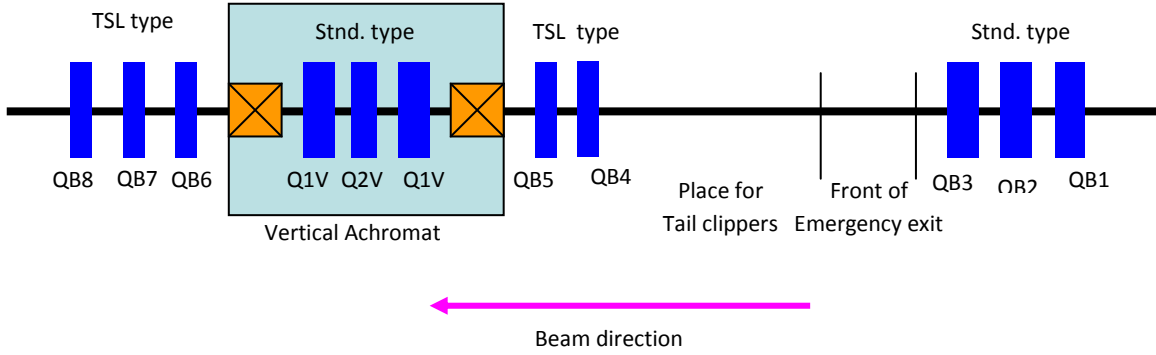


**Fig. 3.4 Schematic layout of Module-2**

In this module, at the beginning there is a quadrupole triplet, which controls the beta function at the location of tail clipper. The two defocusing quadrupole magnets out of the quadrupole triplet in vertical achromat are used to match dispersion and its derivative. A quadrupole doublet just before the vertical achromat is used to control the beta functions inside the vertical achromat as well as for providing Twiss parameters in a suitable range, so that the last quadrupole triplet can match the Twiss parameters within the available magnetic strengths at the entrance of Module-3. In this module, horizontal dispersion is zero and thus quadrupole magnets can be tuned to match Twiss parameters, without disturbing the  $R_{56}$  parameter.

### 3.2.3 Module-3

This module consists of an achromatic arc with a provision to tune the  $R_{56}$  in a wide range. An achromatic optics with a lateral displacement and possible tuning of  $R_{56}$  is discussed in Section 1.8 by joining two dog-leg optics in succession and by an S-arc. In making the arc of Module-3, there are four dipole magnets of two different types and the plan of LPI building is the main driving factor to decide the arrangement of the magnets. For making an achromatic optics with a variable  $R_{56}$ , an S-arc is formed for this module. Following sub-section contains a general description of the S-arc followed by the design of such an arc for Module-3.

## 1. S-Arc

A possible optics (considering only bending plane) of an achromatic S-arc is shown in Fig. 3.5 (dotted line shows a trajectory of a higher momentum electron). Here two different types of dipole magnets are used (keeping the direction of beam propagation the same as in the previous layouts related to TL-2 optics in this chapter, here the beam direction is also kept from right to left). The third and fourth dipole magnets bend the beam in the direction opposite to first and second dipole magnet. First and last dipole magnets have same bending angle while second and third dipole magnet have same bending angle and arc is thus mirror symmetric.

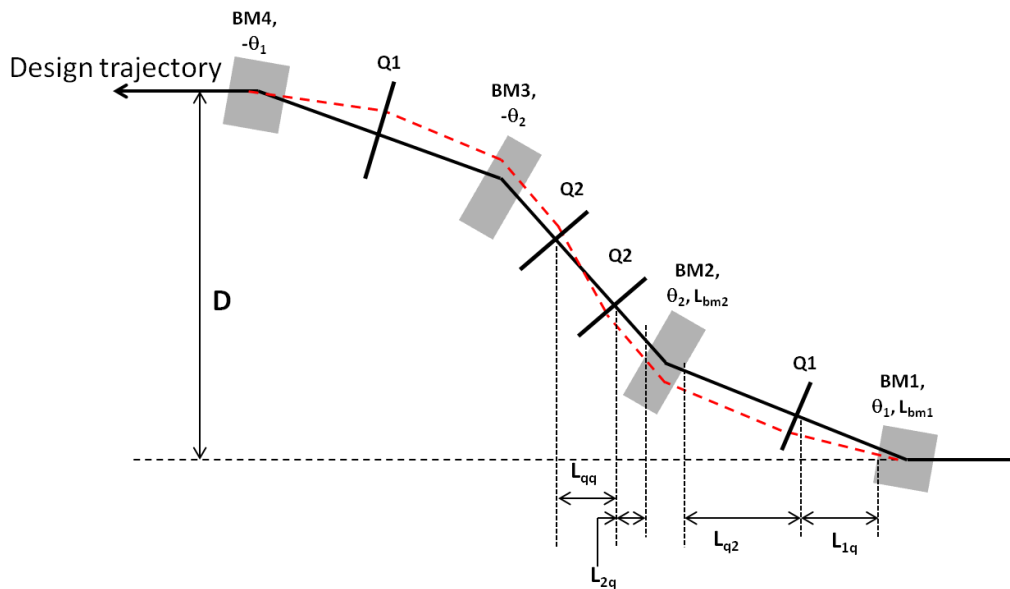


**Fig. 3.5 Layout of an achromatic S-arc with possibility to tune the  $R_{56}$**

In this optics, quadrupole magnet Q1 changes the dispersion and its derivative at the entrance of the second dipole magnet and therefore  $R_{56}$  contribution for this magnet changes and tuning becomes possible. Quadrupole doublet Q2 ensures the achromatic condition. Inclusion of one more quadrupole magnet in first and last straight section enables a control on both, dispersion and its derivative at the entrance to second dipole magnet. It is shown in Fig. 3.6.

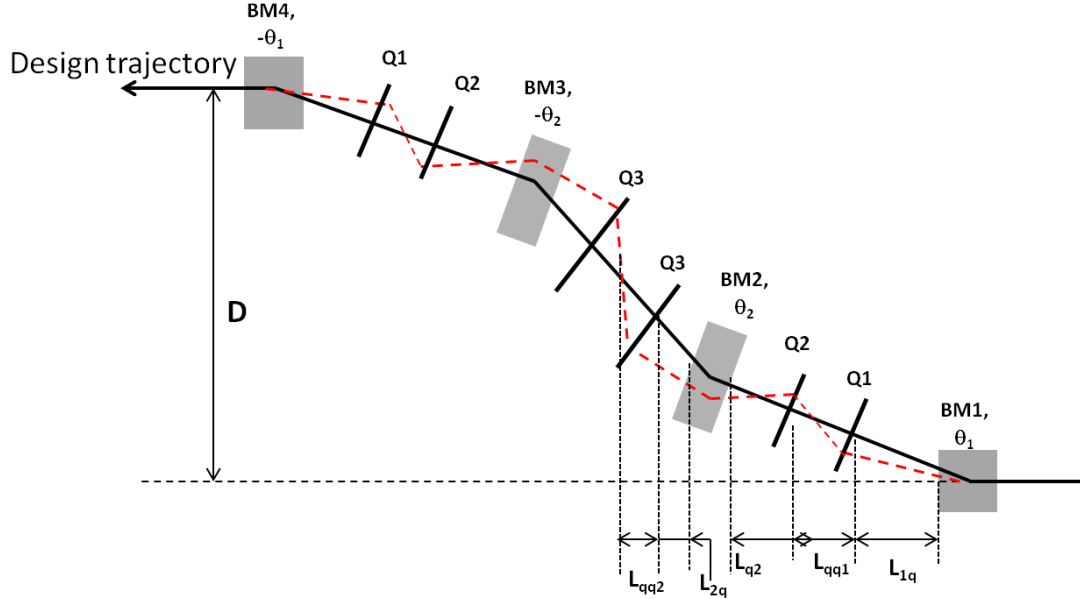


**Fig. 3.6 Layout of an achromatic S-arc with possibility to achieve a value of  $R_{56}$  with different combination of strength of  $Q1$  and  $Q2$  quadrupole magnets**

Using simple geometry and thin lens approximation, as done in Section 1.8, approximate value of  $R_{56}$  for this optics can be obtained and is given below

$$R_{56} = P_0 - \sum_{i=1}^3 K_i P_i - \sum_{i,j=1; i \neq j}^3 K_i K_j P_{ij} \quad [3.1]$$

Here  $P_0$ ,  $P_i$  and  $P_{ij}$  are fixed coefficients for a given optics. A complete derivation of above expression is provided in Appendix B. Here  $R_{56}$  is a function of strength of the quadrupole magnets  $Q1$ ,  $Q2$  and  $Q3$ . Magnet  $Q3$  is used to make the arc as an achromat. Same value of  $R_{56}$  can be obtained using different sets of  $K_1$  and  $K_2$  and thus it adds another degree of freedom for controlling the lattice parameters. Using this degree of freedom, a suitable optics can be tuned for obtaining a given  $R_{56}$ , in which required betatron functions are also not very high. Sets of different  $K_1$  and  $K_2$ , producing same  $R_{56}$  are plotted in Fig. 3.7A (i.e. contours of

$R_{56}$ ). Tuning of  $R_{56}$  with quadrupole strength  $K_1$  and  $K_2$  is shown in Fig. 3.7B. The parameters of this example optics are provided in Table 3.3.

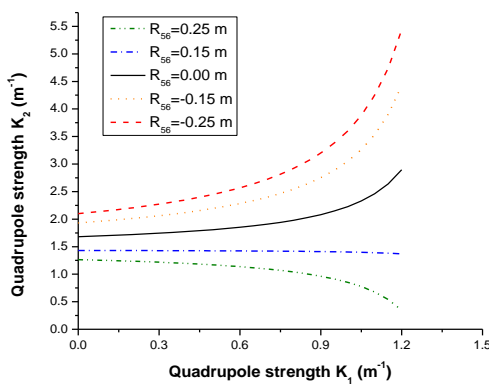
**Table 3.3: Parameters of the example optics for S-arc**

First and last dipole magnet	Length 0.90 m, angle 30.75°
Second and third dipole magnet	Length 0.85 m, angle 17.25°
First dipole magnet exit to first quadrupole magnet ( $L_{1q}$ )	0.70 m
Distance between quadrupoles of first doublets ( $L_{qq1}$ )	0.50 m
From second quadrupole to second dipole magnet entrance ( $L_{q2}$ )	0.70 m
Second dipole magnet to third quadrupole magnet ( $L_{2q}$ )	0.80 m
Distance between quadrupoles of second doublet ( $L_{qq2}$ )	0.50 m

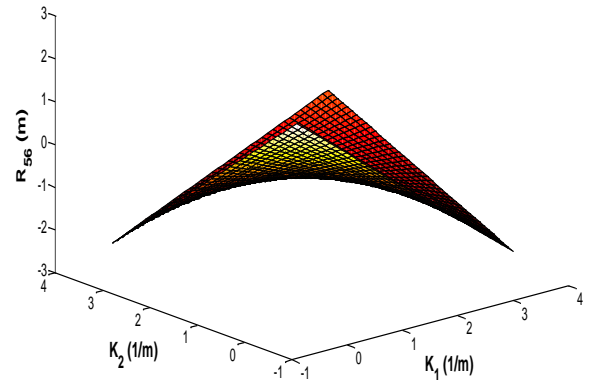
\* The distances are kept close to TL-2 (although in TL-2, instead of doublet, there is triplet) and dipole magnets are also same as of TL-2

In Fig. 3.7C and Fig. 3.7D, the dispersion distribution for  $R_{56} = -0.25$  m and  $+0.25$  m (for some selected  $K_1$  and  $K_2$ ) are shown. The selected set of  $K_1$  and  $K_2$  for producing the required  $R_{56}$  is chosen by keeping constraints on maximum dispersion and beta function in the optics. For  $R_{56} = -0.25$  m,  $K_1$  and  $K_2$  are  $0.6 \text{ m}^{-1}$  and  $1.6 \text{ m}^{-1}$ , respectively. For  $R_{56} = +0.25$  m, the chosen strength of  $K_1$  and  $K_2$  are  $0.8 \text{ m}^{-1}$  and  $3.0 \text{ m}^{-1}$ , respectively. On these settings of optics, maximum dispersion is below 2 m as well as beta functions in both the planes are also below 20 m. The arc has tuning for positive  $R_{56}$  with low dispersion, while for negative  $R_{56}$ , quadrupole strength is much higher and large dispersion is generated. Fig. 3.7E shows the path length variation with momentum offset due to chromatic effect of quadrupole magnets and Fig. 3.7F shows the effects of this chromatic term on the final lateral displacement in the beam as a function of momentum offset. This figure shows that such an arc has a larger

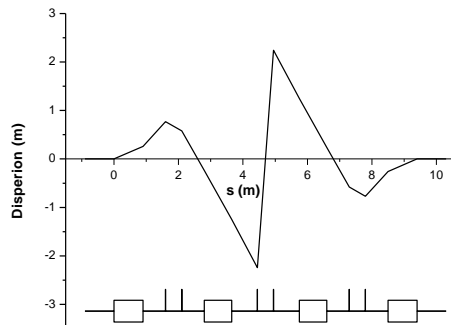
chromatic effect of quadrupole magnets, which generates higher magnitude of nonlinear dispersion.



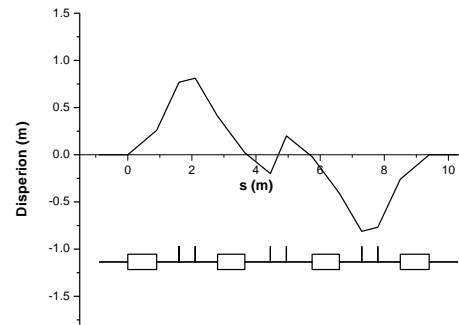
(A) Sets of strength  $K_1$ - $K_2$  for tuning of  $R_{56}$



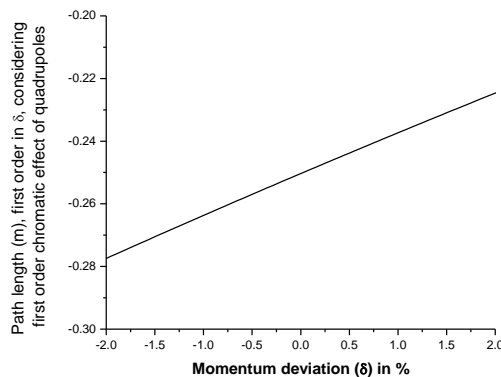
(B) Tuning surface for  $R_{56}$  with  $K_1$  and  $K_2$



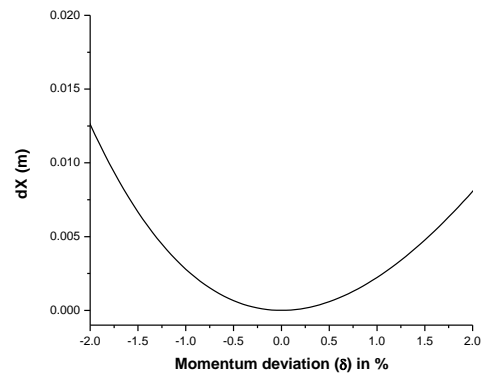
(C) Dispersion curve for  $R_{56} = -0.25$  m



(D) Dispersion curve for  $R_{56} = 0.25$  m



(E) Path length with momentum offset for  $R_{56} = -0.25$  m



(F) Displacement at the exit from design trajectory with momentum offset for first order chromatic effect of quadrupoles at  $R_{56} = -0.25$  m

**Fig 3.7 Different plots, showing the behaviour of an S-arc**

## 2. Optics of S-arc of Module-3

The tuning arc of Module-3 is based on the optics discussed in the above sub-section. In TL-2, second order longitudinal dispersion  $T_{566}$  has to be corrected in entire tuning range of  $R_{56}$ , for which a sufficient magnitude of dispersion is required at the location of  $T_{566}$  correcting sextupole magnets. Therefore, one more control parameter is essential in the optics to achieve a particular value of dispersion at this location, so that with the available strength of sextupole magnets,  $T_{566}$  can be controlled. Keeping this point in view, a defocusing quadrupole is placed between the quadrupole doublet of the first and last section. At middle point of arc, where dispersion is zero, a defocusing quadrupole magnet is added to have a control on vertical betatron function. Due to zero dispersion at this quadrupole magnet, its strength does not affect the setting of  $R_{56}$ . This optics of arc is shown in Fig. 3.8.

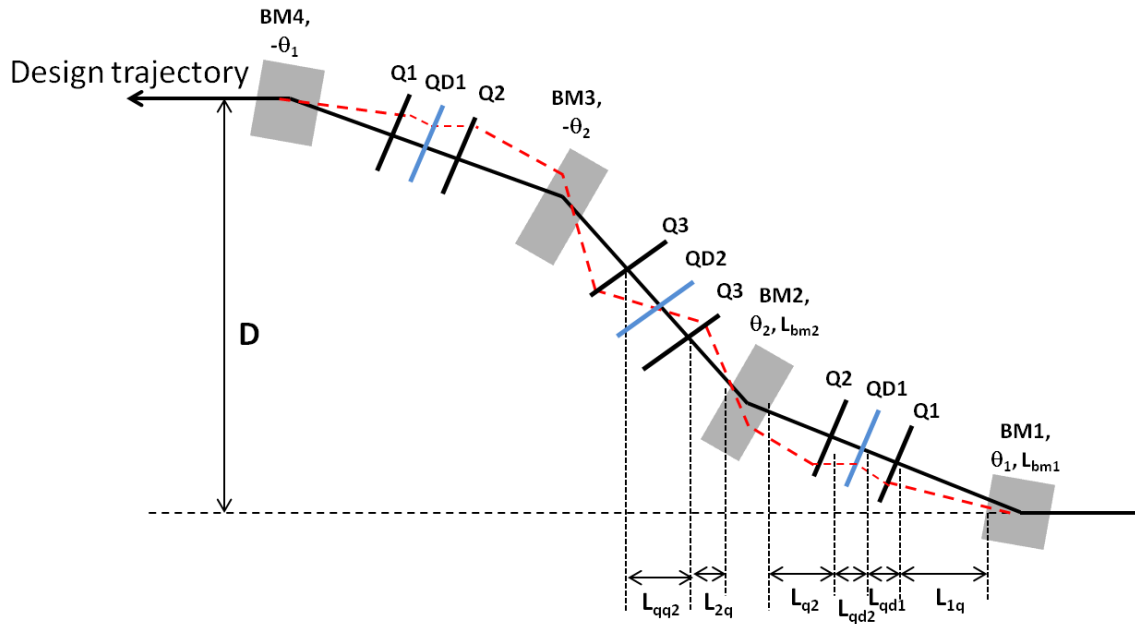


**Fig. 3.8 Layout of the optics of an S-arc, on which tuning  $R_{56}$  arc of Module-3 is based**

In this optics, QD1 increases dispersion and if sextupole magnet is placed just before Q2, a large dispersion can be generated at the sextupole location.

### 3. Design of Module-3

In designing of this part of TL-2, there is a very little scope to vary its geometry and different distances are fixed according to the building plan. After the arc, the distance up to exit wall is very small and therefore, a quadrupole doublet, using "Q3L" type quadrupole (smallest mechanical length among the available quadrupole magnets; Table 3.2) is placed. This doublet is used to match the required beta function at the exit of wall. Two more sextupole magnets are placed in middle arc to suppress the  $T_{566}$ . Locations of sextupole magnets are chosen by considering the correction of  $T_{566}$  in entire range within the available strength. Including all these magnetic elements, the layout of the optics for Module-3 (not to scale) is shown in Fig 3.9.

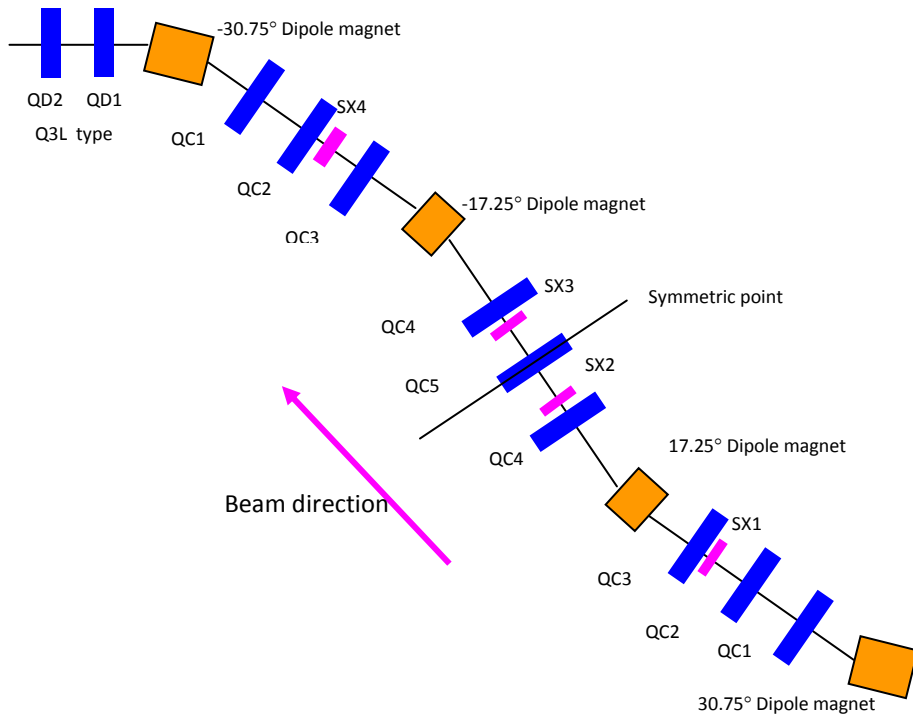


**Fig 3.9 Schematic layout of Module-3 of TL-2**

Dispersion distribution inside this arc is symmetric with respect to quadrupole magnet QC5. This scheme shows that the arc quadrupole magnets are engaged in shaping the dispersion

and these magnets cannot be used to control the Twiss parameters. Therefore the control of Twiss parameters is obtained by matching values of Twiss parameters at the beginning of Module-3 in such a way, that there is no any undesired values of Twiss parameters in the arc as well as the last quadrupole doublet (outside the arc, formed by QD1 and QD2) can ensure the beta function less than 20 m in both the planes in entire separation wall of LPI building and CLEX area. The initial values of Twiss parameters also depend on the correction of  $T_{566}$  by sextupole magnets and will be discussed in next chapter.

### 3.3 Twiss parameters

General purpose accelerator physics code MAD8 [20] is used extensively in design and matching of the line. MAD8 uses either simplex or least square minimization method [44] to match the parameters of optics. These methods require a good initial guess of quadrupole strengths to converge on an optimal solution [45]. Even considering thin lens approximation, the calculations for good initial guess for such a line can be a tedious work for each value of  $R_{56}$ . Thus a computer code in MATLAB is developed for this purpose, which provides initial values using thin lens approximation on the basis of theory outlined in Section 1.8 and Section 3.2, including vertical plane also for obtaining a good initial guess to reach a desired shape of dispersion distribution [46]. These matched values of optics are used to fine tune the optics with MAD8, considering non-zero length of quadrupole magnets.

The optimal lattice parameters on each tuned value of  $R_{56}$  are shown in Fig. 3.10. Parameters in horizontal and vertical plane are shown in black and red colours, respectively. The beta function in the arc is kept below 40 m and dispersion is increased to  $\sim 2$  m to correct the  $T_{566}$  in the entire range of  $R_{56}$ . These values give beam sizes up to  $3\sigma$  well below the aperture of the vacuum chamber.

The chamber aperture is not same throughout the line and is different in different modules.

Table 3.4 given below gives dimensions for aperture of vacuum chamber of this line.

**Table 3.4: Vacuum chamber aperture of the line [43]**

Module	Type of chamber	Aperture full (mm)
Module-1	Racetrack	90×40
Module-2	Round	40
Module-3	Racetrack	90×40

The RMS beam sizes up to  $n\sigma$  in a line is given by  $\sqrt{n^2\epsilon\beta + (D\delta)^2}$ ; where  $\epsilon = \frac{\epsilon_{normalized}}{\gamma\beta}$

[15-17]. In the expression of emittance,  $\gamma$  and  $\beta$  are the relativistic parameters. By taking normalized emittance  $100\pi$  mm-mrad for  $1\sigma$ , the beam sizes in the dispersion free region up to  $3\sigma$  (at 150 MeV, considering beta function 40 m) will be 10.95 mm and with 1% momentum offset, the RMS beam size with almost 2.5 m dispersion function (in horizontal plane in Module-3) will be 25.06 mm. Fig. 3.11 shows the beam size for 1% momentum offset at  $R_{56} = -0.30$  m, 0.00 m and  $+0.30$  m. The maximum beam sizes are  $\sim 18$  mm and  $\sim 10$  mm in horizontal and vertical planes, respectively. In horizontal plane, this maximum beam size reaches in Module-3. This shows that beam sizes are well below the aperture limit. Table 3.5 shows the quadrupole settings for the different  $R_{56}$  tuning. Here, one can note that there is a smooth transition of quadrupole settings of  $R_{56}$  up to  $-0.30$  m to  $+0.25$  m, while at the extreme point (on  $R_{56} = +0.30$  m), there is abrupt changes in settings. To keep the dispersion and maximum beta function within the limits, this is required as continuation of the smooth transition to  $R_{56} = +0.30$  m results in the maximum beta function reaching  $\sim 60$  m and maximum dispersion becoming  $\sim 3.5$  m. To reach the  $R_{56} = +0.30$  m, higher strengths of QC3 and QC4 are required resulting in rapid increase in phase advance in the optics and higher beta and dispersion function.

**Table 3.5A: Quadrupole strength ( $g/B\rho$  in  $m^{-2}$ ) for different  $R_{56}$  settings of TL-2**

Quadrupole & Type	$R_{56}$ (m)						
	0.30	0.25	0.20	0.15	0.10	0.05	0.00
Q0A [Slim]	5.499300						
Q0B [Slim]	-4.889800						
Q0C [TSL]	4.528500						
QB1 [Standard]	3.874428						
QB2 [Standard]	-2.947592						
QB3 [Standard]	0.6759084						
QB4 [TSL]	3.656300	3.602400	3.723600	3.745300	3.736400	3.721600	3.686929
QB5 [TSL]	-6.018900	-5.772700	-6.001800	-6.152800	-6.082400	-6.077500	-6.115232
Q1V [Standard]	-4.93990						
Q2V [Standard]	3.24745						
QB6 [TSL]	-1.631300	-2.239000	-0.091000	-0.059200	-0.000200	-0.425200	-0.055980
QB7 [TSL]	3.526200	4.962300	3.783300	4.010000	3.923400	4.237600	3.941288
QB8 [TSL]	-0.844800	-3.856800	-3.778200	-4.570700	-4.507300	-4.690100	-4.403360
QC1 [TSL]	4.392000	Off	0.520900	1.591602	1.594800	1.635900	2.002300
QC2 [TSL]	-6.309200	-8.147613	-8.127300	-7.165900	-7.273400	-7.180000	-7.616500
QC3 [TSL]	5.092700	7.667834	7.730600	7.441400	7.635000	7.771300	8.015500
QC4 [TSL]	0.004100	9.104372	8.721900	8.569588	8.101671	7.741651	7.436591
QC5 [TSL]	-2.358400	-5.018986	-4.786600	-4.665504	-4.627374	-4.523026	-4.639579
QD1 [Q3L]	-4.552400	-6.750623	-8.082500	-8.945800	-8.904300	-10.121200	-7.861000
QD2 [Q3L]	-5.606900	6.926099	8.061600	7.141900	7.064500	7.993200	7.181300

Here negative sign of strength shows a quadrupole, defocusing in horizontal plane.

**Table 3.5B: Quadrupole strength ( $g/B\rho$  in  $m^{-2}$ ) for different  $R_{56}$  settings of TL-2**

Quadrupole & Type	$R_{56}$ (m)					
	-0.05	-0.10	-0.15	-0.20	-0.25	-0.30
Q0A [Slim]	5.49930 -4.88980 4.52850					
Q0B [Slim]						
Q0C [TSL]						
QB1 [Standard]	3.874428 -2.947592 0.6759084					
QB2 [Standard]						
QB3 [Standard]						
QB4 [TSL]	3.694465	3.709042	3.720976	3.686929	3.720538	3.71460
QB5 [TSL]	-5.940875	-6.000374	-5.994994	-6.115232	-6.117621	-6.29940
Q1V [Standard]	-4.93990 3.24745					
Q2V [Standard]						
QB6 [TSL]	-0.6103124	-0.3429193	Off	Off	-0.6947597	-0.000400
QB7 [TSL]	4.297115	4.116014	3.886963	3.755000	4.301927	3.904900
QB8 [TSL]	-4.268515	-4.308398	-4.334767	-4.273200	-4.364285	-5.064100
QC1 [TSL]	1.989700	2.153567	2.813288	3.189962	4.8462	5.009872
QC2 [TSL]	-7.934264	-7.924808	-8.037459	-8.089192	-8.504432	-8.401705
QC3 [TSL]	8.262446	8.429037	8.642021	8.881988	9.531533	9.964513
QC4 [TSL]	7.217666	7.000154	6.723196	6.504467	5.943693	5.789055
QC5 [TSL]	-4.468653	-4.521916	-4.288874	-4.229013	-4.088262	-4.053587
QD1 [Q3L]	-7.043518	-7.452513	-8.136665	-8.883000	-8.290177	-10.57458
QD2 [Q3L]	5.803209	6.259339	6.520035	8.436400	6.754256	8.581195

Here negative sign of strength shows a quadrupole, defocusing in horizontal plane.

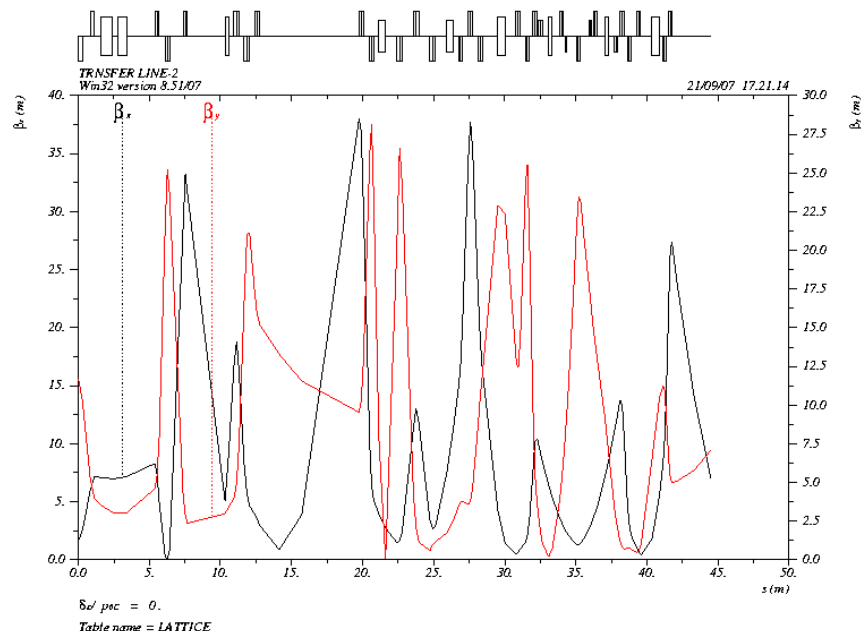
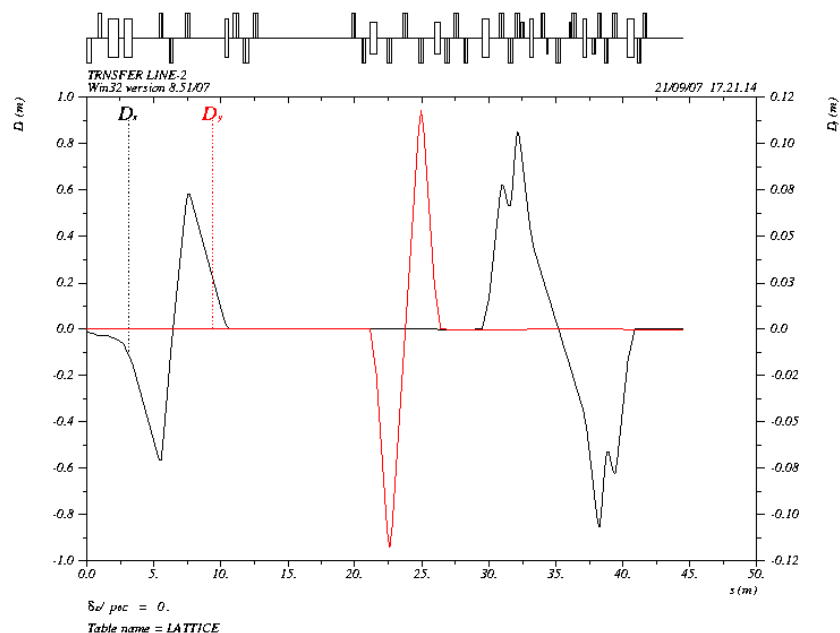


**Fig. 3.10A Dispersion and beta functions @  $R_{56} = +0.30$  m (Black: horizontal, Red: Vertical)**

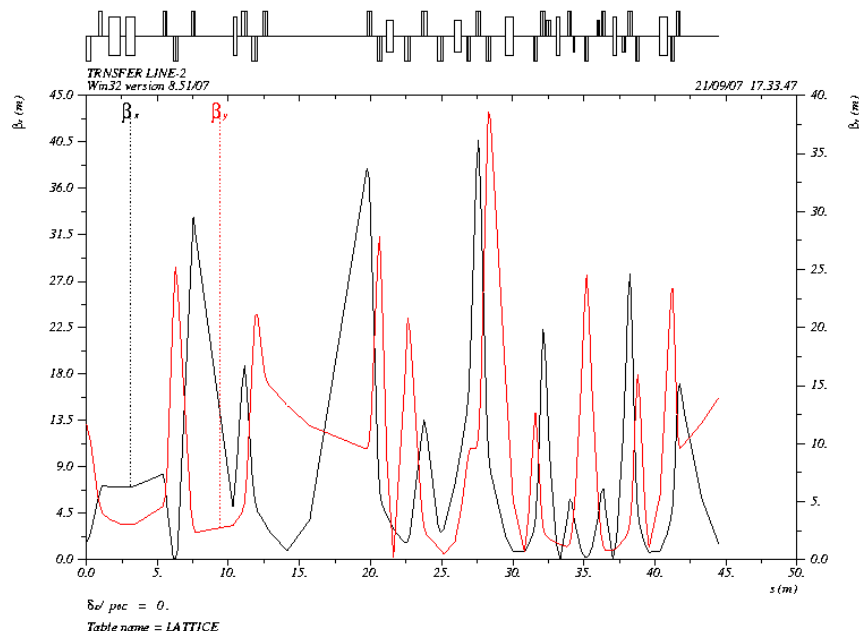
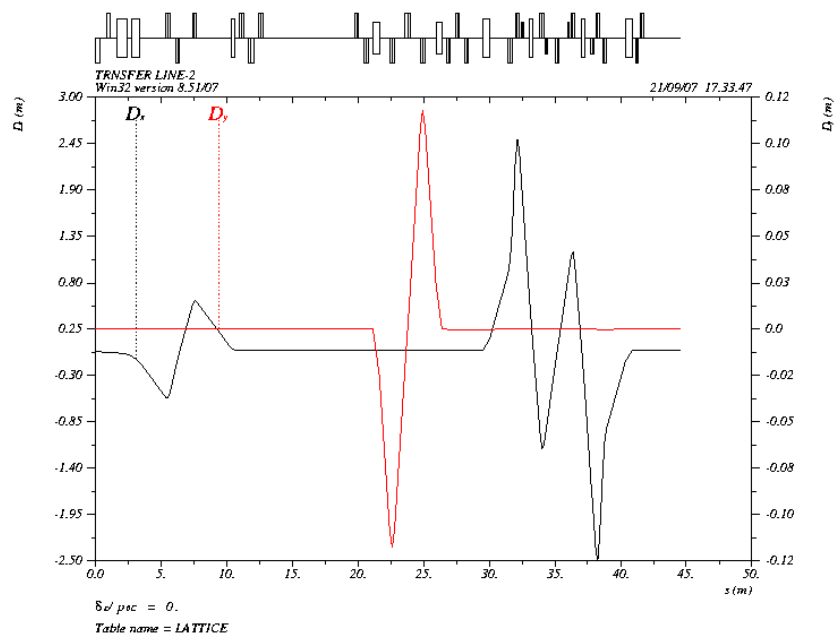


**Fig. 3.10B Dispersion and beta functions @  $R_{56} = +0.25$  m (Black: horizontal, Red: Vertical)**

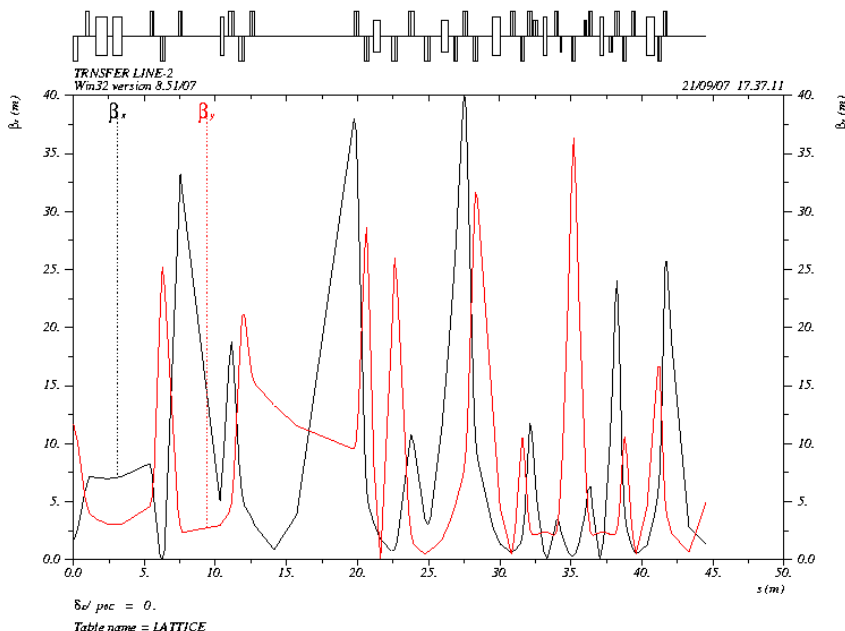
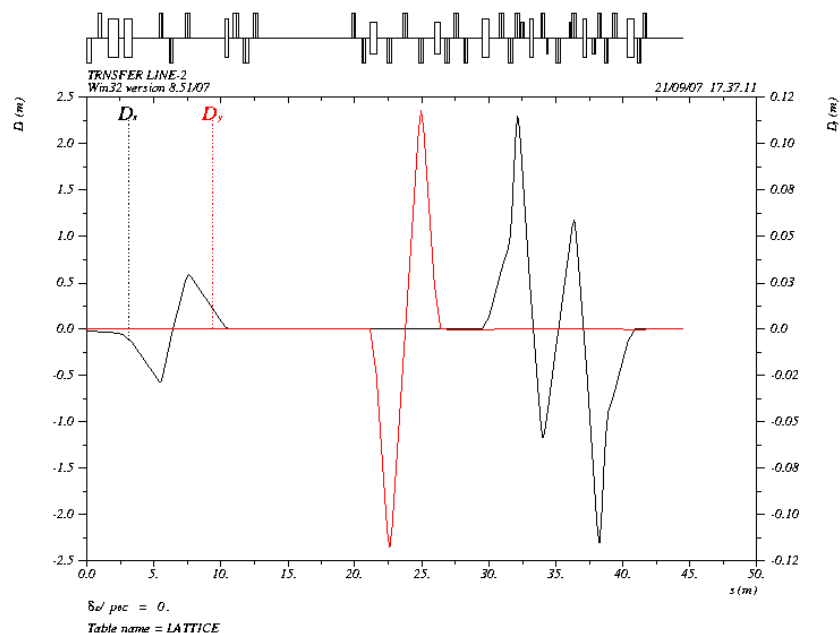


**Fig. 3.10C Dispersion and beta functions @  $R_{56} = +0.20$  m (Black: horizontal, Red: Vertical)**

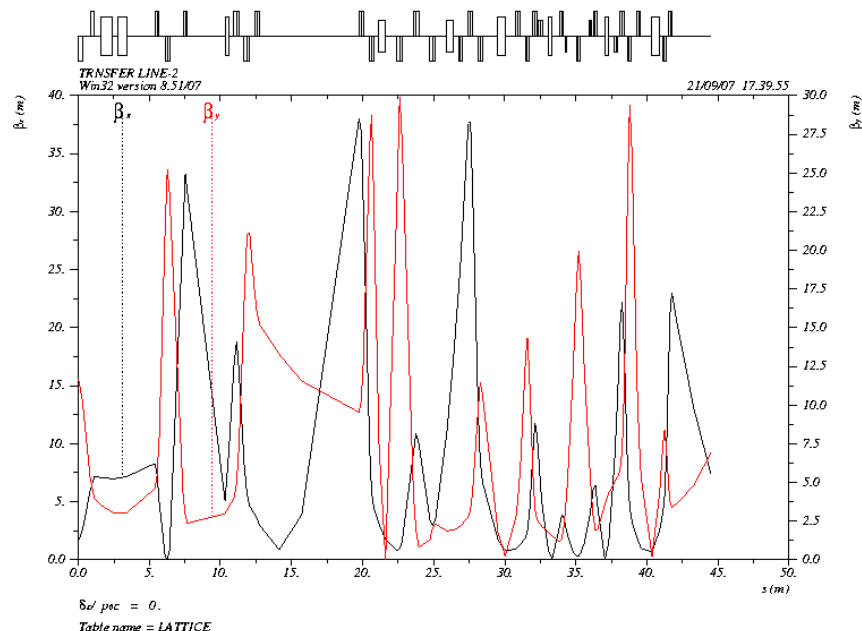
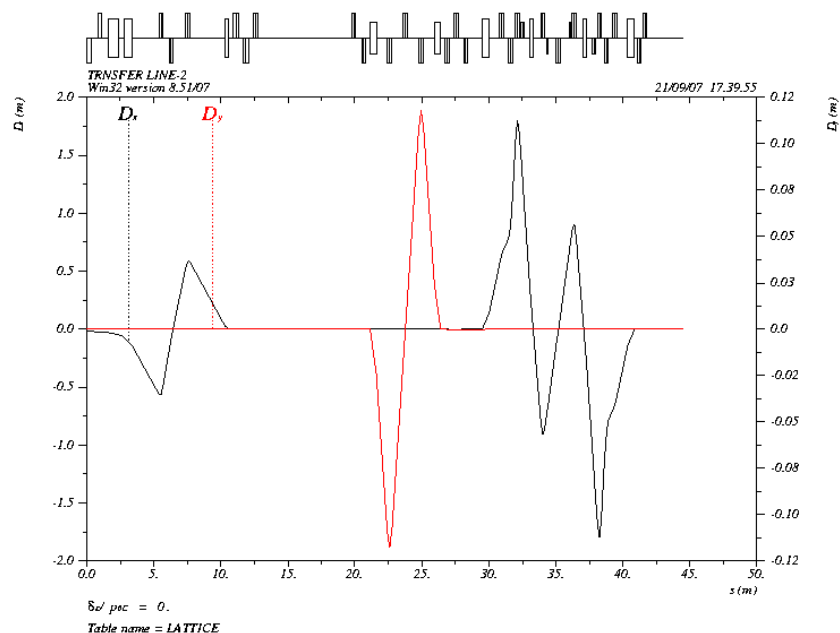


**Fig. 3.10D Dispersion and beta functions @  $R_{56} = +0.15$  m (Black: horizontal, Red: Vertical)**

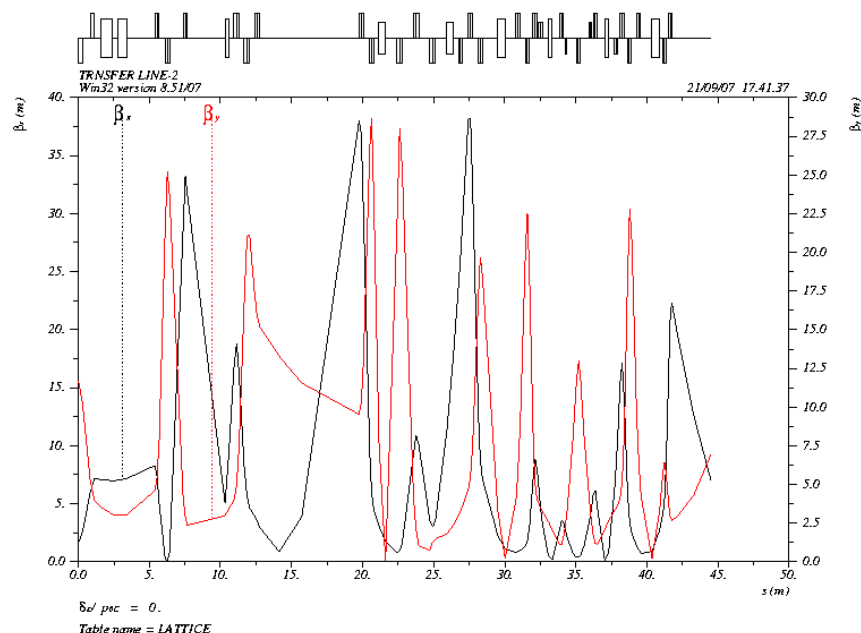
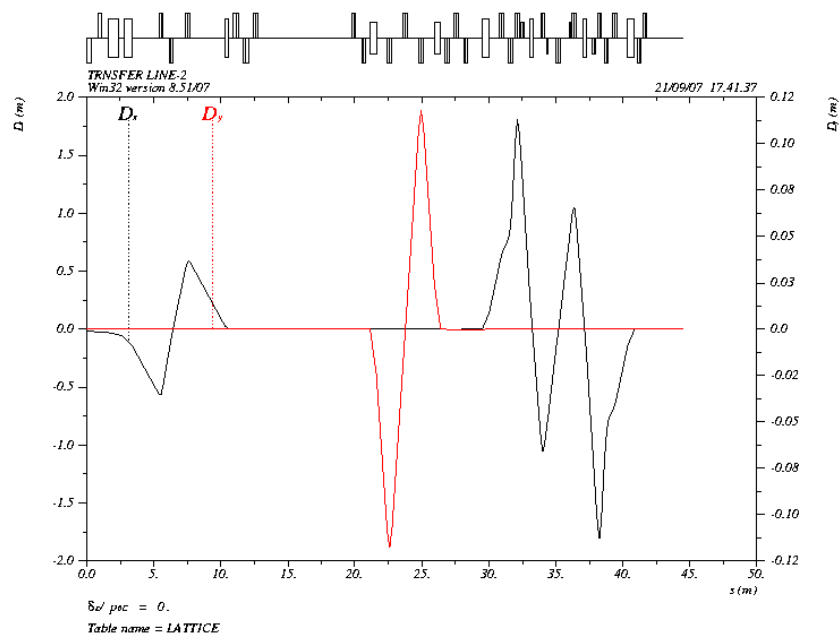


**Fig. 3.10E Dispersion and beta functions @  $R_{56} = +0.10$  m (Black: horizontal, Red: Vertical)**

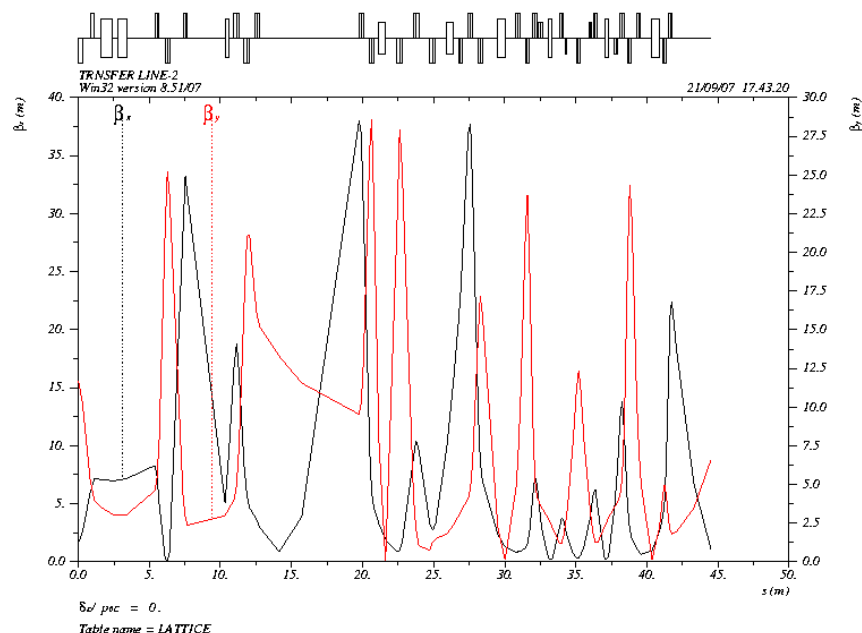
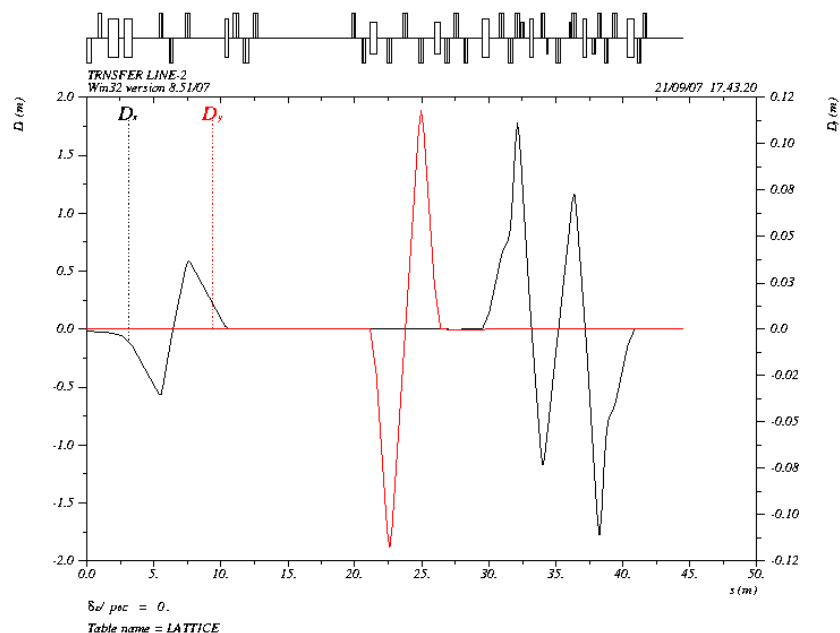


**Fig. 3.10F Dispersion and beta functions @  $R_{56} = +0.05$  m(Black: horizontal, Red: Vertical)**

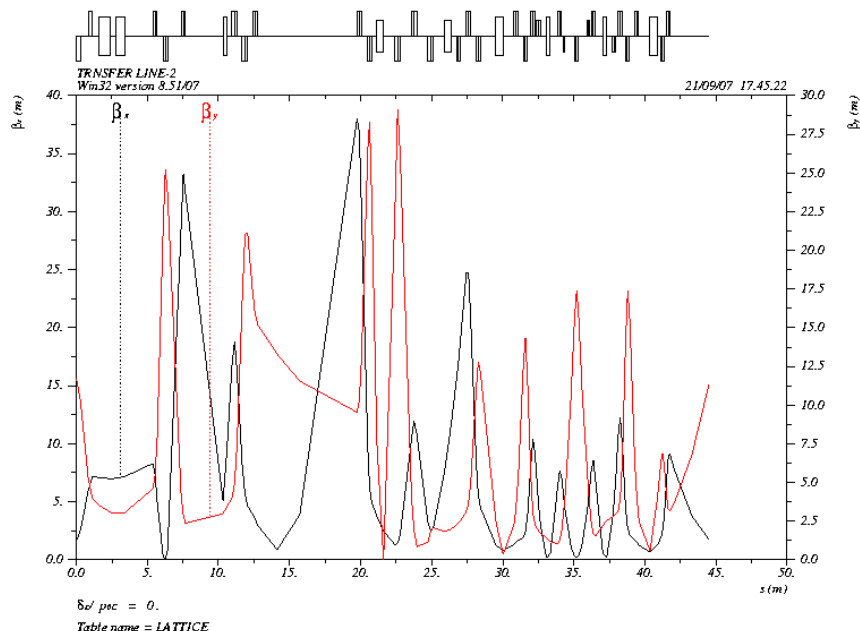
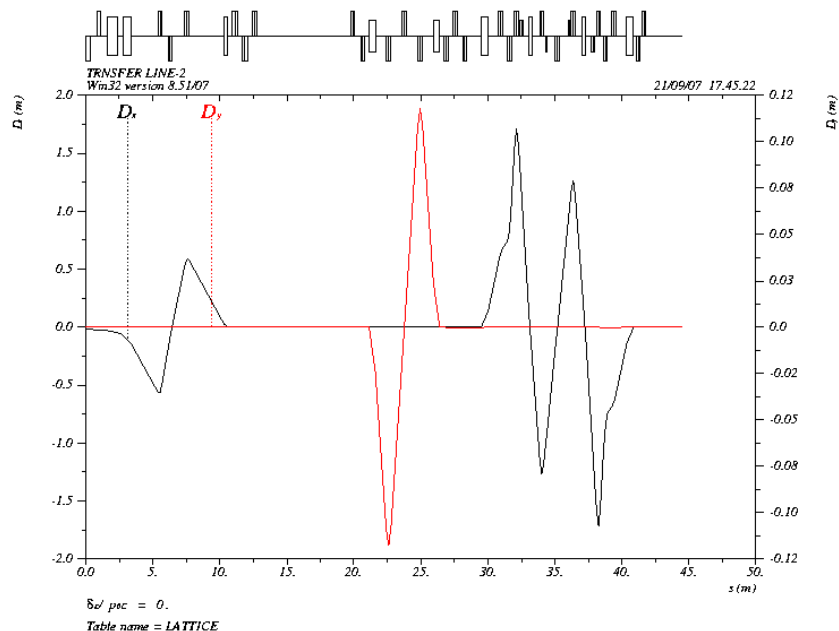


**Fig. 3.10G Dispersion and beta functions @  $R_{56} = 0.00$  m(Black: horizontal, Red: Vertical)**

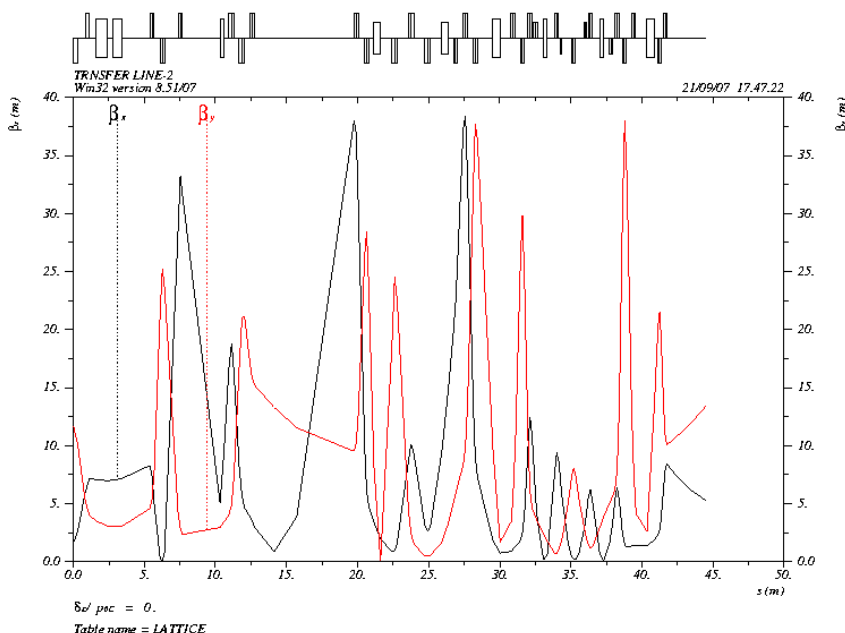
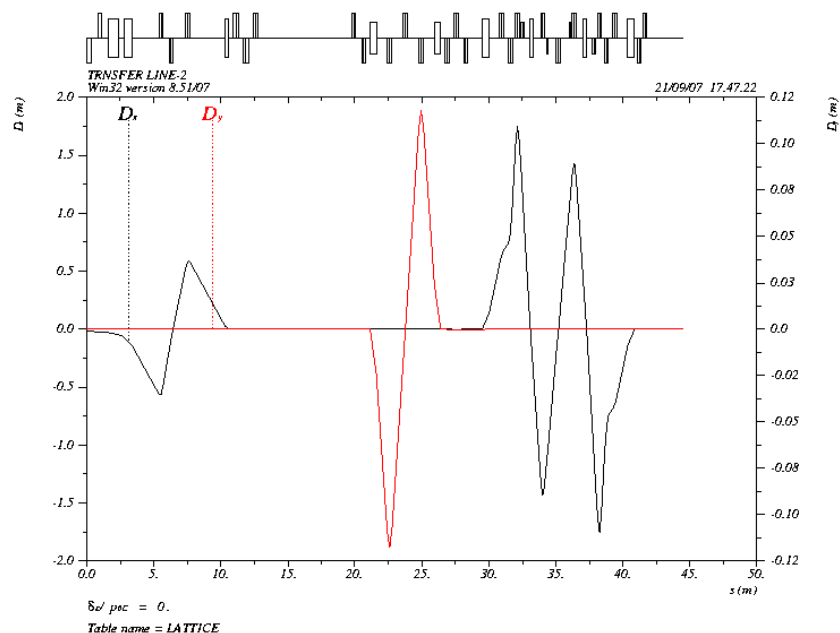


**Fig. 3.10H Dispersion and beta functions @  $R_{56} = -0.05$  m (Black: horizontal, Red: Vertical)**

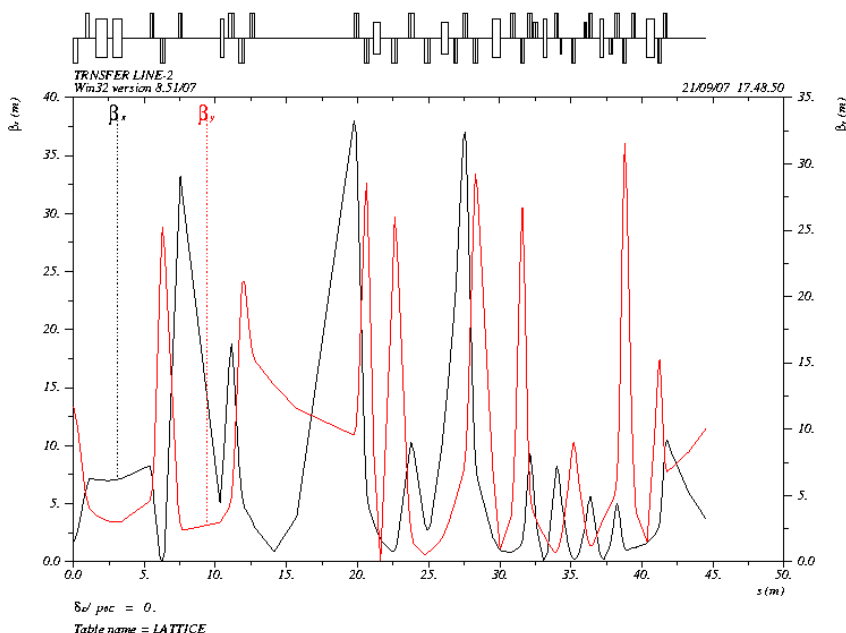
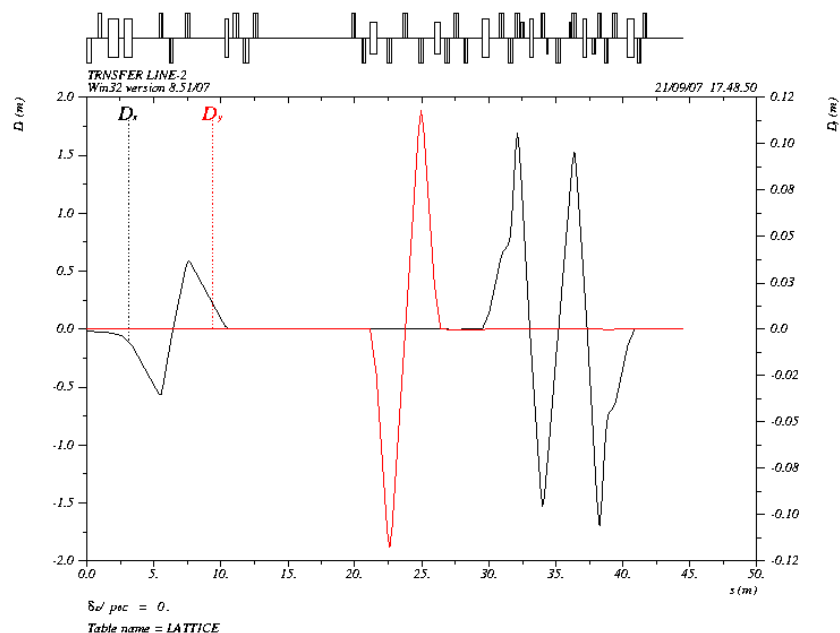


**Fig. 3.10I Dispersion and beta functions @  $R_{56} = -0.10$  m (Black: horizontal, Red: Vertical)**

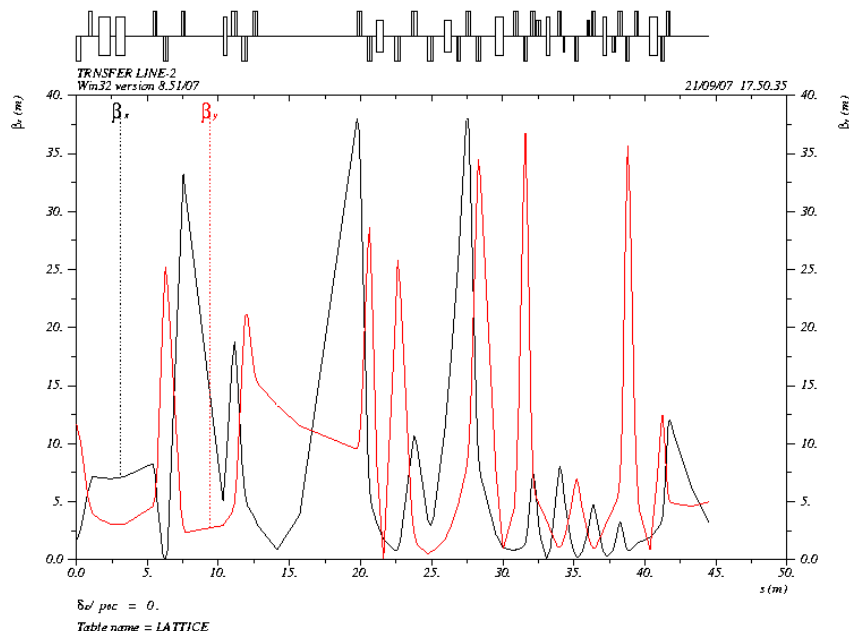
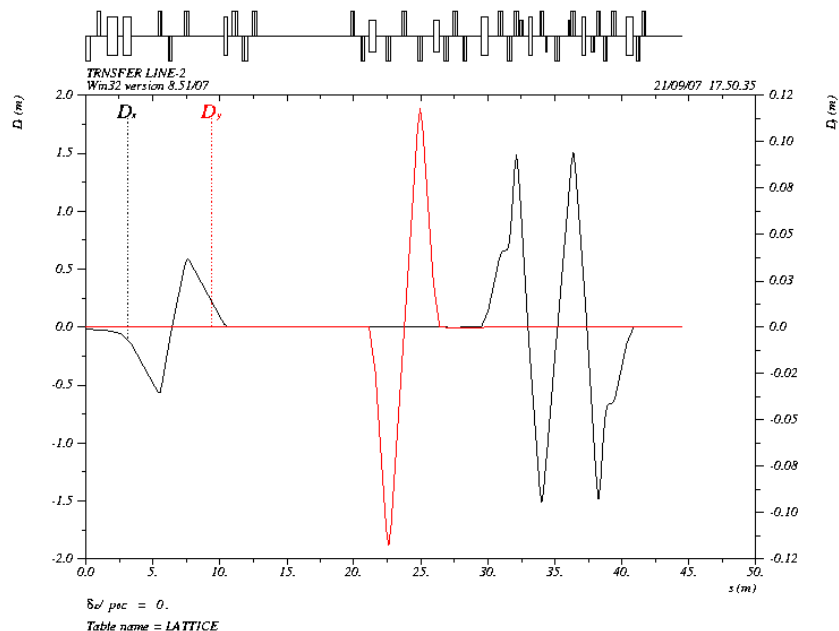


**Fig. 3.10J Dispersion and beta functions @  $R_{56} = -0.15$  m (Black: horizontal, Red: Vertical)**

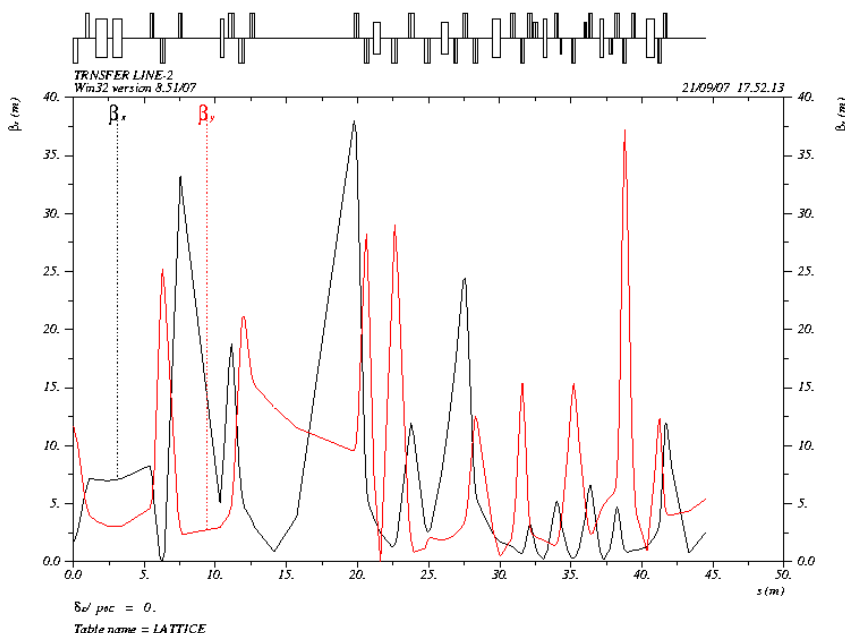
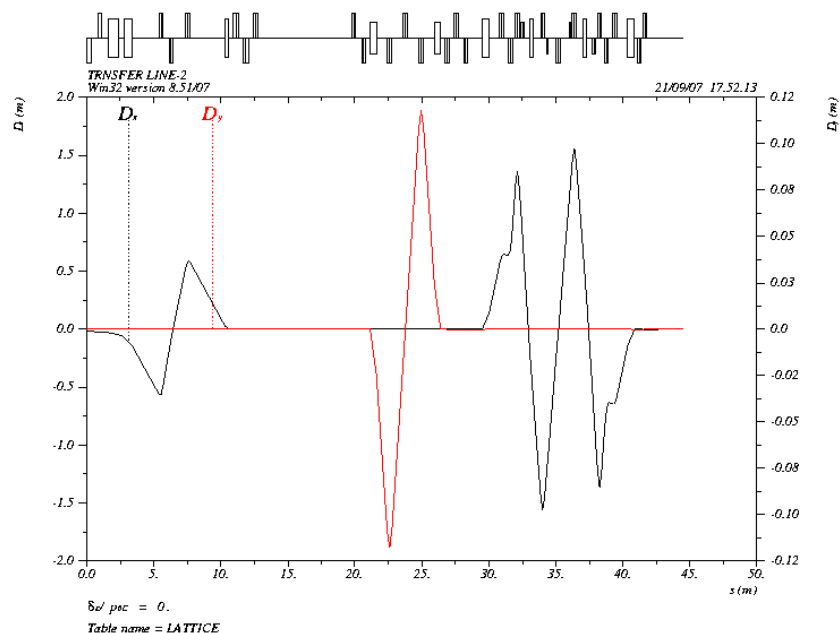


**Fig. 3.10K Dispersion and beta functions @  $R_{56} = -0.20$  m (Black: horizontal, Red: Vertical)**

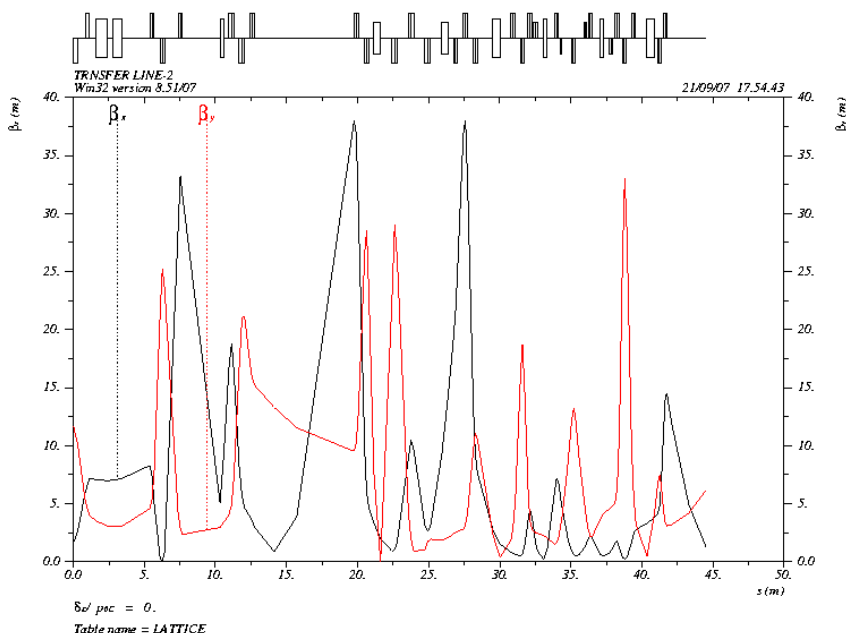
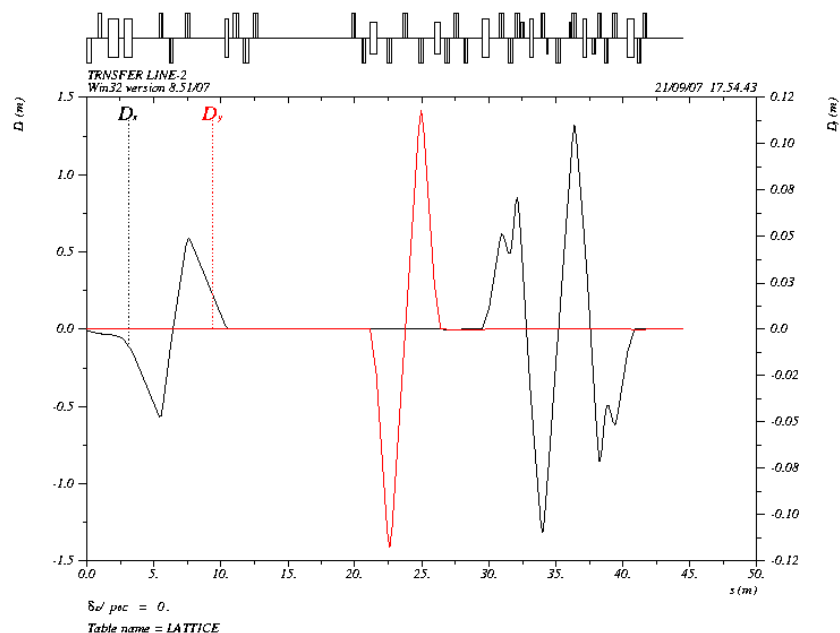


**Fig. 3.10L Dispersion and beta functions @  $R_{56} = -0.25$  m (Black: horizontal, Red: Vertical)**

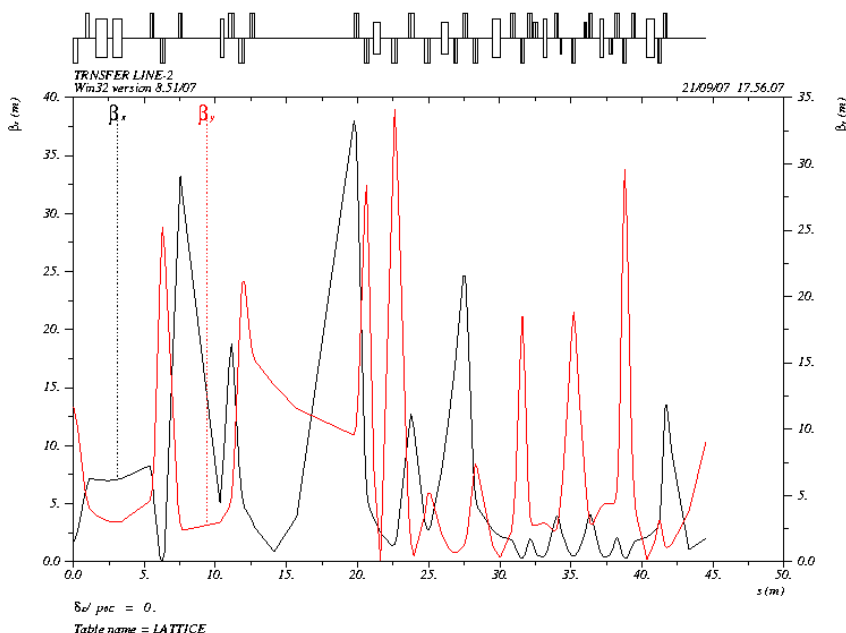
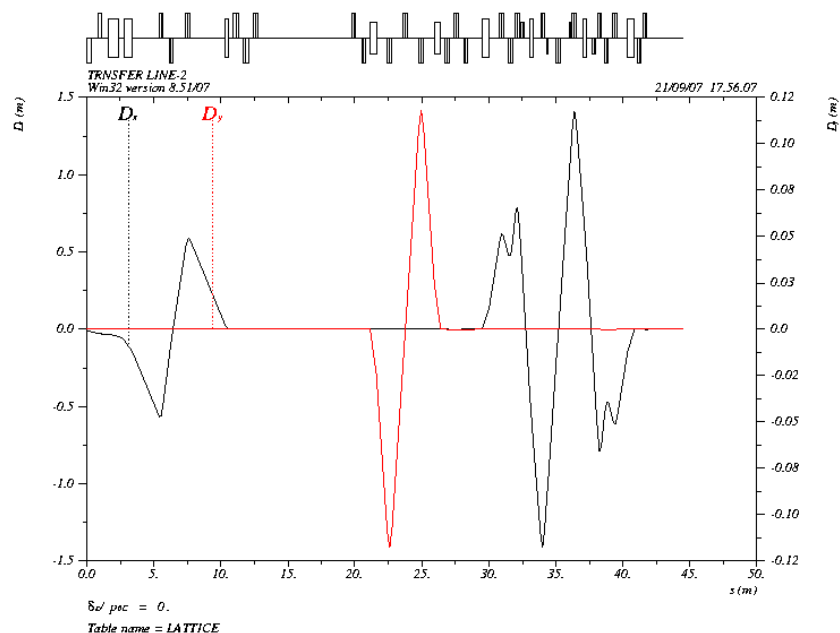


**Fig. 3.10M Dispersion and beta functions @  $R_{56} = -0.30$  m (Black: horizontal, Red: Vertical)**

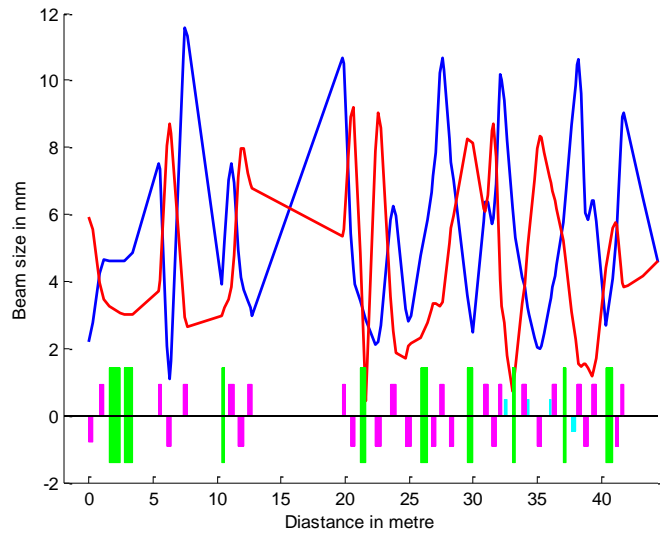


**Fig. 3.11A Beam size (considering 1% momentum spread) for  $R_{56}=+0.30$  m (Blue: horizontal, Red: vertical)**

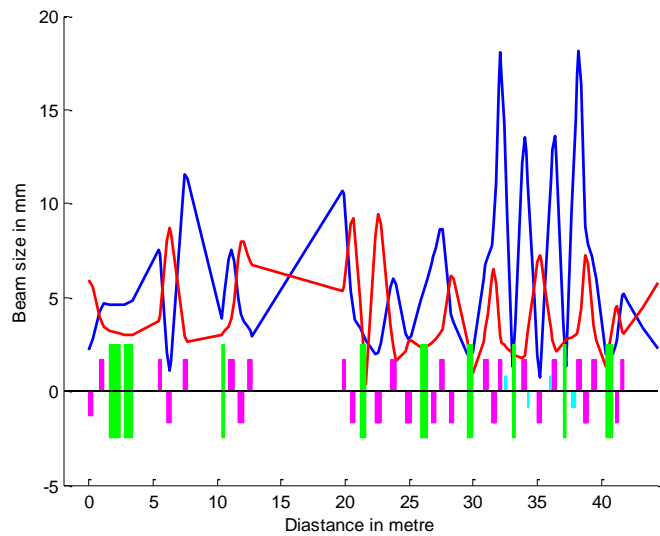


**Fig. 3.11B Beam size (considering 1% momentum spread) for  $R_{56}=0.00$  m (Blue: horizontal, Red: vertical)**

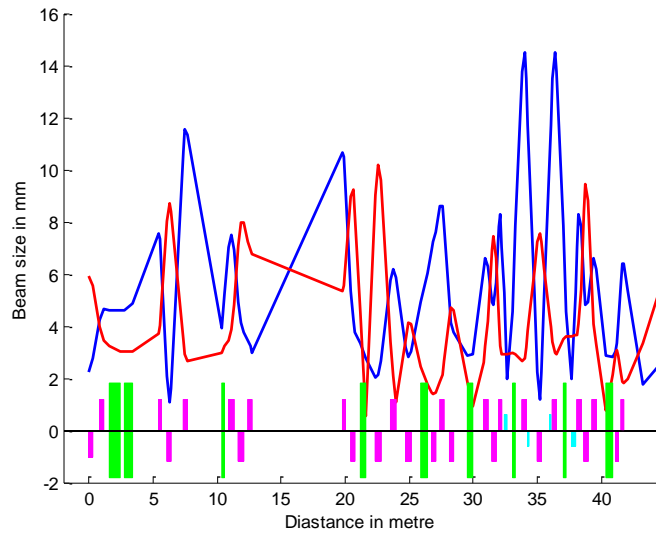


**Fig. 3.11C Beam size (considering 1% momentum spread) for  $R_{56}=-0.30\text{ m}$ (Blue: horizontal, Red: vertical)**

### 3.4 Alternative optics

The optimum solution of optics has large dispersion in  $R_{56}$  arc, so that  $T_{566}$  can be corrected using feasible strength of already available sextupole magnets. Therefore, the strength of quadrupole magnets is higher and optics is sensitive to alignment and gradient errors. In the initial run for commissioning, due to unforeseen errors, these sensitive optics may be difficult to commission. Thus at four different values of  $R_{56}$ , low dispersion mode of optics is also optimized, so that during commissioning, under unforeseen errors, beam can be transmitted easily and elements and errors can be characterized. Due to low dispersion mode,  $T_{566}$  cannot be corrected in this mode in the given strength of sextupole magnets.

**Table 3.6: Quadrupole strength ( $g/B\rho$  in  $m^{-2}$ ) for different settings of  $R_{56}$  of alternative optics for TL-2**

Quadrupole & Type	R <sub>56</sub> settings (m)			
	0.30	0.25	0.00	-0.30
Q0A [Slim]	5.499300 -4.889800 4.528500			
Q0B [Slim]				
Q0C [TSL]				
Q1 [Standard]	3.668100	3.874428	3.668100	3.843000
Q2 [Standard]	-3.876300	-2.947592	-3.876300	-3.801100
Q3 [Standard]	1.950700	0.6759084	1.950700	1.637200
Q4 [TSL]	3.836500	3.612900	3.836500	3.810100
Q5 [TSL]	-6.240200	-5.839600	-6.240200	-6.323200
Q1V [Standard]	-4.939900 3.247453			
Q2V [Standard]				
Q6 [TSL]	-0.9445672	-1.899700	-0.734800	-0.671300
Q7 [TSL]	4.320893	4.980700	4.085400	3.885500
Q8 [TSL]	-2.760655	-2.694100	-2.855600	-2.699187
QC1 [TSL]	3.840300	5.085700	5.121500	6.421631
QC2 [TSL]	-0.460300	-2.117900	-0.411500	-0.1912914
QC3 [TSL]	0.452900	OFF	0.437400	0.181764
QC4 [TSL]	4.226300	4.806300	4.025500	4.162491
QC5 [TSL]	-3.877169	-4.725600	-3.761000	-3.729488
QD1 [Q3L]	-1.846345	-5.756300	-4.360100	-4.426516
QD2 [Q3L]	1.489854	9.791100	5.957600	5.440047

Here negative sign of strength shows a quadrupole, defocusing in horizontal plane.

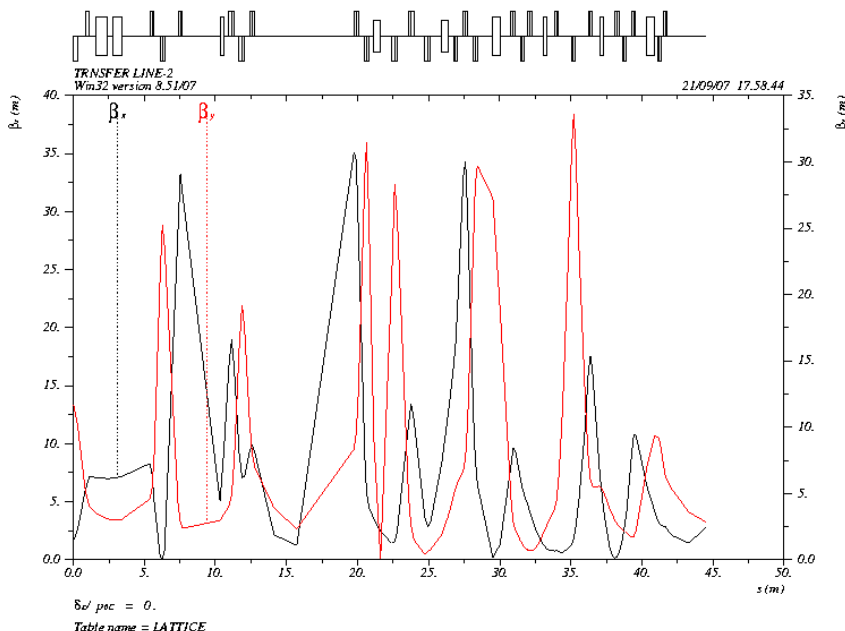
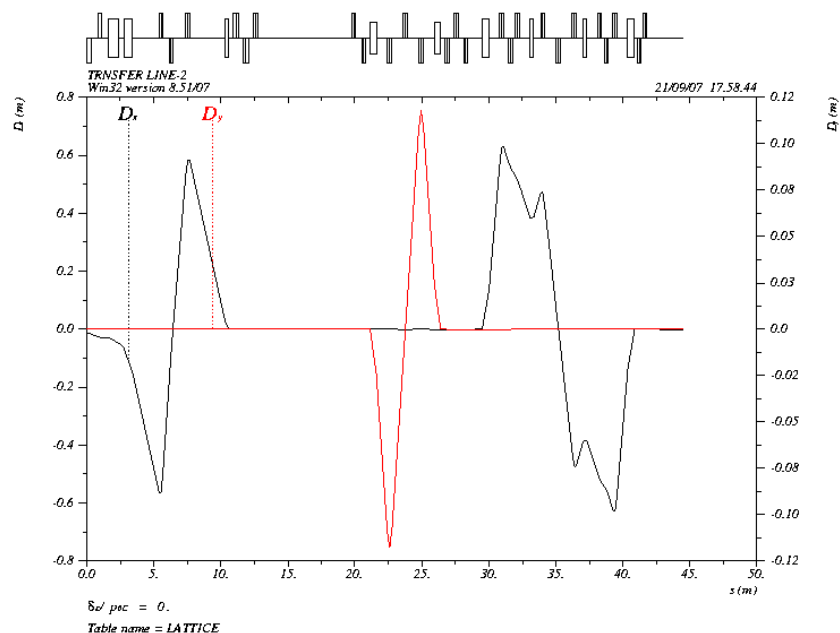


**Fig. 3.12A Dispersion and beta functions @  $R_{56} = +0.30$  m (Black: horizontal, Red: Vertical)**

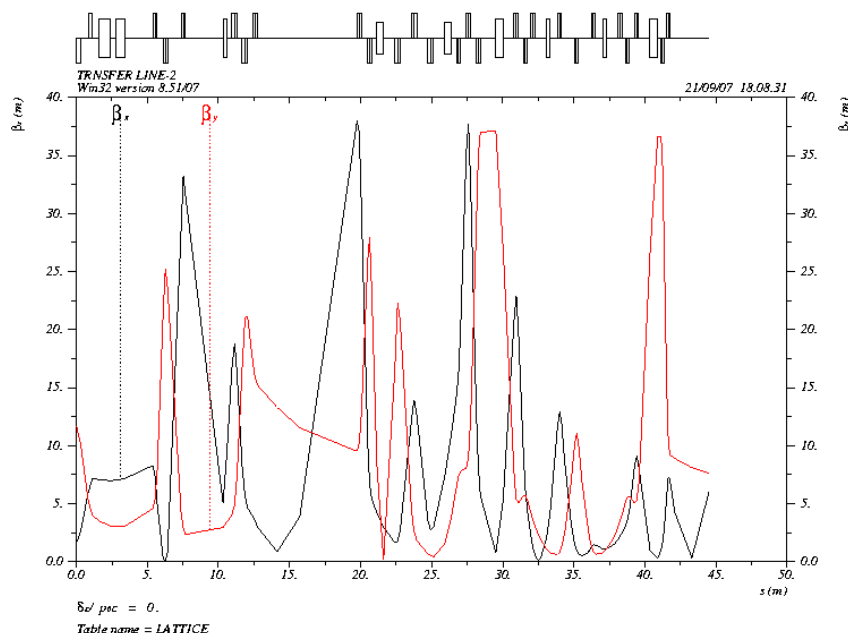
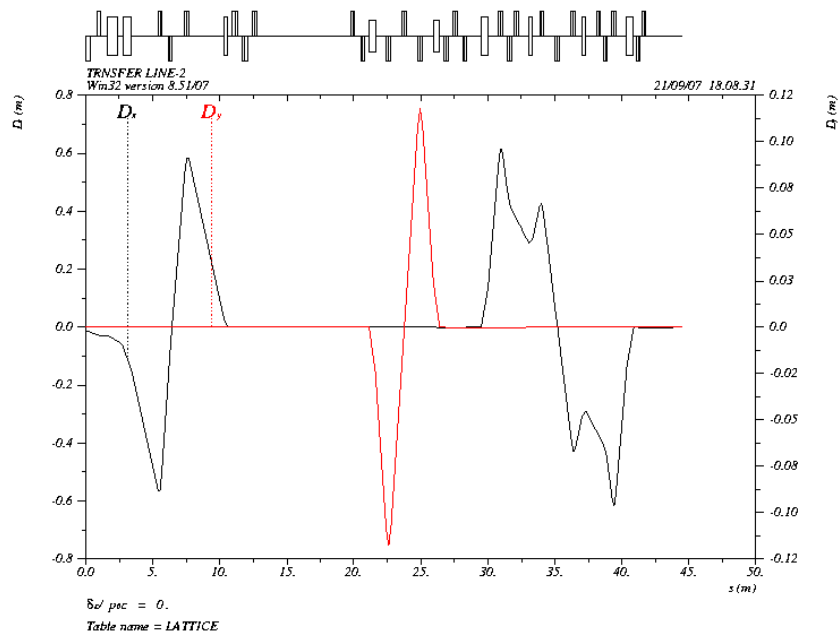


**Fig. 3.12B Dispersion and beta functions @  $R_{56} = +0.25$  m (Proposed nominal operating point; Black: horizontal, Red: Vertical)**

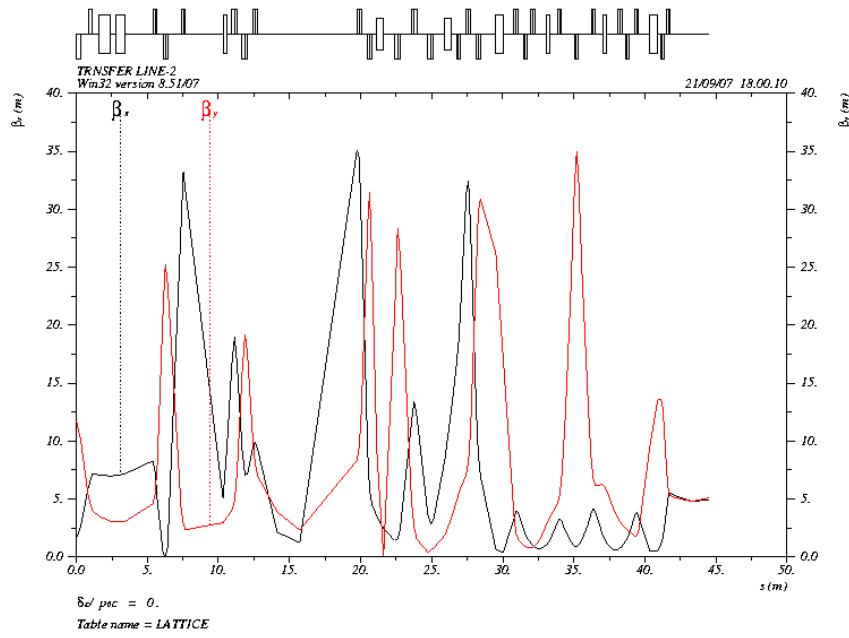
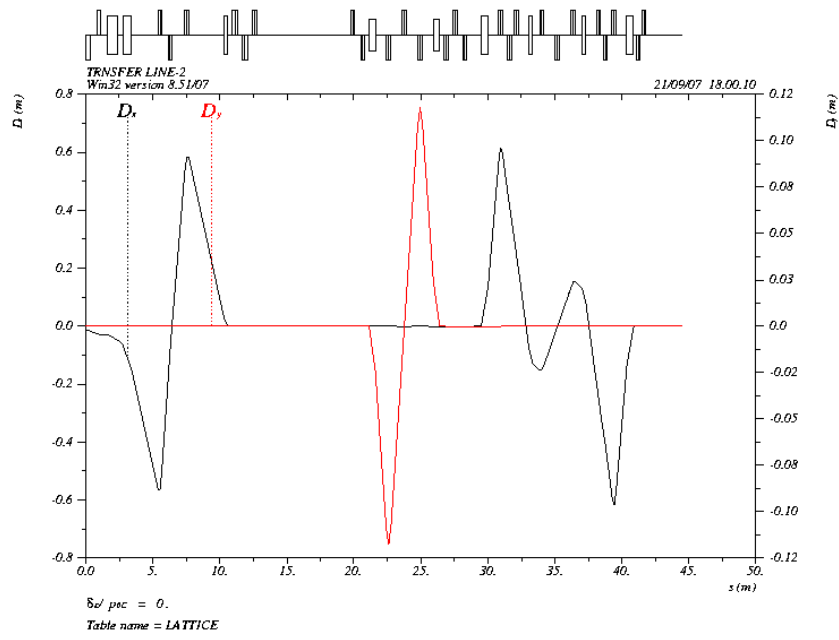
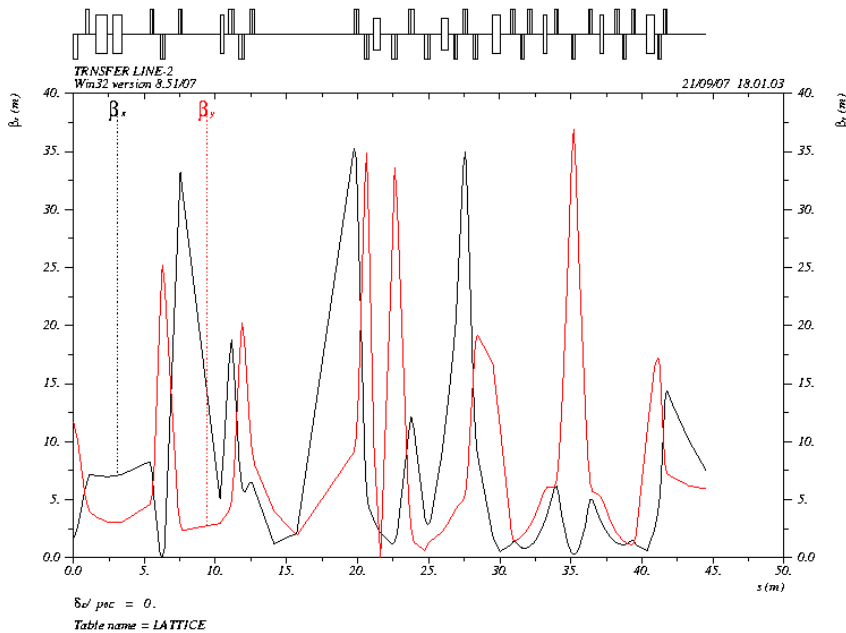
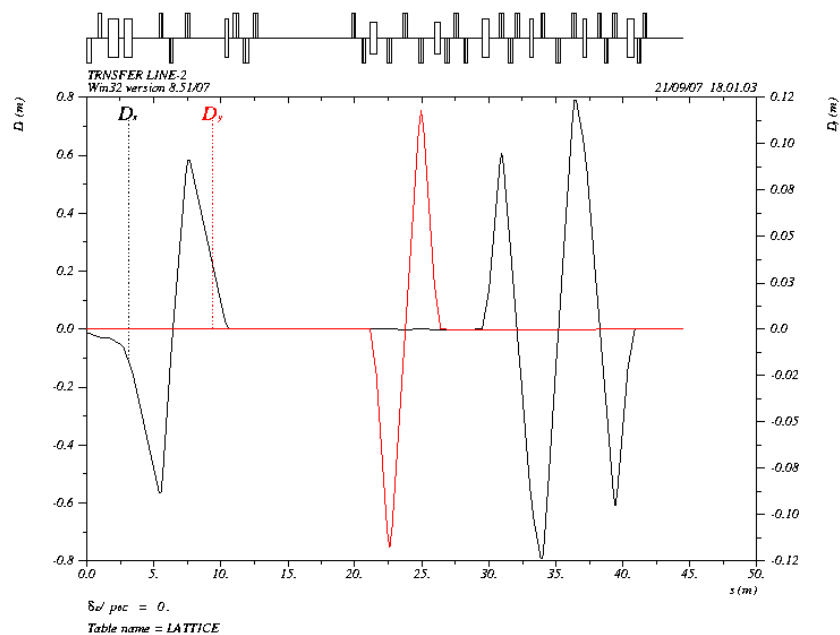


Fig. 3.12C Dispersion and beta functions @  $R_{56} = 0.00$  m (Black: horizontal, Red: Vertical)



**Fig. 3.12D Dispersion and beta functions @  $R_{56} = -0.30$  m (Black: horizontal, Red: Vertical)**

## CHAPTER 4

### SEXTUPOLE OPTIMIZATION FOR TRANSFER LINE-2

In the previous chapter, geometry and linear optical design and optimization of TL-2 is described. In a bunch compressor, even if  $R_{56}$  and  $R_{65}$  are well optimized, second order longitudinal dispersion  $T_{566}$  can lead to a curvature in longitudinal phase space and thus, effective bunch length may increase and longitudinal density distribution of electrons along the bunch length may change. Therefore it is necessary to suppress  $T_{566}$  in the entire range of tuning. In some experiments, where asymmetric density distribution is required, proper value of  $T_{566}$  is of significant importance [47], however this is not required in TL-2.

Second order longitudinal dispersion  $T_{566}$  can be obtained for a curved path inside a dipole magnet using the geometry, depicted in Fig. 1.6. The path length of the trajectory (including effect of  $x'$ ) for an off-momentum electron due to dispersion can be written as

$$ds_\delta = \left[ ((x + \rho)d\theta)^2 + x'^2 ds^2 \right]^{1/2} = \left[ \left( 1 + \frac{x}{\rho} \right)^2 + x'^2 \right]^{1/2} ds \quad [4.1]$$

Expanding the above expression up to second order in co-ordinates and taking the difference from the length of design trajectory ( $\rho d\theta$ ), gives the change in path length for an off-momentum electron as follows

$$\Delta s = \left( \frac{x}{\rho} + \frac{x^2}{2\rho^2} + \frac{x'^2}{2} \right) ds \quad [4.2]$$

Expressing co-ordinates in above expression using first and second order map,  $T_{566}$  is obtained explicitly as given below (for zero initial dispersion and its derivatives)

$$T_{566} = \int \left\{ \frac{R_{16}^2}{2\rho^2} + \frac{R_{26}^2}{2} + \frac{T_{166}}{\rho} \right\} ds \quad [4.3]$$

This expression shows that  $T_{566}$  is related with second order elements  $T_{166}$  [9, 48, 49]. Expression for  $T_{566}$  with non-vanishing initial dispersion and its derivative as well as propagation of second order dispersion in an optics is provided in Appendix C. Inclusion of sextupole magnets in the non-zero dispersion region can be used for controlling  $T_{166}$ . Second order dispersion in an optics is obtained using perturbation technique. Second order dispersion can be described by following differential equation [23, 49]

$$D''_{(2)} + \left( \frac{1}{\rho^2} - K \right) D_{(2)} = f$$

Here  $D_{(2)}$  is the second order dispersion and  $f$  is the driving term for second order dispersion, which is given by [49]

$$f = -\frac{1}{\rho} \left[ 1 - \frac{D'^2}{2} - \frac{D}{\rho} \left( 2 - \frac{D}{\rho} \right) \right] + KD \left( 1 - \frac{2D}{\rho} \right) - \frac{1}{2} m D^2$$

Here ' $m$ ' is the sextupole strength ( $\frac{1}{B\rho} \frac{\partial^2 B_y}{\partial x^2}$ ) and  $K$  is the quadrupole strength. This expression reveals that sextupole magnet has an effect on the second order dispersion (if magnet is placed at the non-zero dispersion location). This effect on  $T_{166}$  is utilized to control  $T_{566}$  in an optics, leaving  $R_{56}$  unaffected.

Field of a sextupole magnet varies as  $B_y = \frac{1}{2} m(x^2 - y^2)$  and  $B_x = mxy$ . Thus kick imparted by a sextupole magnet on an electron in the beam is a nonlinear function of co-ordinates and therefore, sextupole magnets generates geometric aberrations, which increase the emittance of the beam. Keeping this in view, sextupole scheme should be optimized in such a way so that in suppression of  $T_{566}$ , effect on emittance is minimum.

If two sextupole magnets are placed in an optics at the symmetric location with  $\pi$  betatron phase apart, there will be no net transverse kick on the design momentum electron due to

these sextupole magnets [17]. The transfer matrix for such an optics becomes unit matrix with negative sign and the optics is known as  $-I$  transformer i.e. identity transformer. In this scheme, as the net transverse kick is zero, there will be no emittance dilution. Thus if  $T_{566}$  is corrected using this type of scheme,  $T_{566}$  will be suppressed without dilution of the emittance. In thick lens, this condition cannot be met exactly, however if within the length of sextupole magnets, if beta function does not vary with large values, the emittance dilution still remains insignificant.

#### **4.1 Sextupole scheme for TL-2**

In an optics, there are various second order geometric terms ( $T_{5ij}$ ;  $i$  and  $j=1$  to 4), geometric-chromatic cross terms ( $T_{5i6}$ ,  $i=1$  to 4) and pure chromatic term ( $T_{566}$ ), which contribute to the path length, hence finally to bunch length. Variation in bunch length due to geometric and geometric-chromatic cross terms depend on transverse beam emittance and for a very small beam emittance, these contributions are negligible. In TL-2, the total contribution in path length from geometric and geometric-chromatic cross terms is only about 10% of the contribution of only  $T_{566}$ . Therefore, it is sufficient to suppress  $T_{566}$  in entire range of tuning. In TL-2, four sextupole magnets, grouped in two families are installed in Module-3 to control  $T_{566}$ . The major challenge in sextupole scheme is to suppress  $T_{566}$  in the entire range of  $R_{56}$  tuning, keeping the transverse emittance dilution below 10%. To suppress  $T_{566}$  within the available strength of sextupole magnets, sufficient dispersion is generated in Module-3 at the location of sextupole magnets as described in Section 3.2.

Due to various constraints, the optical functions in Module-3 are not symmetric as discussed in detail in the previous chapter. Also, there is a requirement of wide tuning range of  $R_{56}$  in the transfer line and optical functions vary by large magnitude (dispersion at the entrance of

second dipole magnet varies from nearly -1 m to +1 m in the entire range of tuning). So conditions for placing the sextupole magnets in a standard scheme, like  $-I$  transformer etc. cannot be satisfied. Therefore, sextupole scheme for TL-2 is optimized in an another way to suppress  $T_{566}$ , keeping the dilution of transverse emittance small.

The kick of a thin sextupole magnet on an electron in horizontal plane is given by

$$\theta_x = \frac{\int B_y ds}{B\rho} = \frac{1}{2} ml(x^2 - y^2) \quad [4.4]$$

Here ' $l$ ' is the effective length of the sextupole magnet. Similarly, in vertical plane, the kick is given by

$$\theta_y = \frac{\int B_x ds}{B\rho} = mlxy \quad [4.5]$$

The displacements  $x$  and  $y$  for an electron due to betatron oscillations and dispersion are

$$x = \sqrt{\varepsilon_x \beta_x} \cos(\phi_x - \phi_{x0}) + D\delta \quad [4.6]$$

$$y = \sqrt{\varepsilon_y \beta_y} \cos(\phi_y - \phi_{y0}) \quad [4.7]$$

Here  $\varepsilon_x$  and  $\varepsilon_y$  are the emittance in horizontal plane and vertical plane, respectively. Betatron phases at the location of sextupole magnets are  $\phi_x$  and  $\phi_y$  and subscript '0' shows the initial phase in the respective plane. We are interested in geometrical aberrations, which increases emittance, so chromatic term (momentum dependent) of Eq. 4.6 can be dropped in further studies. Using Eq. 4.6 and 4.7 in Eq. 4.4 and 4.5, sextupolar kicks in the both the planes can be obtained as a function of Twiss parameters and betatron phases. In TL-2, horizontal and vertical emittance of the beam are same, hence we will use  $\varepsilon_x = \varepsilon_y = \varepsilon$  in further discussions.

The kick in horizontal plane is

$$\theta_x = \frac{1}{2} ml \left( \varepsilon \beta_x \cos^2(\phi_x - \phi_{x0}) - \varepsilon \beta_y \cos^2(\phi_y - \phi_{y0}) \right)$$

Which can be written as

$$\theta_x = \frac{1}{4} \varepsilon ml \{ (\beta_x - \beta_y) + (\beta_x \cos[2(\phi_x - \phi_{x0})] - \beta_y \cos[2(\phi_y - \phi_{y0})]) \} \quad [4.8]$$

In vertical plane, kick is given by

$$\theta_y = \varepsilon ml \left\{ \sqrt{\beta_x \beta_y} \cos(\phi_x - \phi_{x0}) \cos(\phi_y - \phi_{y0}) \right\} \quad [4.9]$$

In a transfer line, consisting of  $N$  sextupole magnets, total kick becomes

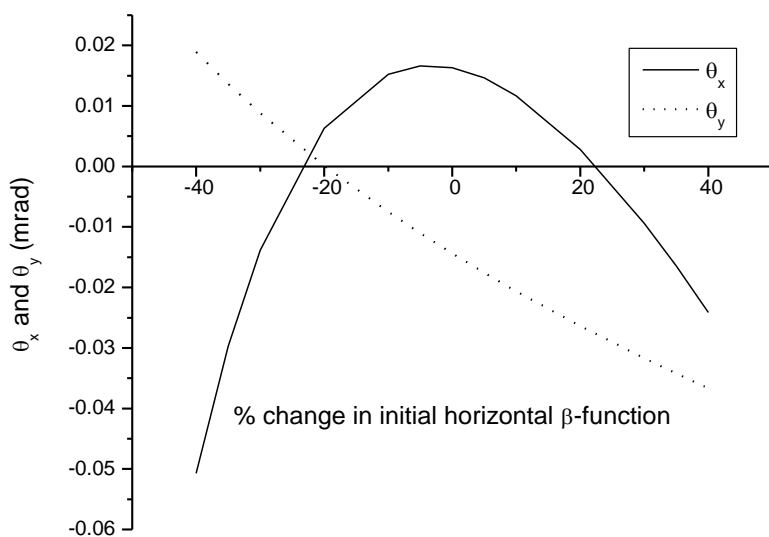
$$\begin{aligned} \theta_x &= \frac{1}{4} \varepsilon \sum_{i=1}^N (ml)_i \{ (\beta_{xi} - \beta_{yi}) \\ &\quad + (\beta_{xi} \cos[2(\phi_{xi} - \phi_{x0})] - \beta_{yi} \cos[2(\phi_{yi} - \phi_{y0})]) \} \end{aligned} \quad [4.10]$$

$$\theta_y = \varepsilon \sum_{i=1}^N (ml)_i \left\{ \sqrt{\beta_{xi} \beta_{yi}} \cos(\phi_{xi} - \phi_{x0}) \cos(\phi_{yi} - \phi_{y0}) \right\} \quad [4.11]$$

Minimizing the effects of sextupole magnets on emittance is equivalent to minimizing the total kick on an electron due to all the  $N$ -sextupole magnets as given in Eq. 4.10 and 4.11. In the horizontal kick, there are two terms, first is phase independent and second is phase dependent, while in vertical kick, only phase dependent term exists. For a symmetric  $-I$  transformer, the kick of Eq. 4.10 and 4.11 becomes zero between two sextupole magnets with opposite polarities, resulting in zero dilution of transverse emittance. For the optics, in which such phase advance is not possible, we can still minimize the kick angles by having an optimized distribution of beta functions and phases at the locations of sextupole magnets and dilution in transverse emittance can be bought down.

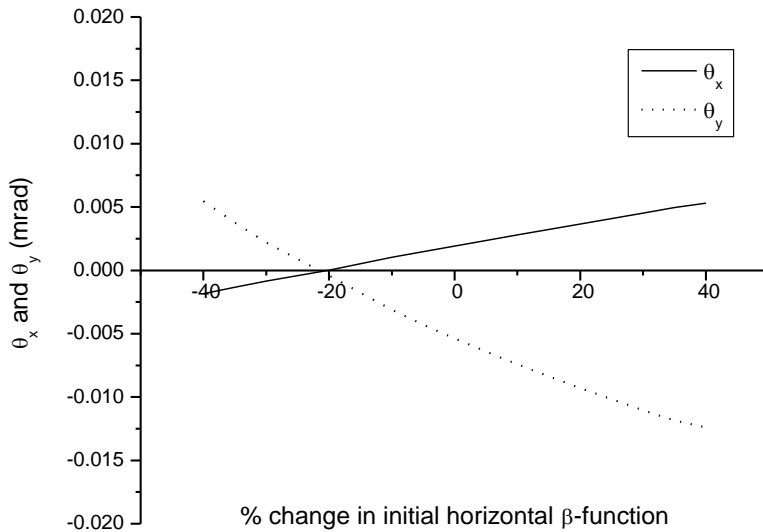
In Module-3 optics, as described in the previous chapter, optimization is mainly carried out to have a suitable distribution of dispersion and generate the desired  $R_{56}$  in tuning range. There is very little scope in optics of Module-3 to optimize it for minimizing the kick angles from sextupole magnets. Therefore, last quadrupole triplet of Module-2 is used to generate a suitable initial Twiss parameters at the entrance of Module-3, so that the distribution of Twiss parameters in Module-3 generates smaller kick angles computed from Eq. 4.10 and 4.11 and also beta function remain in suitable range to allow adequate clearance of the beam in the vacuum chamber aperture. This optimization leads to a reduced dilution of phase space, while keeping  $R_{56}$  and  $T_{566}$  unchanged.

We present the optimization procedure in detail for two extreme  $R_{56}$  values of tuning range i.e. for  $R_{56} = +0.30$  m and -0.30 m. Fig. 3.10A and Fig. 3.10M show the optimized beta functions and dispersion for these two optics for which aberrations, generated by sextupole magnets are minimized to keep the dilution in transverse emittance low. By changing the initial beta functions at Module-3 from these optimized values, kick angles also vary. The variations in kick angles for these two extreme  $R_{56}$  are shown in Fig. 4.1, given below.



**Fig. 4.1A Variation in kick angles generated by sextupole magnets [Eq. 4.10 and 4.11] for**

$$R_{56} = +0.30 \text{ m optics [50]}$$

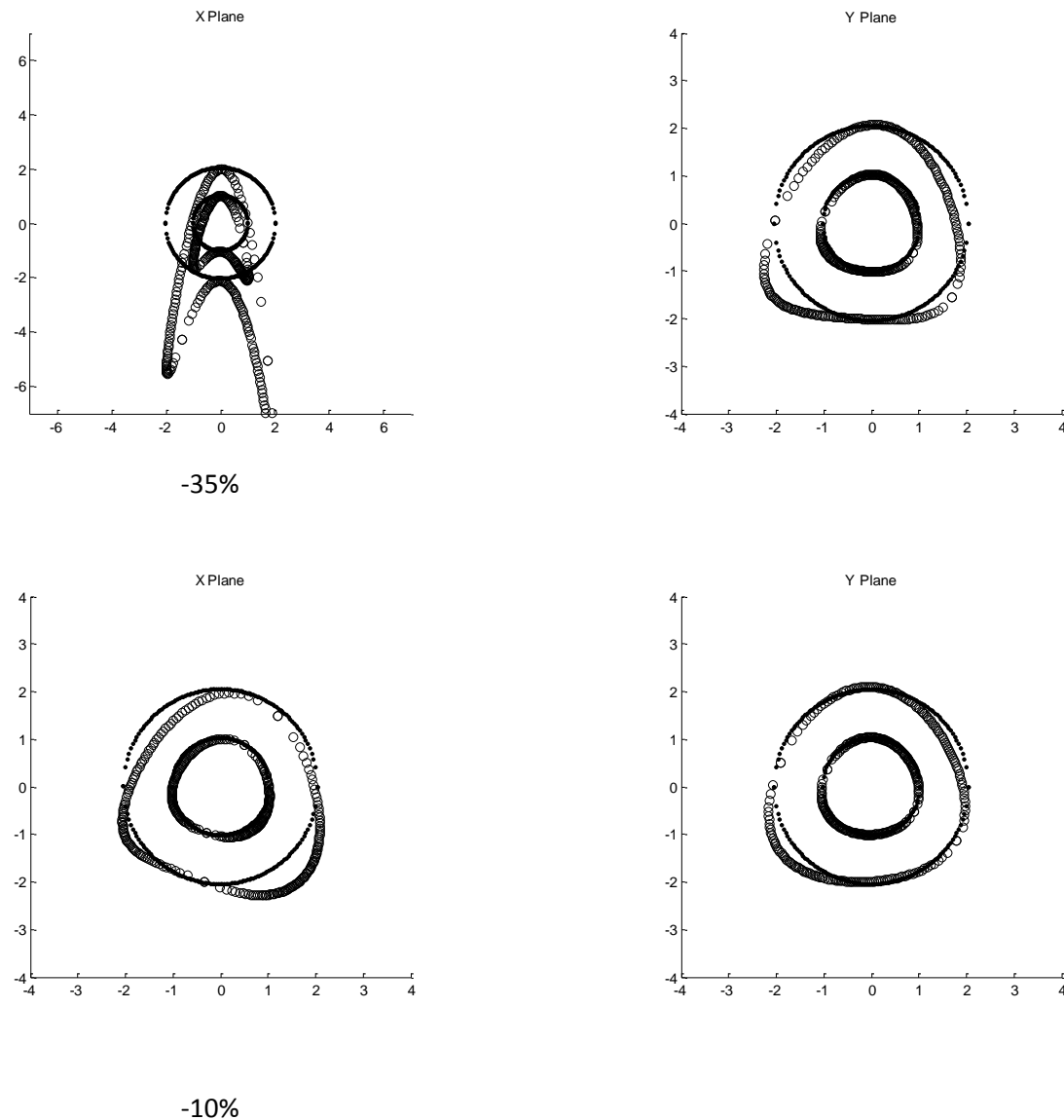


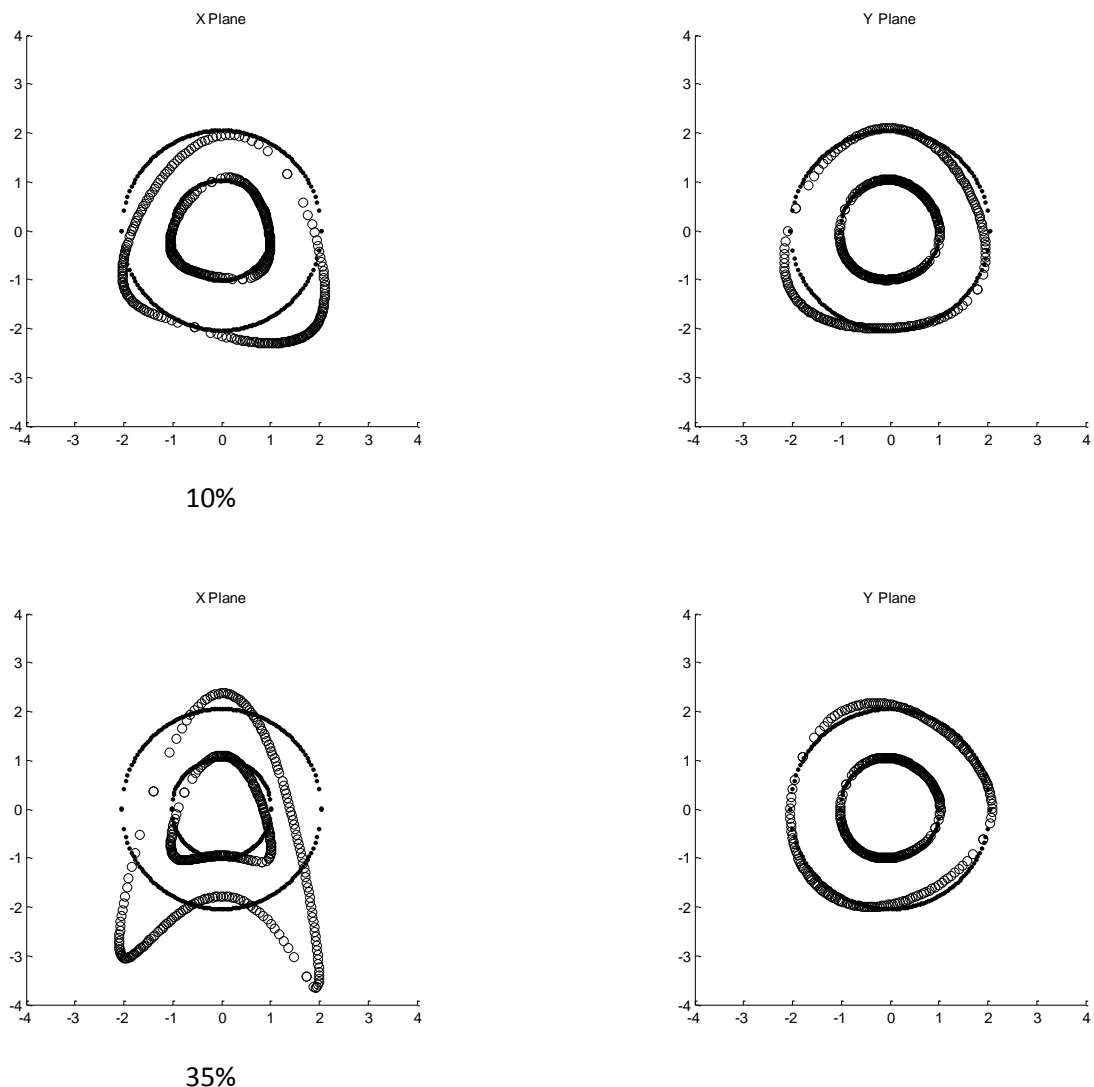
**Fig. 4.1B Variation in kick angles generated by sextupole magnets [Eq. 4.10 and 4.11] for  $R_{56} = -0.30$  m optics [50]**

Fig. 4.1A shows that at the tuned optics (0% on horizontal axis) for  $R_{56} = +0.30$  m, kick angles are larger in magnitude for both the planes than the optics tuned at the initial beta functions less than 20% from the present values. But figure shows clearly, that the kick angle is very sensitive to initial value of beta function at this reduced value. If optics is tuned to this lower values of beta function, where kick angles are close to minimum (near to zero), a slight variation in initial beta function brings a large change in kick angles. So even if this initial value provide a small kick angles, there are issues related to practical operation of line. At the tuned optics, variation in beta function does not bring a sudden change in kick angles and hence provide good robust operating conditions. In addition, at operating points, the dilutions in emittance due to kick angles are within the limit. Fig. 4.2A shows the distortion in phase space at different initial beta functions, obtained by tracking of electrons using MAD8. As the beta function becomes 35% lower than the chosen operating point, there is large distortion in phase space. Up to  $\pm 10\%$  change in initial beta function does not cause much distortion in phase space and confirms that the chosen operating point on the basis of kick angles are well

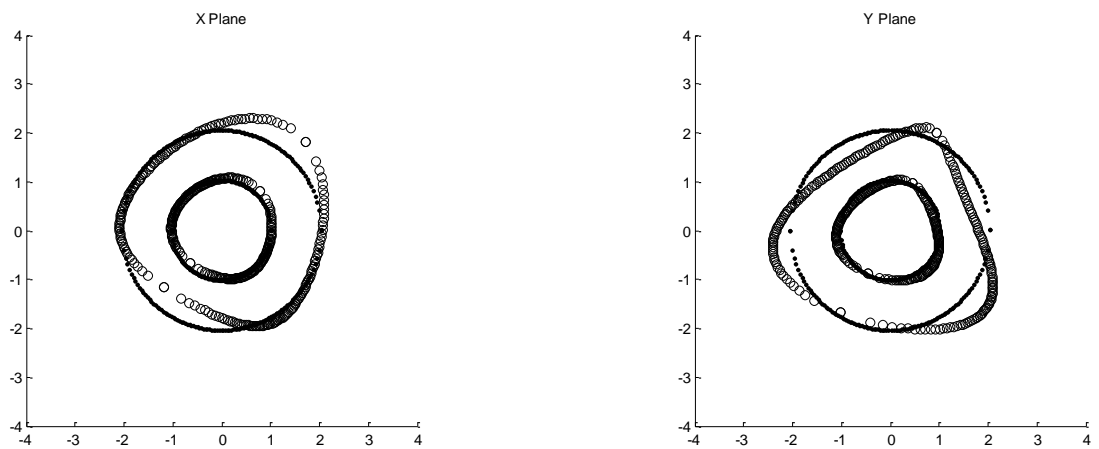
optimized. Due to change in initial beta function, at the location of sextupole magnets, phase independent term in kick angle (Eq. 4.10) changes rapidly, which brings sensitivity in kick angles for the initial values of beta function.

Fig. 4.1B shows that in case of  $R_{56} = -0.30$  m, the kick angles do not vary significantly with change in initial beta function. Therefore, here operating point is chosen where beta functions are not very high in Module-3. Very low sensitivity on kick angles with initial beta function for this optics is also confirmed by the tracking results, shown in Fig. 4.2B.

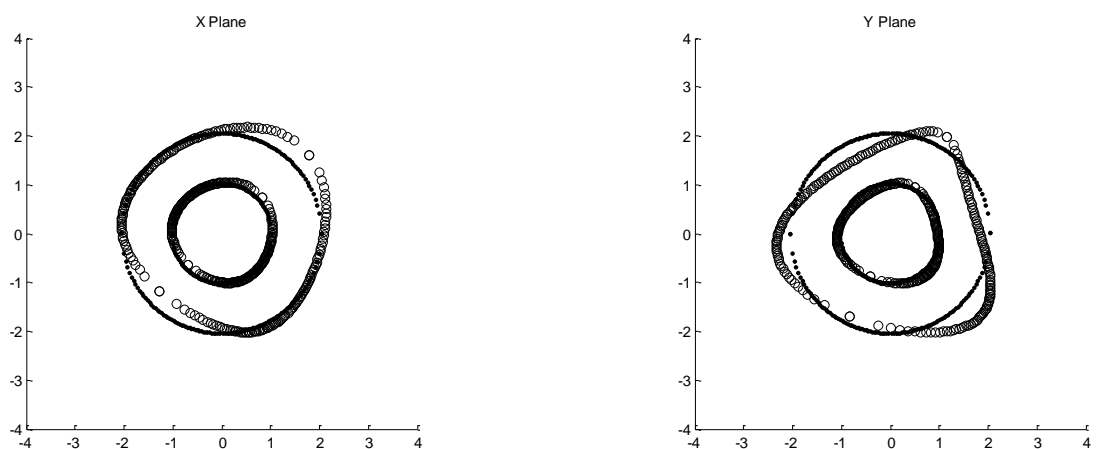




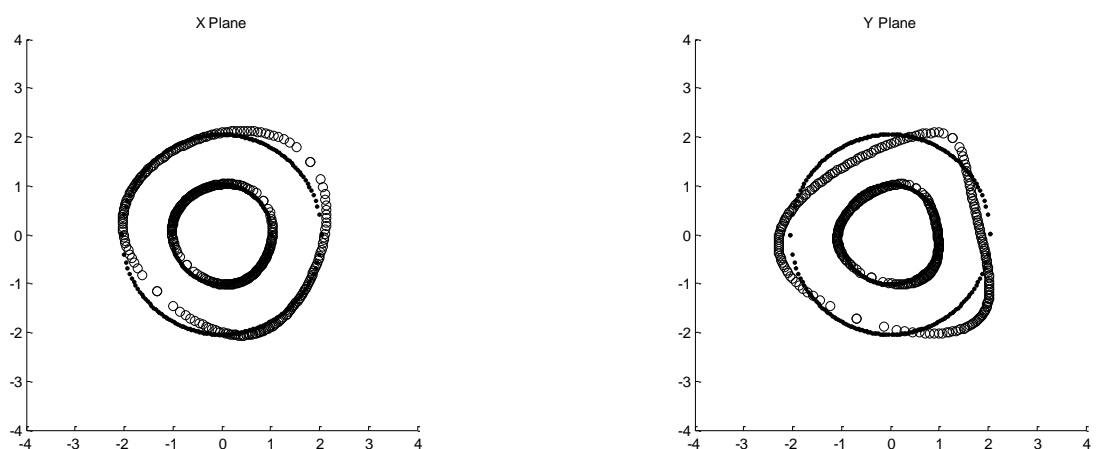
**Fig. 4.2A** Tracking results, showing phase space distortion in both the planes ( $1\sigma$  and  $2\sigma$ ) at different initial horizontal  $\beta$  function (-35%, -10%, +10% and +35%) at Module-3 for  $R_{56} = +0.30m$ . Horizontal scale is in mm and vertical is in mrad

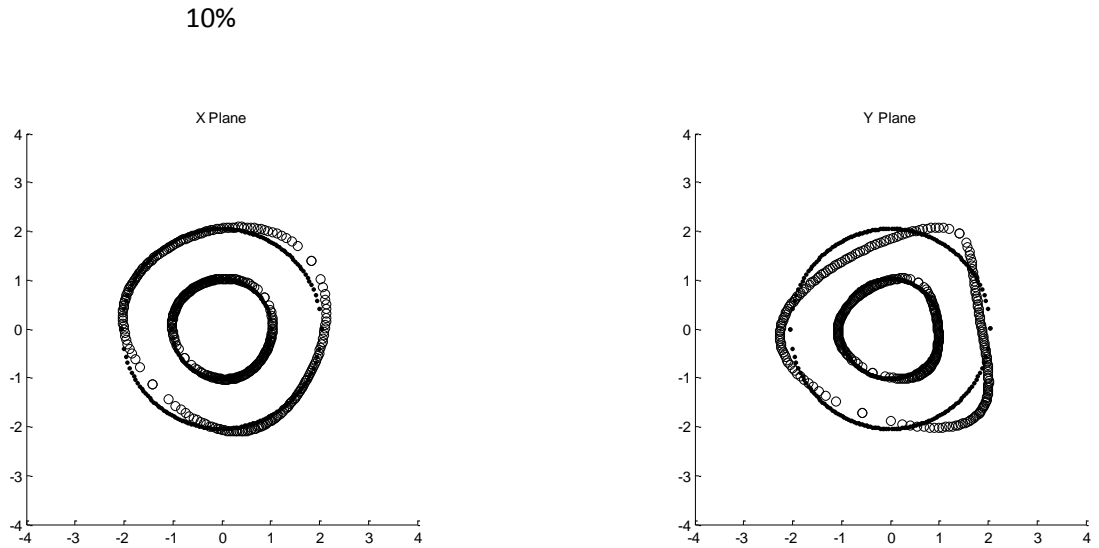


-35%



-10%

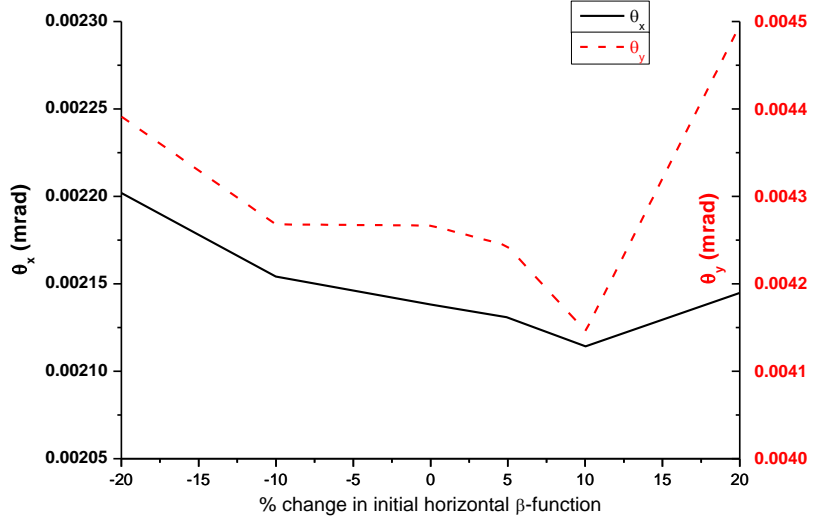




35%

**Fig. 4.2B Tracking results, showing phase space distortion in both the planes (1 $\sigma$  and 2 $\sigma$ ) at different initial horizontal  $\beta$  function (-35%, -10%, +10% and +35%) at Module-3 for  $R_{56} = +0.30\text{m}$ . Horizontal scale is in mm and vertical is in mrad**

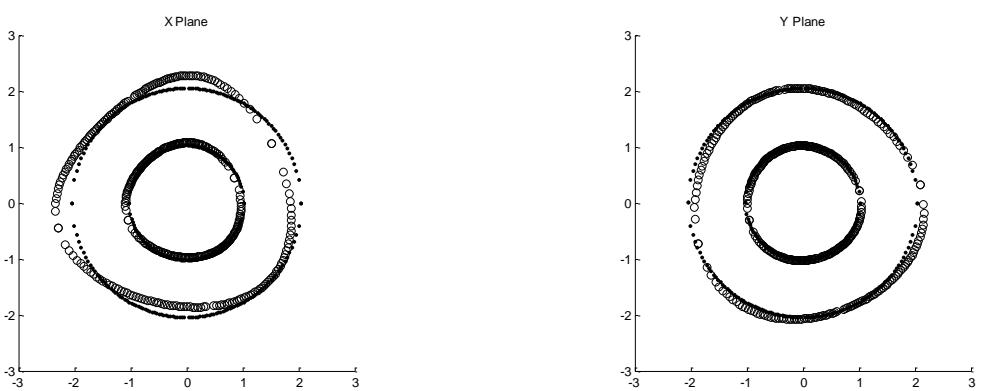
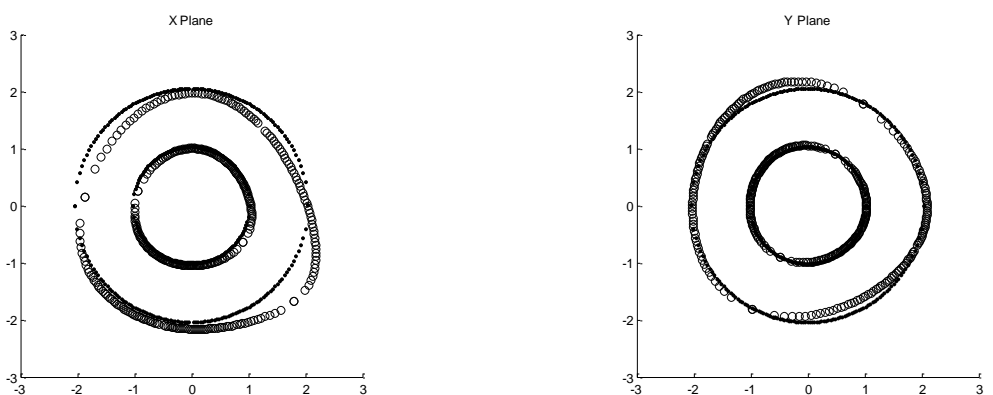
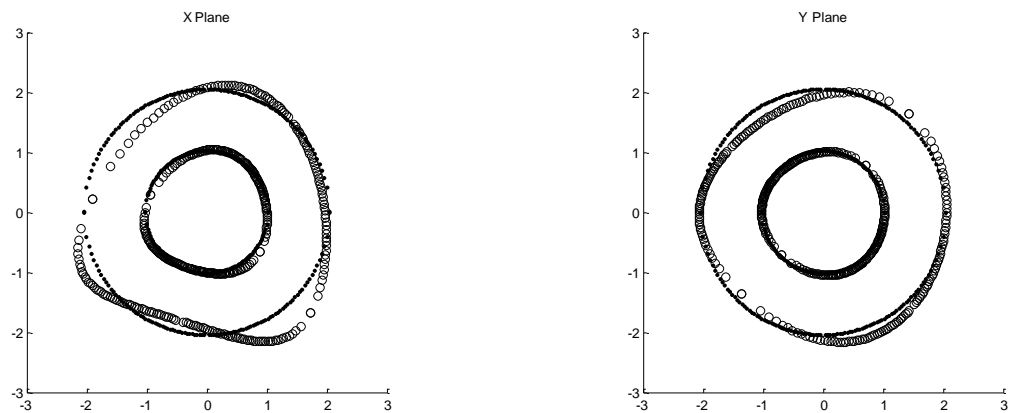
One more example for optimization of sextupole scheme through the kick computation is given in Fig. 4.3 for  $R_{56} = +0.25\text{ m}$  optics. This example is chosen because of the steep change in quadrupole settings from  $R_{56} = +0.30\text{ m}$  to  $R_{56} = +0.25\text{ m}$ .

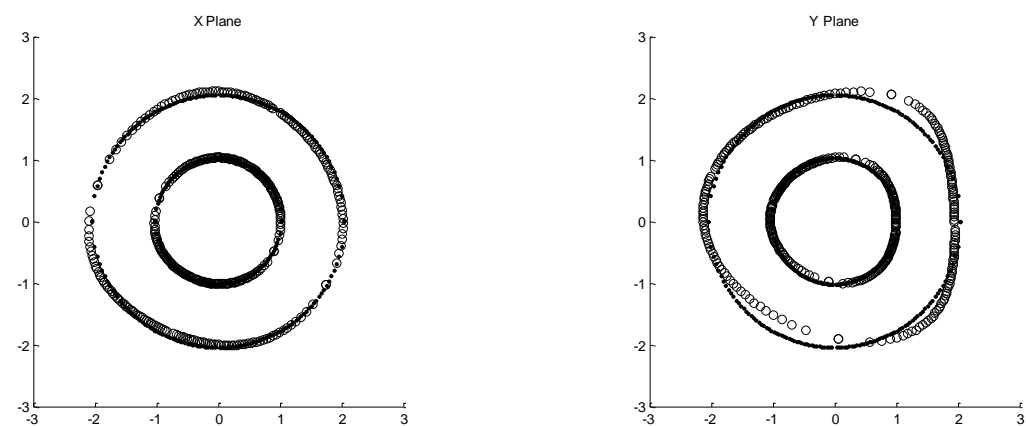
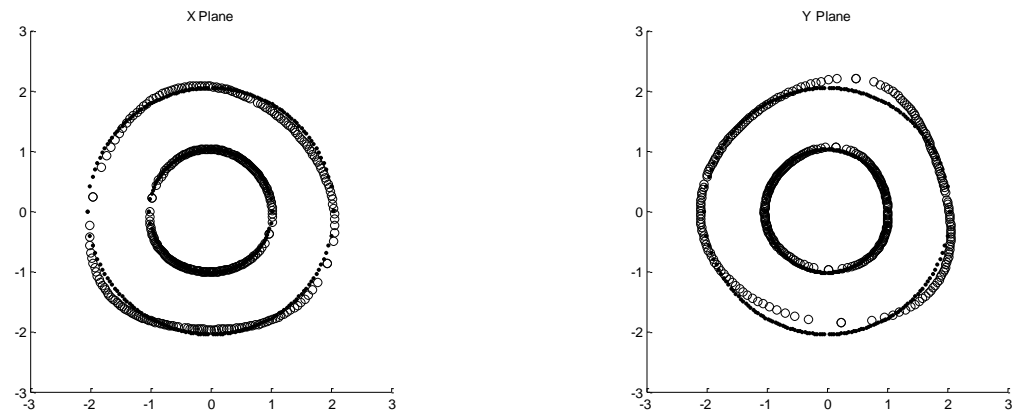
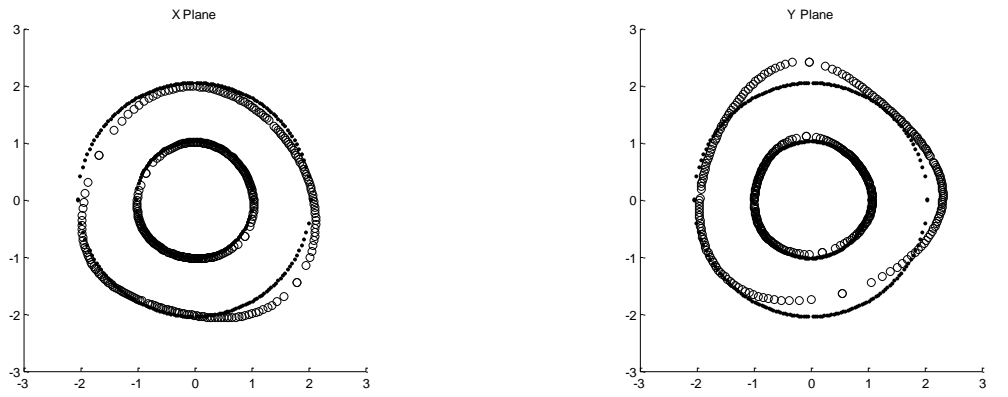


**Fig. 4.3 Variation in kick angles generated by sextupole magnets [Eq. 4.10 and 4.11] for  $R_{56} = +0.25 \text{ m optics}$**

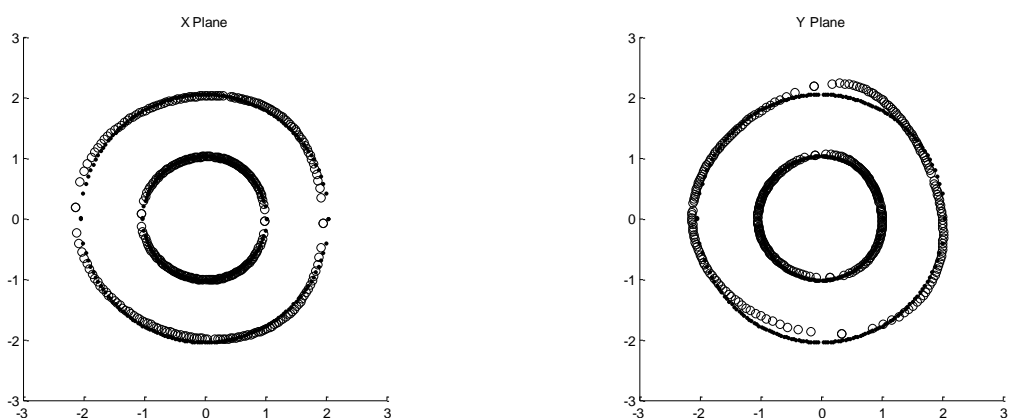
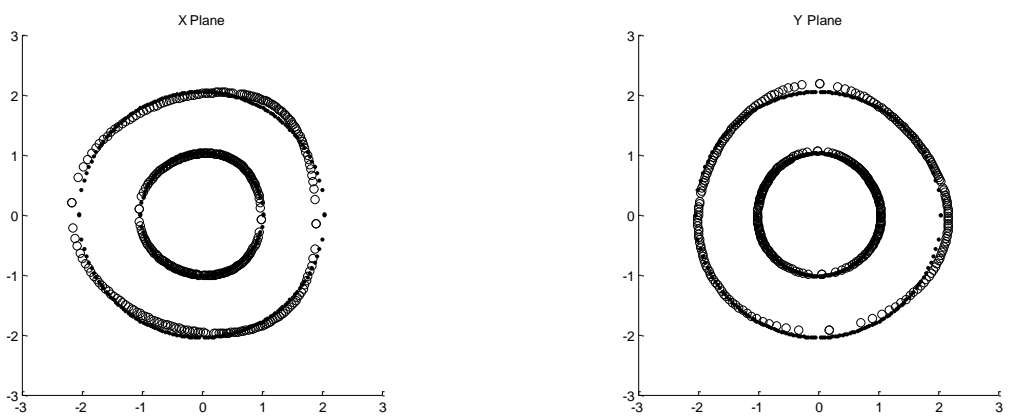
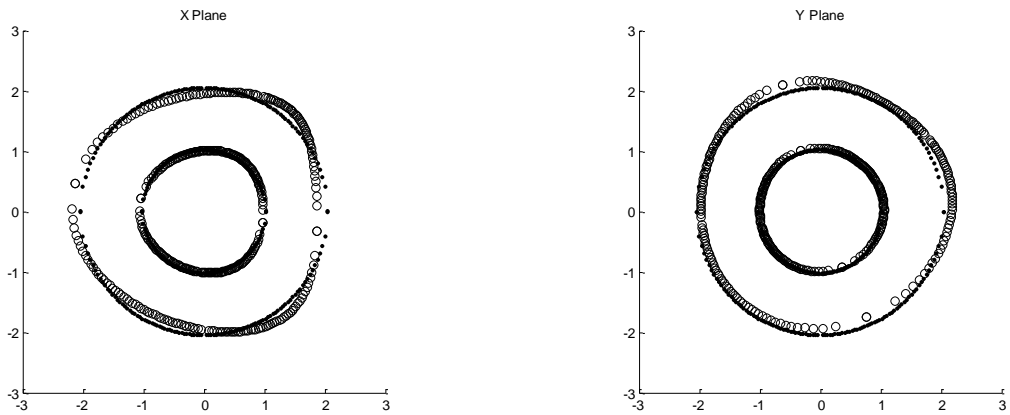
Kick angles are minimum for 10% higher horizontal beta function and therefore, phase space dilution will be minimum at this beta function. Again, here choosing a beta function different from the above (10% higher) value of initial horizontal beta function is based on the minimum among the beta-max values in both the planes. Also the optimum setting of optics is in the middle of almost stable kick angles. Kick angle increases steeply for beta function lower or higher by 10% from the chosen optimum values of initial beta functions.

Using this method, at each value of  $R_{56}$ , beta functions are optimized to minimize the kick angles, keeping the emittance dilution within control in presence of  $T_{566}$  correcting sextupole magnets. The tracking results for each  $R_{56}$  for optimized optics are shown in Fig 4.4A, 4.4B and 4.4C [50].





**Fig 4.4A Distortion in horizontal and vertical phase space in both the planes ( $1\sigma$  and  $2\sigma$ ) at positive  $R_{56}$  (0.30, 0.25, 0.20, 0.15, 0.10, and 0.05m) due to  $T_{566}$  correcting sextupoles in normalized phase space. Horizontal scale is in mm and vertical is in mrad**



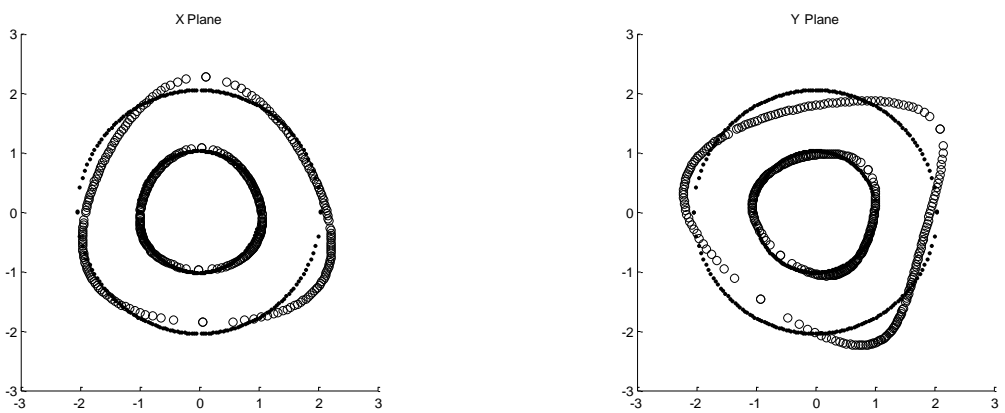
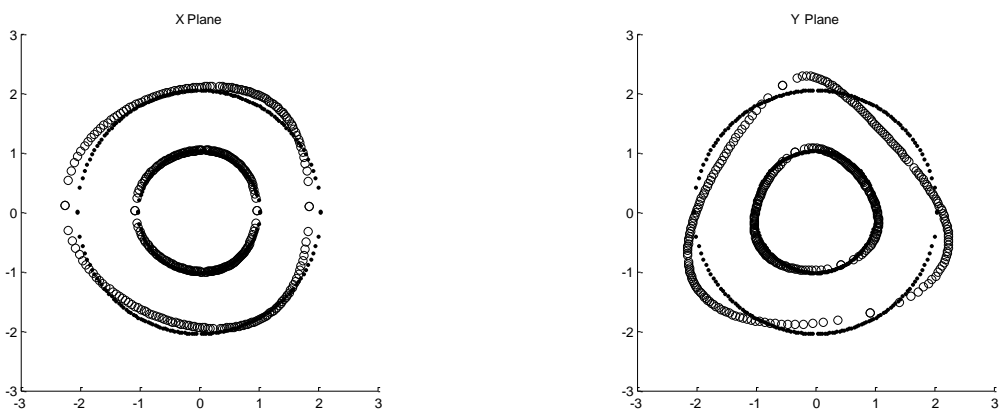
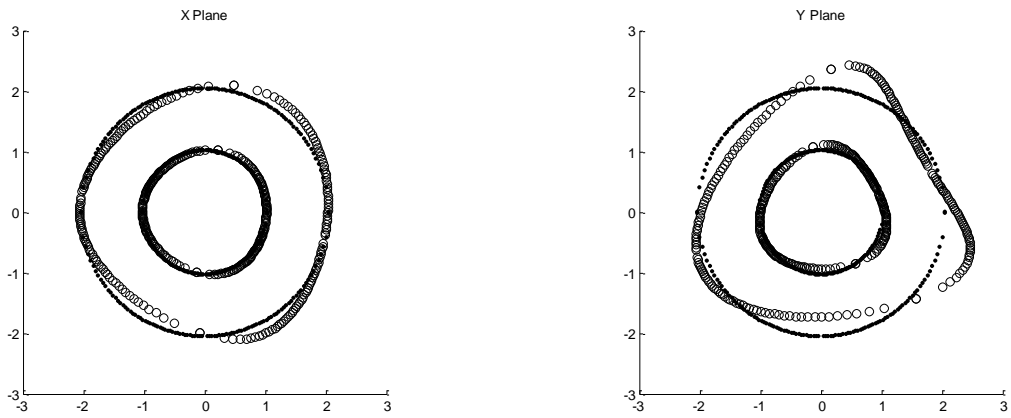


**Fig 4.4B Distortion in horizontal and vertical phase space in both the planes ( $1\sigma$  and  $2\sigma$ ) at negative  $R_{56}$  (-0.05, -0.10, -0.15, -0.20, -0.25 and -0.30m) due to  $T_{566}$  correcting sextupoles in normalized phase space. Horizontal scale is in mm and vertical is in mrad**

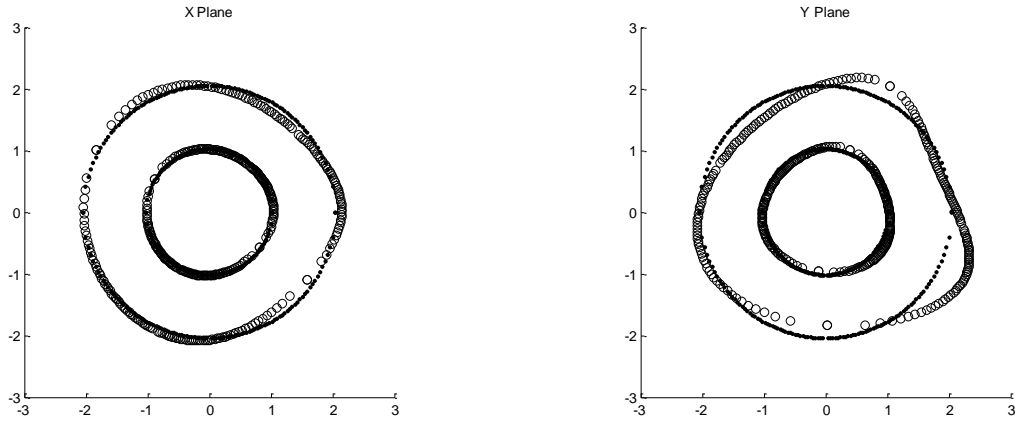


**Fig. 4.4C Distortion in horizontal and vertical phase space in both the planes (1 $\sigma$  and 2 $\sigma$ ) at zero  $R_{56}$  (isochronous mode) due to  $T_{566}$  correcting sextupoles in normalized phase space. Horizontal scale is in mm and vertical is in mrad**

Table 4.1A and 4.1B give the  $T_{566}$  for different values of  $R_{56}$  in TL-2 and the required sextupole strength to suppress the  $T_{566}$ .

**Table 4.1A: Sextupole strength ( $m^{-3}$ ) for  $T_{566}$  correction for positive and zero  $R_{56}$**

Sextupole	R <sub>56</sub> settings (m)						
	0.30	0.25	0.20	0.15	0.10	0.05	0.00
SX1	41.368925	26.797500	32.094230	42.307200	39.357680	42.531715	41.779525
SX2	OFF	OFF	OFF	OFF	-88.703140	-94.505860	-119.552150
SX3	OFF	OFF	OFF	OFF	88.703140	94.505860	119.552150
SX4	-41.368925	-26.797500	-32.094230	-42.307200	-39.357680	-42.531715	-41.779525
T <sub>566</sub> without sextupoles (m)	-38.710	-41.910	-37.205	-22.733	-25.272	-26.783	-27.650
T <sub>566</sub> after correction (m) $\times 10^4$	-7.443	3.358	-0.73	3.547	2.847	-9.118	-7.575

**Table 4.1B: Sextupole strength ( $m^{-3}$ ) for  $T_{566}$  correction for negative  $R_{56}$**

Sextupole	$R_{56}$ settings (m)					
	-0.05	-0.10	-0.15	-0.20	-0.25	-0.30
<b>SX1</b>	42.006775	41.902875	43.538175	43.616720	43.700000	43.703990
<b>SX2</b>	-112.543600	-115.361700	-127.993550	-126.457750	-154.538700	-135.895150
<b>SX3</b>	112.543600	115.361700	127.993550	126.457750	154.538700	135.895150
<b>SX4</b>	-42.006775	-41.902875	-43.538175	-43.616720	-43.700000	-43.703990
<b><math>T_{566}</math> without sextupoles (m)</b>	-31.541	-32.462	-28.467	-27.724	-16.761	-17.661
<b><math>T_{566}</math> after correction (m) <math>\times 10^{-4}</math></b>	7.005	-4.847	3.552	-3.760	-4.252	-3.200

## 4.2 Sextupole error in dipole magnets

In dipole magnets, sextupole components are main systematic errors. Design of dipole magnets for TL-2 were already available and it is essential to check if these errors are within tolerable limit or not. For estimating the allowable limit on sextupole component in dipole magnets, electrons within  $2\sigma$  beam sizes are tracked considering sextupole components at both the edges of each dipole magnet along with  $T_{566}$  correcting sextupole magnets. Tolerable error components in dipole magnets are estimated on the basis of  $\sim 5\%$  increase in beam size as compared to the beam size in the absence of sextupole errors. Table 4.2 shows the allowable error components at different  $R_{56}$  tuning.

**Table 4.2: Tolerable integrated sextupole component in dipole magnets for different  $R_{56}$**

*settings*

<b><math>R_{56}</math> (m)</b>	<b>Maximum tolerable sextupole strength (sl) (<math>m^{-2}</math>)</b>
+0.30	-2.0
0.00	-5.0
-0.30	-5.0

Above table shows that maximum allowable integrated sextupole error (*sl*) in a dipole magnet is  $-2 \text{ m}^{-2}$ . The sextupole component in the design of dipole magnets are well below this limit, hence there no problem is expected with sextupole errors in dipole magnets in the line.

## CHAPTER 5

### CSR STUDIES OF TRANSFER LINE-2

When the path of an electron is curved through a dipole magnet in a beam transport system or in an accelerator, it emits radiation, known as synchrotron radiation (SR) [32]. In an ultra-relativistic case, the emitted radiation is highly collimated in the forward direction. The electron therefore loses energy in the form of this radiation and energy loss increases rapidly with the electron energy. At shorter bunch length radiation may become coherent and significant amount of power is emitted in SR. This energy loss changes the beam dynamics and is one of the major concerns in the design of a bunch compressor. In this chapter, in first section, we provide a general but a very brief overview of synchrotron radiation and in next section, the effects of this radiation on beam parameters of a bunch compressor is discussed. In last section simulation results of TL-2 in presence of emitted radiation is presented.

#### 5.1 General overview of Synchrotron Radiation (SR)

In a bunch of  $N$  electrons, if distances between electrons are longer than the emitted wavelength, all electrons radiate independent of each other and the radiation is incoherent. The emitted radiation has a wide continuous spectrum as shown in Fig. 5.1. The incoherent radiated power from this bunch is given by [51]

$$P_{inc} = \frac{c}{6\pi\epsilon_0} \frac{Ne^2\gamma^4}{\rho^2} \quad [5.1]$$

Here  $\gamma$  is the relativistic factor and  $\rho$  is the radius of curvature of the path. Other symbols carry their usual meaning. The spectrum is characterised by one wavelength, known as critical wavelength ( $\omega_c = \frac{3c}{2\rho}\gamma^3$ ), which divides the emitted spectral power in two halves [52].

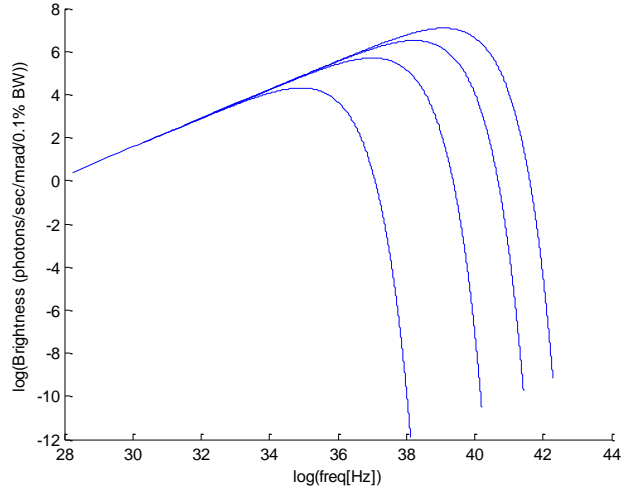


**Fig. 5.1 Spectrum of synchrotron radiation for four different electron beam energies (150 MeV, 300 MeV, 450 MeV and 600 MeV). Bending radius  $\rho$  is taken 1 m**

In other extreme case, when bunch length is very small as compared to emitted wavelength, all the electrons emit radiation as a single entity. In this case radiation is coherent and radiated power of coherent synchrotron radiation (CSR) is given by

$$P_{coh} = \frac{c}{6\pi\epsilon_0} \frac{N^2 e^2 \gamma^4}{\rho^2} \quad [5.2]$$

Here total power from the bunch is  $N^2$  times the power from a single electron. Between these two limits, the emitted power is partially coherent and is given by

$$P_{part-coh} = \frac{c\Gamma\left(\frac{5}{6}\right)}{6^{1/3}4\pi^{3/2}\epsilon_0\rho^{2/3}\sigma^{4/3}} \frac{N^2 e^2}{\rho^{2/3}\sigma^{4/3}} \quad [5.3]$$

The partially coherent power varies with bunch length ( $\sigma$ ), while incoherent and coherent power do not depend on the bunch length.

The emitted synchrotron radiation from electrons has a broad continuous spectrum ranging from micro waves to X-ray (Fig. 5.1). The radiation spectrum of an electron bunch in circular motion is given by [30, 53]

$$\frac{dP}{d\omega} = \frac{dP_1}{d\omega} \left\{ N + N(N-1)e^{-\left(\frac{\sigma\omega}{c}\right)^2} \right\} \quad [5.4]$$

$$\frac{dP_1}{d\omega} = \frac{\sqrt{3}e^2\gamma}{8\pi^2\epsilon_0\rho} \left( \frac{\omega}{\omega_c} \right) \int_x^\infty K_{5/3}(x') dx'$$

Here  $K_{5/3}$  is Bessel function. This spectrum consist of above mentioned three regimes i.e. incoherent, partially coherent and coherent, depending on the bunch length.

As the energy of the electron beam increases, spectrum shifts towards the right side i.e. towards higher frequencies (shorter wavelengths). Spectrum at lower frequencies (longer wavelengths) remains almost independent to beam energy. The spectrum at lower frequency side becomes coherent at shorter bunch lengths and intensity at lower side of spectrum increases with decreasing the bunch length. The three regimes of spectrum can be described using two bunch lengths, one is critical bunch length defined below

$$\sigma_c = \frac{2\rho}{3\gamma^3} \quad [5.5]$$

This critical bunch length is equal to critical wavelength vector of the emitted spectrum. If bunch length in a line becomes shorter than this bunch length, the emitted radiation becomes coherent. Second limiting bunch length depends on the number of electrons in a bunch and is given by

$$\sigma_{inc} = \sigma_c N^{3/4} \quad [5.6]$$

If bunch length is bigger than  $\sigma_{inc}$ , the emitted radiation is incoherent. Bunch length in between these two limits, emits radiation which is partially coherent. Fig 5.2 shows these three regimes with emitted power [30, 54]. Power is normalized to incoherent power and bunch length is normalized with critical bunch length.

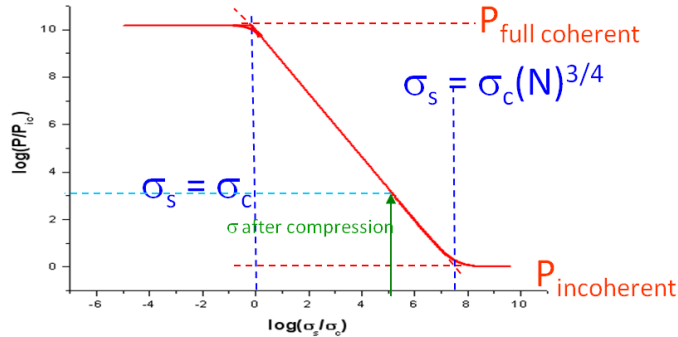


**Fig 5.2 Emited power (normalized) with bunch length (normalized)**

The maximum charge in TL-2 bunch is 2.33 nC, which gives number of electrons ( $N$ ) in the bunch as  $\sim 1.4 \times 10^{10}$ . The bunch length at the entrance of TL-2 is  $2.5 \times 10^{-3}$  m ( $\sim 8.3$  ps), which becomes after compression as  $4.5 \times 10^{-4}$  m ( $\sim 1.5$  ps). There are two types of dipole magnets in TL-2 and in the following table 5.1, parameters related to synchrotron radiation emitted by the electron bunch of 300 MeV at these two dipole magnets, used in Module-3 of TL-2 are provided.

**Table 5.1 CSR related parameters for TL-2 dipole magnets**

Parameter	Dipole-1	Dipole-2
Bending angle	30.75°	17.25°
Bending radius ( $\rho$ )	0.96518	0.89106
$\sigma_c$ (m)	$3.18 \times 10^{-9}$	$2.93 \times 10^{-9}$
$\sigma_{inc}$ (m)	$129.3 \times 10^{-3}$	$119.2 \times 10^{-3}$
$P_{inc}$ (W)	86.05	93.30
$P_{coh}$ (W)	$1.2 \times 10^9$	$1.3 \times 10^9$
$P$ in SR at the compressed $\sigma$ (W)	$152.5 \times 10^3$	$161.0 \times 10^3$
Log( $\sigma/\sigma_c$ )	5.15	5.18

Parameters in last two rows of the above table are computed at the finally compressed bunch length of  $\sim 1.5$  ps. Above table shows that the bunch length in TL-2 is not extremely short ( $\sigma \gg \sigma_c$ ) i.e. the emitted power is much less than the coherent power, but it is significantly higher than the incoherent power. In Fig. 5.2, green arrow marked the position of bunch size after compression in TL-2.

## 5.2 Effects of CSR on beam dynamics

The emitted radiation from the one electron can interact with the another electron of the bunch and therefore may have an effect on the dynamics. On the curved path of an electron bunch, the emitted radiation from the tail of the bunch follows a straight path and have interaction with head of the bunch. Fig. 5.3 shows a schematic of this mechanism.

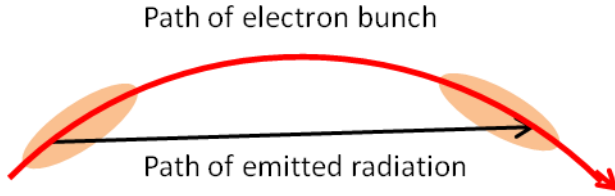


**Fig 5.3 Tail-head interaction of an electron bunch due to emitted CSR**

If bending angle in Fig 5.3 is  $\theta$ , then path length difference between electron trajectory and photon trajectory is

$$l \approx \frac{\rho\theta^3}{24} \quad [5.7]$$

Therefore, two electrons can interact if distance between these two, is smaller than this "slippage length". Thus tail-head interaction in a bunch of length  $\sigma$  is possible, if arc length of design trajectory is larger than  $l_o = (24\sigma\rho^2)^{1/3}$ .

All the formulations presented in the previous section is developed for a circular motion inside the magnetic field and therefore do not account for the finite length of a magnet. Radiative interaction of two electrons in a bunch, which leads to the generation of CSR, depends on the length of the magnet i.e. transient effects. These interaction with an account of transient and relativistic effects are described in Ref [55]. The total energy loss of a bunch in CSR is given by

$$E_{SR} = - \left( \frac{\frac{2}{3}N^2 e^2}{4\pi\epsilon_0\rho^{\frac{2}{3}}\sigma^{\frac{4}{3}}} \right) \rho\theta \left( 1 + \frac{\frac{1}{3}\frac{4}{3}}{9} \frac{\sigma^{\frac{1}{3}}}{\rho^{\frac{1}{3}}\theta} \left\{ \ln\left(\frac{\sigma\gamma^3}{\rho}\right) - 4 \right\} \right) \quad [5.8]$$

The formula is applicable for the range  $\frac{1}{\gamma} \ll \left(\frac{24\sigma}{\rho}\right)^{\frac{1}{3}} \leq \theta$

The total energy loss of a bunch is not much a problem rather than a redistribution of the energy inside the bunch. As bunch enters a magnet, a longitudinal force due to CSR is build up and this causes an energy redistribution in the bunch depending on the position of an electron inside the bunch. For 1D charge distribution, this change in energy with position in a bunch is also derived in Ref [55] and is given by

$$\frac{dE}{d(ct)} = -\frac{2e^2}{4\pi\epsilon_0 3^{\frac{1}{3}} \rho^{\frac{2}{3}}} \left\{ \left( \frac{24}{\rho\theta^3} \right)^{\frac{1}{3}} \left[ \lambda \left( s - \frac{\rho\theta^3}{24} \right) - \lambda \left( s - \frac{\rho\theta^3}{6} \right) \right] + \int_{s - \frac{\rho\theta^3}{24}}^s \frac{ds'}{(s - s')^{\frac{1}{3}}} \frac{d\lambda(s')}{ds'} \right\} \quad [5.9]$$

Here  $\lambda$  is the linear charge density of the bunch (as a function of  $s$ ). The first part in bracket shows the transient effects, which fade out in long magnets as the bunch progresses. The second part describes the transition to the steady state and reflects that the electrons which are closer than slippage length, have interaction.

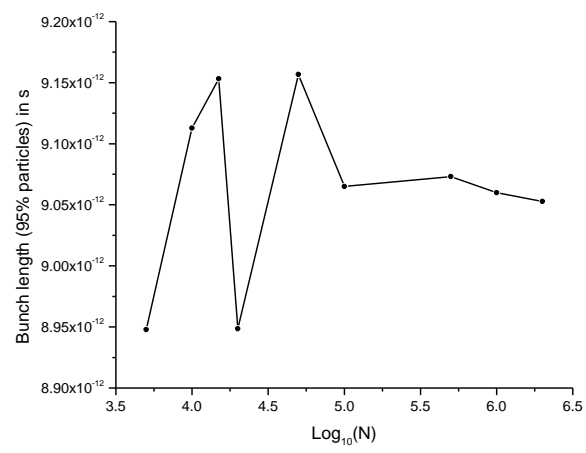
The emission of radiation and interactions take place on a curved path, where dispersion is non-zero. Thus each slice of the bunch along the propagation axis has betatron oscillations about the different trajectory due to difference of energy in each slice and overall emittance of the bunch increases. Due to this difference in energy of each slice, the slices also have different path lengths and distribution of electron in a bunch along the length also changes and effective bunch length may increase. In this way, CSR may increases transverse emittance and bunch length. It is thus necessary to study these effects.

Apart from the above mentioned longitudinal effects, there are also transverse effects in a curved path, however the effects of this transverse part on the beam dynamics is very small [56, 57].

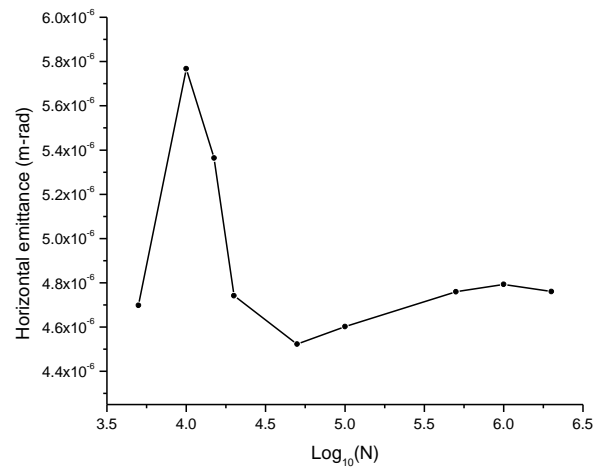
### 5.3 CSR simulation and studies for TL-2

Although it is stated in Section 5.1, bunch length are not extremely short in TL-2, however it still emits radiation which is partially coherent with a significant power. Therefore, it is essential to study the beam behaviour in TL-2 in presence of CSR. For simulating the behaviour of beam with CSR in TL-2, computer code ELEGANT [58] is used. This code is based on Saldin's model [59]. For computing the CSR, code bins the 'macro particle' arrival time at the end of each dipole piece and then this distribution is smoothed out using filters. Using this distribution, derivative of density with respect to  $s$  is obtained and then both parts of the Eq. 5.9 are computed. Using these calculations, energy kicks are applied to the each macro particle. This code does not take transverse distribution into account for this computation and also does not use true retarded time to save the computational time. Due to smoothening of density histogram using filters, number of macro particles in simulation becomes a critical parameter. Also the number of pieces of dipole magnets also becomes important [60].

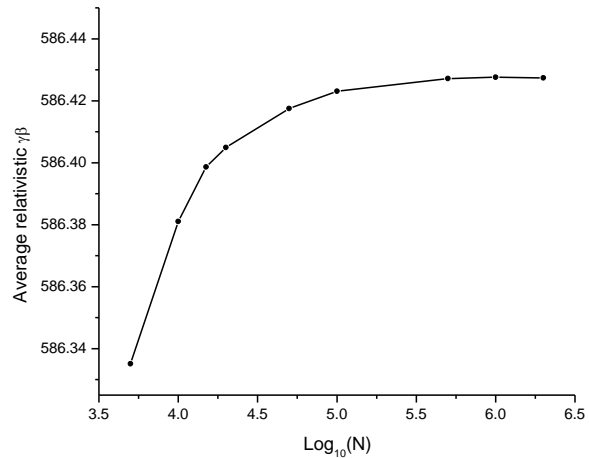
In our simulation to fix these parameters, we increased number of electrons (macro particles), number of pieces of dipole magnets, number of bins etc. to see the effects on the bunch length, transverse emittance and final energy of bunch after CSR loss. When these results becomes almost independent to the chosen parameters, we fixed theses parameters with slight increase in these values. Fig. 5.4 shows variation in simulation results with number of electrons at one of the selected  $R_{56}$  optics. The chirping is set to get the minimum bunch length from the optics.



(A) Bunch length variation with  $N$



(B) Horizontal emittance variation with  $N$



(C) Variation in final average bunch energy with  $N$

**Fig 5.4 Variation in beam parameters at exit from TL-2 for different number of electrons (macro particles) in the simulation [61]**

The finally chosen parameters for further study are as (1) Number of macro particles  $5 \times 10^5$  (2) Number of kicks in each dipole magnet 4 (3) Number of bins 500.

Fig. 5.5 shows the initial electron distribution (at the extraction septum of CR) in the electron bunch with  $1\sigma$  of  $\sim 2.5$  mm (8.3 ps). Final density distribution of the electrons in this bunch (at the end of  $R_{56}$  tuning arc) are shown in Fig. 5.6 at two extreme settings of tuning range ( $R_{56} = 0.30$  m and -0.30 m). The required compressed  $1\sigma$  of bunch length is  $\sim 0.45$  mm (1.5 ps). The distributions on each setting show bunch without considering CSR effects and with CSR effects, respectively.

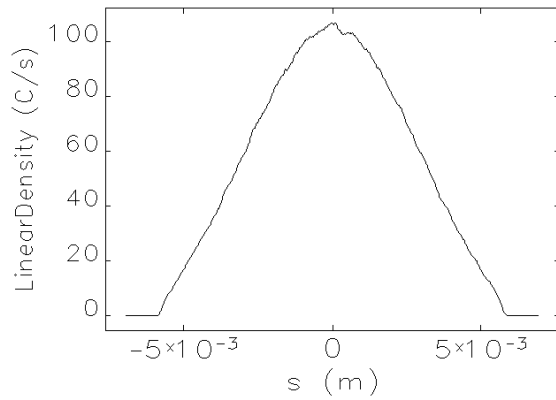
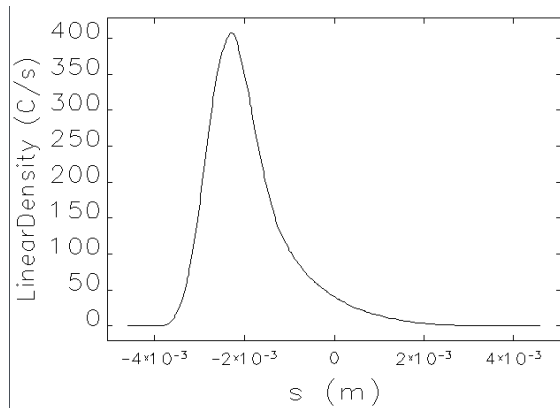
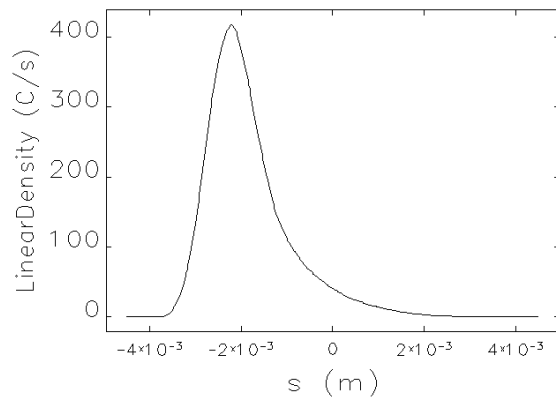


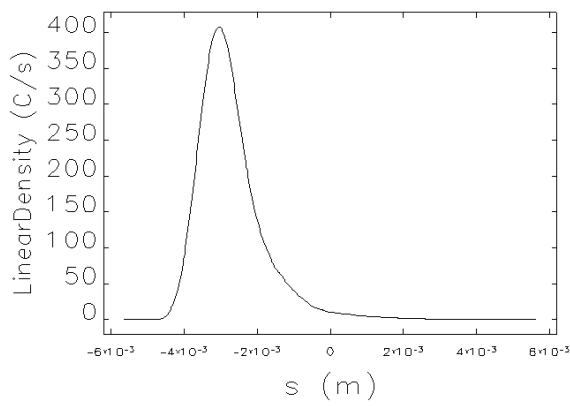
**Fig. 5.5 Initial electron distribution in bunch**



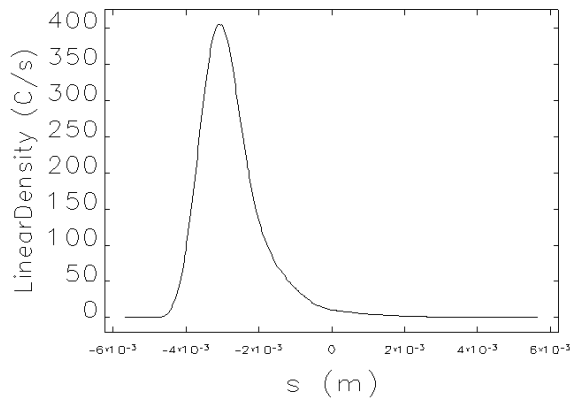
(A)  $R_{56}=0.30$  m without CSR



(B)  $R_{56}=0.30$  m with CSR



(C)  $R_{56}=-0.30$  m without CSR



(D)  $R_{56}=-0.30$  m with CSR

**Fig. 5.6 Electron density distribution in bunch along the longitudinal direction at different  $R_{56}$  settings without and with CSR effects [61]**

These results show that in the longitudinal direction, there is no any noticeable change. A very minute analysis shows that there is only very little (insignificant) redistribution of some electrons in the bunch. On these two important settings of  $R_{56}$ , transverse emittance are shown without and with CSR in Fig. 5.7. In transverse plane also CSR does not bring any change.

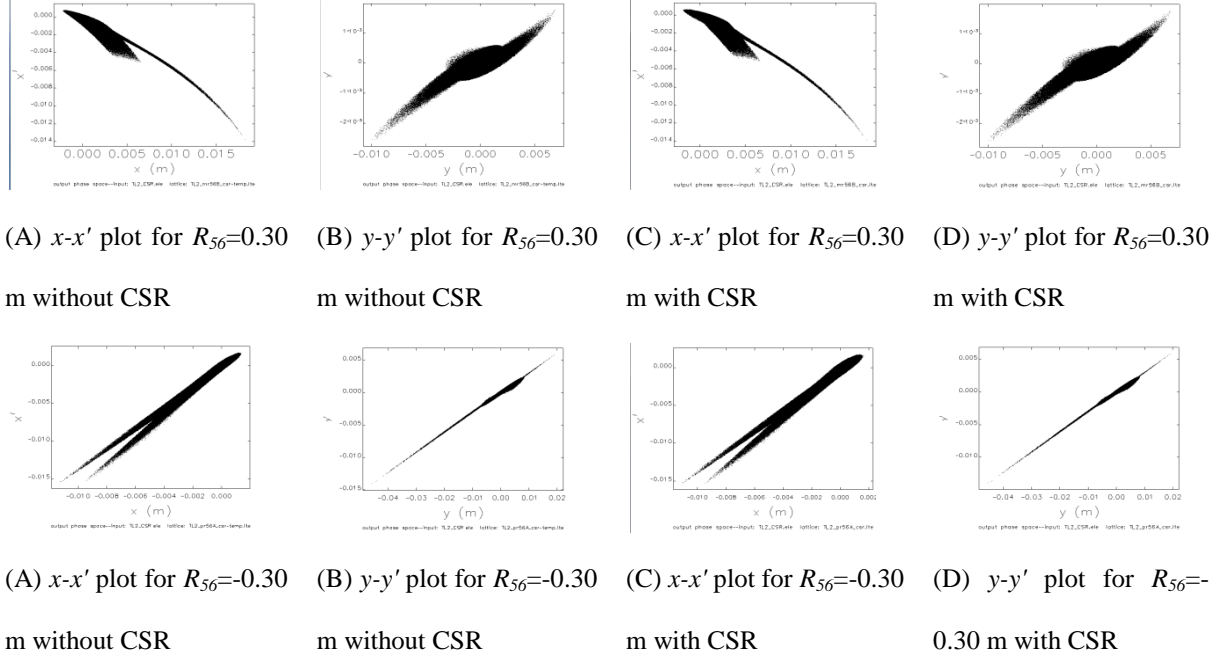


**Fig. 5.7 Horizontal and vertical phase space for extreme tuning of  $R_{56}$  with and without CSR effects [61]**

These studies show that CSR effects are not a serious problem in TL-2, up to 1.5 ps of bunch length. To see the effects of CSR, we further carried out studies by simulating the short bunches in TL-2 and noticeable CSR effects starts from the bunch length of  $\sim 0.5$  ps and shorter. Therefore TL-2 operating range is almost safe from the CSR point of view.

## CHAPTER 6

# ANALYTICAL MAP FOR DIPOLE MAGNET AND ITS APPLICATION TO BUNCH COMPRESSOR

The most important magnetic element in a bunch compressor is a dipole magnet. The maximum contribution and control in path length deviation due to momentum offset comes through dipole magnets in an optics. For compressing the bunch length with feasible values of  $R_{56}$  requires a large value of  $R_{65}$  i.e. large correlated momentum spread. Thus a precise path length computation requires higher order dependence of path length on momentum. For a high emittance beam, even geometric higher order terms can contribute to the path length. Therefore, for obtaining the precise final bunch length from an initial distribution of electrons in the beam in 6D phase space for a bunch compressor would require a higher order map for a dipole magnet. Although at very short bunch length, CSR related effects are more prominent than the nonlinear effects of dipole magnets, however it is always useful to have an exact analytical expression producing results, correct up to all orders.

Presently, analytically higher order maps are obtained either through inclusion of higher order perturbation terms in Hill's equation step by step and then using Green function theory to solve it or describing the magnet with a Hamiltonian and using Lie operator theory [21-23, 62-68]. In these methods, mathematical complexities are involved. We want to quote here from one of the landmark papers [67] in this field "*Indeed even if one is aware of the symplectic condition of the map generated by the Hamiltonian  $H$  of special relativity, it is not clear to most physicists that the return map from an arbitrary surface of section leads to a*

*canonical symplectic map in some properly selected coordinates. Without going into mathematical details which are obscure to most accelerator physicists, ..."*

The numerical integration for the equation of motion is available up to very high orders [69-71], but increasing order of integration in numerical simulations costs time. Besides this, it is not feasible to get an insight with the problem using numerical techniques. We have obtained an analytical formulation of map using hard edge approximation for dipole magnets, which is correct up to all orders and thus provides an alternate method. The formulation is obtained using geometrical arguments and therefore, no mathematical complexities are faced in understanding the problem with this alternate method. In Section 6.1 we present this formulation for a sector magnet. In Section 6.2, we showed an example of the bunch length computation using formulation and compared it with numerical methods for a chicane type bunch compressor. In subsequent section, we extended this formulation for wedge magnets.

## 6.1 Map for sector dipole magnet

In this section, we describe the geometry of a sector dipole magnet and then using geometrical methods, the map for a sector dipole magnet is obtained. Similar approach is used in work of Wollnik [72] to obtain the linear map of a dipole magnet. For describing the problem there are two co-ordinate systems, one is  $u$ - $v$  co-ordinate system in which  $u$ - $v$  plane is the median plane in which design trajectory bends. It is a fixed co-ordinate system whose origin coincides with the apex of the sector magnet and one of the co-ordinate axes coincide with the magnet edge. Other co-ordinate system  $x$ - $y$  is the usual accelerator co-ordinate system. The geometry is shown in Fig 6.1 [73]. The arc marked by  $\mathbf{C}_1$  is the design trajectory and defines the  $x$ - $y$  co-ordinate system (usual accelerator co-ordinates). The radius of curvature and bending angle for the design trajectory are  $\rho$  and  $\theta$  respectively. Let us choose

another particle, deviated from the design trajectory and this enters the magnet at the point **B**. Its trajectory is defined by the arc **C**<sub>2</sub> in the figure. The displacement and angle with respect to design trajectory at the entrance of this particle are  $x_i$  and  $\alpha_i$ , respectively. Let the momentum deviation of the particle be  $\delta$ . At the exit of the magnet, the displacement and angle of this particle with design trajectory are  $x_e$  and  $\alpha_e$ , respectively. The aim is to find a map which provides  $x_e$  and  $\alpha_e$  as a function of  $x_i$ ,  $\alpha_i$  and  $\delta$ .

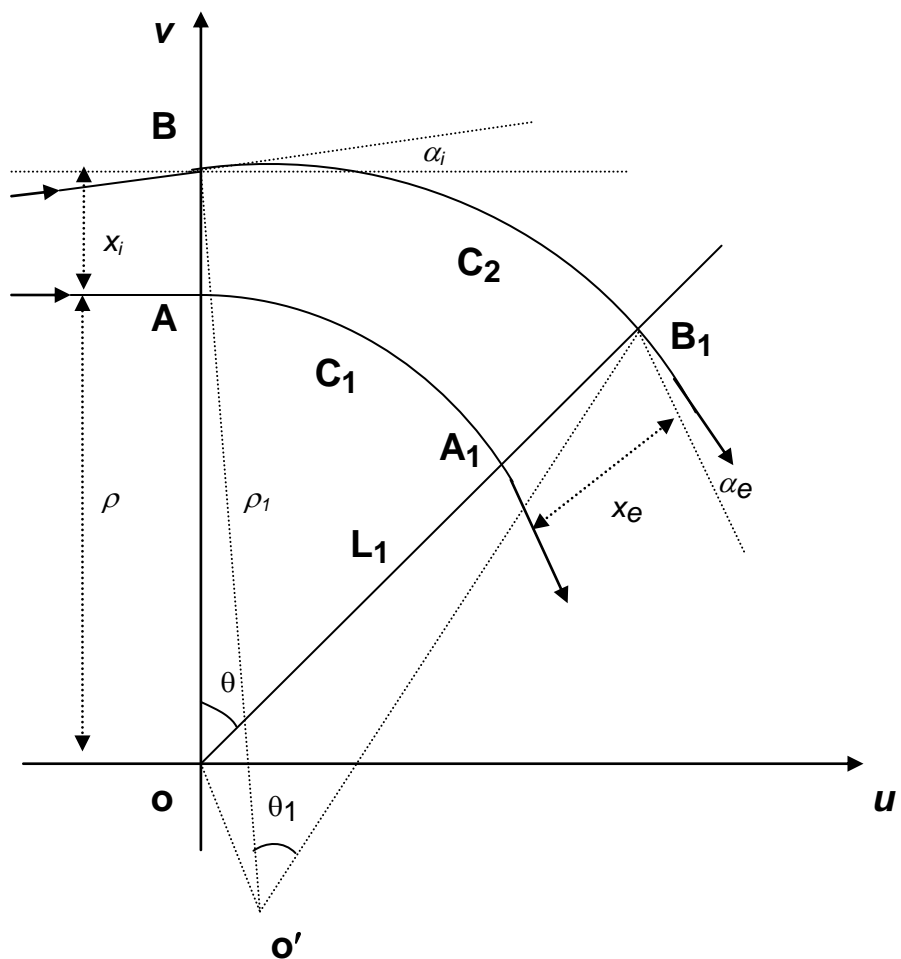


**Fig 6.1 Geometry of the sector dipole magnet with co-ordinate system and particle trajectory**

The trajectory **C**<sub>2</sub>, traced by the deviated particle has a radius of curvature  $\rho_l$  with the centre at O'. Let co-ordinates of the centre  $(u_c, v_c)$  in the fixed co-ordinate system. The bending

angle for this arc is  $\theta_l$ . The co-ordinates of the centre as a function of initial co-ordinates and radius of curvature  $\rho_l$  is given by

$$u_c = \rho_l \sin \alpha_i \quad [6.1]$$

$$v_c = (x_i + \rho) - \rho_l \cos \alpha_i \quad [6.2]$$

Here  $\rho_l = \rho(1 + \delta)$ . This deviated particle exits from the magnet at point **B**<sub>1</sub> ( $u_1, v_1$ ) and its exit co-ordinates are following

$$u_1 = (\rho + x_e) \sin \theta \quad [6.3]$$

$$v_1 = (\rho + x_e) \cos \theta \quad [6.4]$$

From Eq. 6.3 we get

$$x_e = \frac{u_1}{\sin \theta} - \rho \quad [6.5]$$

The angle at the exit can be obtained by taking the difference between the slopes of two trajectories **C**<sub>1</sub> and **C**<sub>2</sub> at points **A**<sub>1</sub> and **B**<sub>1</sub> as following

$$\alpha_e = \tan^{-1} \left( -\frac{u_1 - u_c}{m u_1 - v_c} \right) - \tan^{-1} \left( -\frac{1}{m} \right) \quad [6.6]$$

Here the  $\theta_{c1} = \tan^{-1} \left( -\frac{1}{m} \right)$  and  $\theta_{c2} = \tan^{-1} \left( -\frac{u_1 - u_c}{m u_1 - v_c} \right)$  are the slopes of trajectories **C**<sub>1</sub> and **C**<sub>2</sub> at points **A**<sub>1</sub> and **B**<sub>1</sub> respectively. In these expressions,  $m$  ( $= \cot \theta$ ) is the slope of the exit

edge of the dipole magnet. Eq. 6.5 and 6.6 give co-ordinates of the deviated particle at the exit of the magnet and both of these co-ordinates depend on the co-ordinate  $u_1$ . If  $u_1$  can be expressed exactly as a function of initial co-ordinates and momentum offset of the particle, exact map for a hard edge sector magnet can be obtained. Point **B<sub>1</sub>** in Fig. 6.1 is an intersection point of circle **C<sub>2</sub>** and edge **OB<sub>1</sub>**. Therefore, it is a common point for these two following curves

$$(u - u_c)^2 + (v - v_c)^2 = \rho_1^2 \quad [6.7]$$

$$v = mu \quad [6.8]$$

These two equations above, give the intersection point  $u_1$  as following

$$u_1 = \frac{u_c + mv_c}{1+m^2} \pm \frac{\rho(1+\delta)}{\sqrt{1+m^2}} \sqrt{(1+P)(1-Q)} \quad [6.9]$$

Here

$$P = \frac{(u_c + mv_c)^2}{(1+m^2)} \frac{1}{\rho_1^2} \frac{1}{(1-Q)} \quad [6.10]$$

and

$$Q = \frac{u_c^2 + v_c^2}{\rho_1^2} \quad [6.11]$$

Using Eq. 6.9 in 6.5 and 6.6 provides the co-ordinates of the deviated particles at the exit of the magnet as a function of initial co-ordinates and momentum offset i.e. it is a map in the median plane of a sector magnet. There are no approximations, except that the hard edge is used in deriving these expressions and therefore, the map is exact up to all orders.

Now we add another degree of freedom i.e. particle at the entrance is inclined at an angle  $\beta_i$  with the median plane and a displacement of  $y_i$  in vertical direction. For this trajectory, magnetic field will not be in the perpendicular direction to the plane of motion. In this case, the particle will trace out a trajectory, which will be a part of a helix ( $\mathbf{AA}_2$ ) and particle will exit from the magnet with a vertical displacement of  $y_e$ . The geometry is shown in Fig. 6.2. The effective magnetic field for bending the trajectory is  $B \cos \beta_i$  and radius of curvature ( $\rho'_1$ ) for helix path will be  $\rho_1 / \cos \beta_i$ . Due to helix, this trajectory will follow a longer path inside the dipole magnet than the trajectory without inclination to the median plane and due to this longer path, co-ordinates  $x_e$  and  $\alpha_e$  will be modified. Due to changed radius of curvature, the projection of trajectory  $\mathbf{AA}_2$  on the median plane  $\mathbf{AA}'_1$  will be different from the trajectory  $\mathbf{AA}_1$ , which is the path of the particle having same initial condition except initial vertical angle. This shows the origin of coupling in the motion in a dipole magnet.

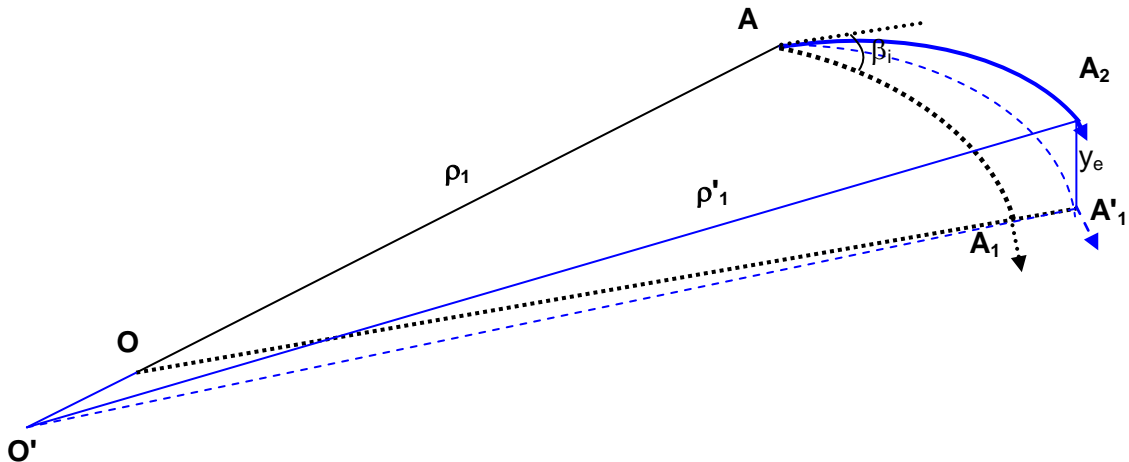


**Fig. 6.2 Trajectory of a particle having vertical inclination ( $\beta_i$ ) from the median plane**

The centre of curvature for the trajectory of this particle is  $\mathbf{O}'$  and its co-ordinates are given by following relations

$$u_c' = \rho_1' \sin \alpha_i = \frac{\rho_1 \sin \alpha_i}{\cos \beta_i} \quad [6.12]$$

$$v_c' = (x_i + \rho) - \rho_1' \cos \alpha_i = (x_i + \rho) - \frac{\rho_1 \cos \alpha_i}{\cos \beta_i} \quad [6.13]$$

Replacing values of  $u_c$ ,  $v_c$  and  $\rho_1$  in Eq. 6.9, 6.10 and 6.11 by  $u_c'$ ,  $v_c'$  and  $\rho_1'$  from above expressions, provide  $u_1$  for the particle with vertical angle  $\beta_i$ . Using this value of  $u_1$  in Eq. 6.5 and 6.6, the horizontal co-ordinate  $x_e$  and angle  $\alpha_e$  at the exit of the magnet can be obtained for this particle.

In order to obtain the vertical co-ordinate at the exit, the path length dependence on initial horizontal co-ordinate  $x_i$  and angle  $\alpha_i$  is to be known. The path length in the median plane can be obtained by integrating the circular trajectory from initial to final co-ordinates in the fixed  $u-v$  co-ordinate system.

$$S = \int_{u=0}^{u=u_1} \sqrt{1 + \left\{ \frac{dv}{du} \right\}^2} du = \int_0^{u_1} \frac{\rho_1}{v - v_c} du = \rho_1 \int_0^{u_1} \frac{1}{\sqrt{\rho_1^2 - (u - u_c)^2}} du$$

$$S = \rho_1 \left[ \sin^{-1} \left( \frac{u_1 - u_c}{\rho_1} \right) - \sin^{-1} \left( \frac{-u_c}{\rho_1} \right) \right] \quad [6.14]$$

For the particle, entering the magnet at a vertical angle  $\beta_i$ , the co-ordinates  $u_c$  and radius of curvature  $\rho_1$  will be replaced by  $u'_c$  and  $\rho_1'$  respectively. For this inclined trajectory, the path length ( $S'$ ) becomes  $S/\cos \beta_i$ . The path length of the design trajectory is given by

$$S_0 = \rho \theta$$

The difference between  $S'$  and  $S_0$  provides path length deviation of a particle's trajectory from the design trajectory and it is one of the most important parameters in the bunch compressor. Using  $S$ , the vertical exit co-ordinate  $y_e$  can be obtained by the following relation

$$y_e = y_i + S \tan \beta_i \quad [6.15]$$

The vertical angle at the exit  $\beta_e$  is same as initial vertical angle  $\beta_i$ . Above mentioned procedure gets all the co-ordinates ( $x_e$ ,  $\alpha_e$ ,  $y_e$ ,  $\beta_e$  and path length) as a function of initial co-ordinates ( $x_i$ ,  $\alpha_i$ ,  $y_i$ ,  $\beta_i$  and  $\delta$ ). In this procedure, no any approximation except hard edge is assumed and final expressions are purely algebraic in nature i.e. no differentials or integrals are required and hence expressions can be calculated analytically completely. The complete procedure is outlined in Fig. 6.3, given below.

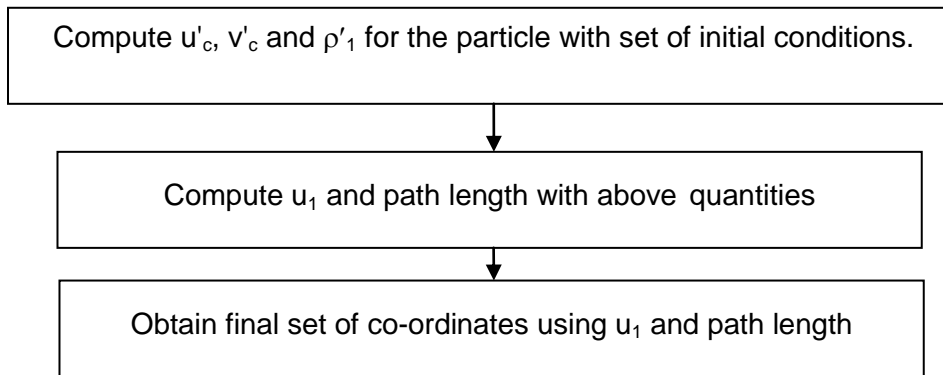


**Fig 6.3 Procedure for obtaining final co-ordinates of a particle travelled through a sector dipole magnet as a function of initial co-ordinates**

These analytical results are applied to a sector dipole magnet with a bending angle of  $30.75^\circ$  and a bending radius of 0.96 m. A Gaussian distributed beam of 3000 particles in 6D is taken and the final bunch length and transverse emittance growth of this beam is studied as a function of initial bunch length and transverse emittance. Results are compared with

numerical results using MAD8. In computation, difference in bunch length is found with increase in initial transverse emittance between the analytical and numerical results. The difference is due to effect of transverse geometrical terms on bunch length. In Fig. 6.4, results are depicted in which a monochromatic beam of correct energy is tracked through the magnet.

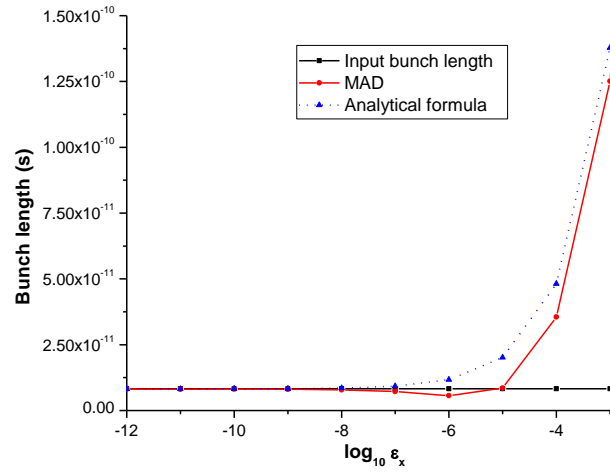


**Fig. 6.4 Variation in final bunch length with initial transverse emittance in m-rad. Initial bunch length is taken as 8.3 ps.**

The effect on transverse emittance growth is almost same for analytical and numerical results. There is also difference between the analytical and numerical results for the final bunch length as a function of initial bunch length for a monochromatic beam of correct energy. this deviation is plotted in Fig. 6.5. The deviation increases to  $\sim 10\%$  for very short initial bunch length (sub ps range). Again, transverse emittances are almost same, obtained analytically and numerically.

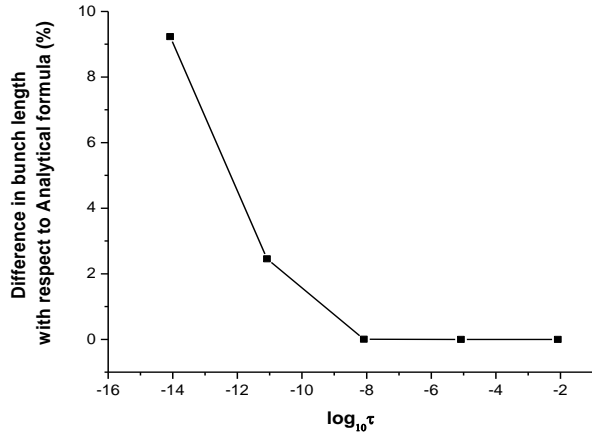
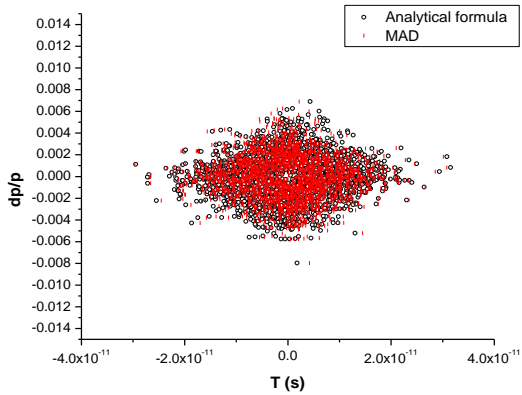


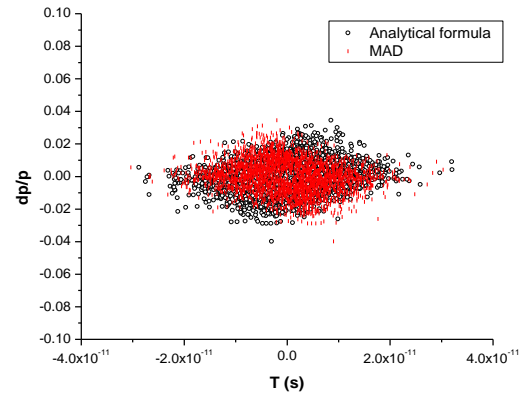
**Fig. 6.5 Variation in difference in final bunch length obtained from analytical expression and MAD as a function of initial bunch length ( $\tau$  in s)**

These results show that the bunch length obtained by analytical expressions deviates from the numerical computation and therefore these expressions are important for estimating correct bunch length from a bunch compressor.

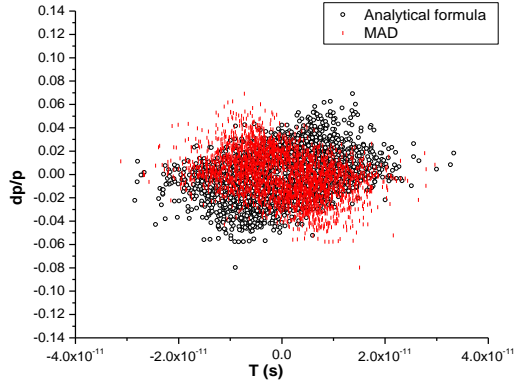
Including momentum spread in initial beam (instead of monochromatic beam), does not bring much deviation in the results of transverse plane from analytical expressions and numerical computation. However, there is difference in longitudinal phase plane, which increases with increase in momentum spread. Fig. 6.6 shows the results for a 8.3 ps initial bunch length.



Initial emittance ( $10^{-9}$  m-rad in both the planes);  $\Delta p/p = 0.2\%$  ( $1\sigma$ ) and bunch length 8.3ps ( $1\sigma$ )



Initial emittance ( $10^{-9}$  m-rad in both the planes);  $\Delta p/p = 1\%$  ( $1\sigma$ ) and bunch length 8.3ps ( $1\sigma$ )



Initial emittance ( $10^{-9}$  m-rad in both the planes);  $\Delta p/p = 2\%$  ( $1\sigma$ ) and bunch length 8.3ps ( $1\sigma$ )

**Fig. 6.6 Longitudinal phase space after passing through magnet (obtained from MAD and formula)**

## 6.2 Validation of the derived analytical map

The derived expressions for the map encompasses all the orders and are exact in hard edge approximation. In this section, we carry out analysis of the derived map by separating different terms of each order and show that formulation provides the usual expressions.

### 6.2.1 Linear terms

In first order,  $u_c$  and  $v_c$  becomes (from Eq. 6.1 and 6.2)

$$u_c \approx \rho\alpha_i \text{ and } v_c \approx x_i - \rho\delta_i$$

The co-ordinates  $u_c$  and  $v_c$  contain minimum first order terms in initial co-ordinates i.e. these do not contain constant terms and thus  $P$  and  $Q$  will contain minimum second order terms (see Eq. 6.10 and 6.11). Therefore,  $u_1$  can be written up to first order easily as

$$u_1 \approx \frac{\rho}{\sqrt{1+m^2}} + \frac{m}{1+m^2} x_i + \frac{\rho}{1+m^2} \alpha_i - \frac{m\rho}{1+m^2} \delta + \frac{\rho}{\sqrt{1+m^2}} \delta$$

Now using Eq. 6.5,  $x_e$  can be obtained

$$x_e \approx \frac{m}{\sqrt{1+m^2}} x_i + \frac{\rho}{\sqrt{1+m^2}} \alpha_i - \frac{m\rho}{\sqrt{1+m^2}} \delta + \rho\delta$$

Putting the value of  $m=\cot\theta$  in above expression gives  $x_e$  finally as follows

$$x_e \approx \cos\theta \cdot x_i + \rho \sin\theta \cdot \alpha_i + \rho(1-\cos\theta)\delta \quad [6.16]$$

This is the usual first order relation for a sector dipole magnet. Using trigonometric identity, Eq. 6.6 can be reduced to

$$\alpha_e = \tan^{-1} \left\{ \left[ -\frac{1}{m} \left( 1 - \frac{u_c}{u_1} \right) \left( 1 - \frac{v_c}{mu_1} \right)^{-1} + \frac{1}{m} \right] \left[ 1 + \frac{1}{m^2} \left( 1 - \frac{u_c}{u_1} \right) \left( 1 - \frac{v_c}{mu_1} \right)^{-1} \right]^{-1} \right\}$$

After simplification, this expression can be written as

$$\alpha_e = \tan^{-1} \left[ -\frac{mZ}{1+m^2} \left( 1 + \frac{Z}{1+m^2} \right)^{-1} \right] \quad [6.17]$$

$$\text{Here } Z = \left( \frac{v_c}{m} - u_c \right) u_1^{-1} + \frac{v_c}{m} \left( \frac{v_c}{m} - u_c \right) u_1^{-2} + \left( \frac{v_c}{m} \right)^2 \left( \frac{v_c}{m} - u_c \right) u_1^{-3} + \dots$$

In linear approximation, Eq. 6.16 reduces to

$$\alpha_e \approx -\frac{m}{1+m^2} Z \approx -\frac{1}{\rho\sqrt{1+m^2}} x_i + \frac{m}{\sqrt{1+m^2}} \alpha_i + \frac{1}{\sqrt{1+m^2}} \delta$$

This gives

$$\alpha_e \approx -\frac{\sin \theta}{\rho} x_i + \cos \theta \cdot \alpha_i + \sin \theta \cdot \delta \quad [6.18]$$

This expression is usual linear function for horizontal angle for a sector magnet.

Again in linear approximation,  $S=\rho\theta$  and this gives co-ordinates in vertical plane

$$y_e = y_i + S\beta_i \quad [6.19]$$

$$\beta_e = \beta_i \quad [6.20]$$

Thus formulation correctly reduces to usual relations in linear approximation.

### 6.2.2 Higher order terms

Now we outline the procedure which obtains the higher order terms using the analytical expression. Higher order map elements ( $R$ -,  $T$ - and  $U$ - maps) are given in [48, 66, 67]. As already stated that the derived expression encompasses all the orders and therefore there is no need to separate the terms of different orders, however we present this separation of terms only to validate the formulation. In order to obtain higher order terms,  $P$  and  $Q$  (as given in Eq. 6.10 and 6.11) are also expanded up to higher orders. Variation in  $P$  and  $Q$  for different bending radii and bending angles are shown in Fig. 6.7A and Fig. 6.7B, respectively.

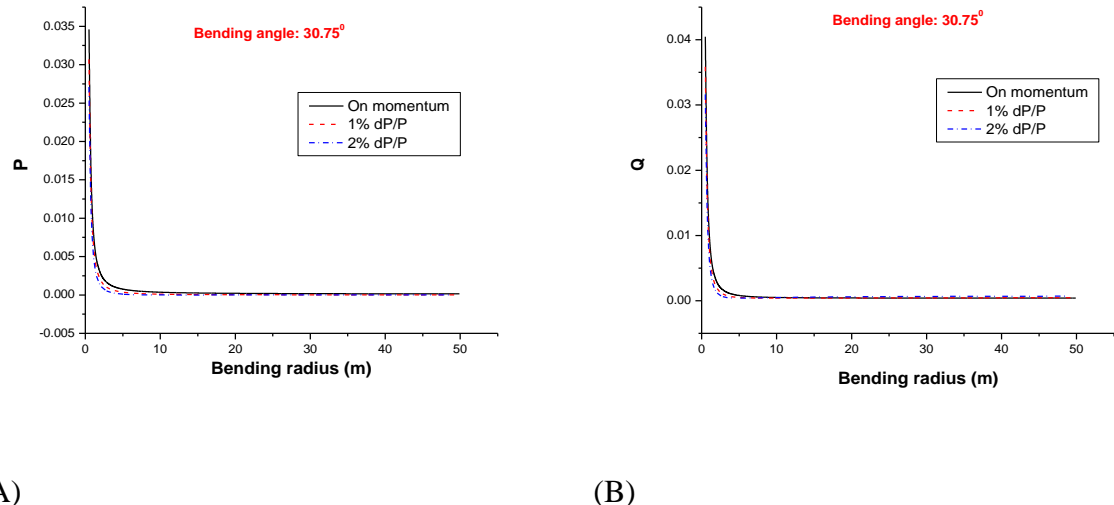


**Fig. 6.7A Variation in  $P$  and  $Q$  with bending radius for fixed bending angle of  $30.75^\circ$ . The  $x_i$  and  $\alpha_i$  are taken as 100 mm and 20 mrad respectively**

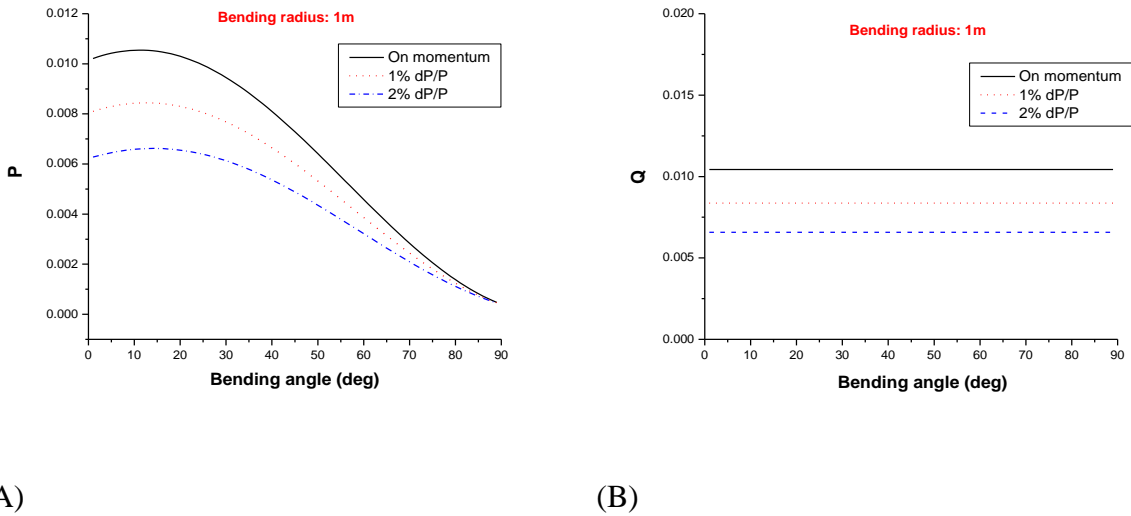


**Fig. 6.7B Variation in  $P$  and  $Q$  with bending angle for fixed bending radius of 1 m. The  $x_i$  and  $\alpha_i$  are taken as 100 mm and 20 mrad respectively**

In practical situations,  $P$  and  $Q$  are smaller than one and thus in Eq. 6.9, expansion can be used easily to obtain the higher order terms as well as expansion up to certain orders in coordinates for  $P$  and  $Q$  using Eq. 6.10 and 6.11 can also be obtained. From Eq. 6.11, we get up to third order (up to elements of  $U$ -map)

$$Q = \frac{1}{\rho^2} x_i^2 + \alpha_i^2 - \frac{2}{\rho} x_i \delta + \delta^2 + \frac{1}{\rho} x_i \alpha^2 - \frac{2}{\rho^2} x_i^2 \delta + \frac{4}{\rho} x_i \delta^2 - \alpha_i^2 \delta - 2\delta^3$$

Eq. 6.10 and above expression lead to higher order (up to third order) expansion of  $P$  as follows

$$\begin{aligned} P = \frac{1}{M} & \left\{ \frac{m^2 x_i^2}{\rho^2} + \frac{2m x_i \alpha_i}{\rho} + \alpha_i^2 - \frac{2m^2 x_i \delta}{\rho} - 2m \alpha_i \delta + m^2 \delta^2 + \frac{m^2 x_i \alpha_i^2}{\rho} + m \alpha_i^3 \right. \\ & \left. - \frac{2m x_i \alpha_i \delta}{\rho} - \frac{2m^2 x_i^2 \delta}{\rho^2} + \frac{4m^2 x_i \delta^2}{\rho} - m^2 \alpha_i^2 \delta + 2m \alpha_i \delta^2 - 2m^2 \delta^3 \right\} \end{aligned}$$

Here  $M=1+m^2$ . Using these two expressions, explicit higher order terms of Eq. 6.9 can be computed. The first part of this equation is as

$$\frac{u_c + mv_c}{1+m^2} = \frac{1}{M} \left\{ mx_i + \rho \alpha_i - m \rho \delta + \frac{m \rho}{2} \alpha_i^2 + \rho \alpha_i \delta - \frac{\rho}{6} \alpha_i^3 + \frac{m \rho}{2} \alpha_i^2 \delta \right\}$$

Second part is given by

$$\frac{\rho(1+\delta)}{\sqrt{1+m^2}} (1+P)^{\frac{1}{2}} (1-Q)^{\frac{1}{2}} = \frac{1}{M^{\frac{3}{2}}} \left\{ M\rho + M\rho\delta - \frac{x_i^2}{2\rho} + mx_i\alpha_i - \frac{m^2\rho\alpha_i^2}{2} + x_i\delta - m\rho\alpha_i\delta - \frac{m\rho\delta^2}{2} \right. \\ \left. - \frac{x_i\alpha_i^2}{2} + \frac{m\rho\alpha_i^3}{2} + \frac{x_i^2\delta}{2\rho} + (1-2m^2)x_i\delta^2 + \rho(1-m^2)\alpha_i^2\delta + \frac{\rho}{2}\delta^3 \right\}$$

Addition of these two parts produce  $u_1$  and using  $u_1$  in Eq. 6.5,  $x_e$  can be obtained up to third order. Similarly, using Eq. 6.16 and expansion of  $Z$ ,  $\alpha_e$  can be obtained up to third order from the following expression

$$\alpha_e = -\frac{m}{1+m^2} Z + \frac{m}{(1+m^2)^2} Z^2 - \frac{m}{(1+m^2)^3} \left(1 + \frac{m^2}{3}\right) Z^3$$

From these two equations, we get the well known elements of  $R$ - ,  $T$ - and  $U$ -maps same as defined in [22, 23, 48, 66, 67]. This shows that the derived analytical expression is correct and can be used in analysis and design of an optics.

### 6.3 Example of a bunch compressor

From Section 6.1, it is evident from the example of a dipole magnet that the deviation between numerical method and analytical map is larger in longitudinal plane than the deviation in transverse emittance and therefore the analytical formula becomes more important from the bunch compressor point of view. Therefore, in this section, we provide a specific example of a chicane bunch compressor. Chicane optics is in general made by using rectangular dipole magnets with proper orientation (Section 1.8.2), but here in this section, chicane is formed using sector dipole magnets with inclusion of quadrupole magnets. The

aim of example is to show that in computing the bunch length from an optics which employs sector dipole magnet, there is remarkable difference in analytical results and numerical computation. The optics used in this example is shown in Fig. 6.8 and parameters of this optics is shown in Table 6.1.

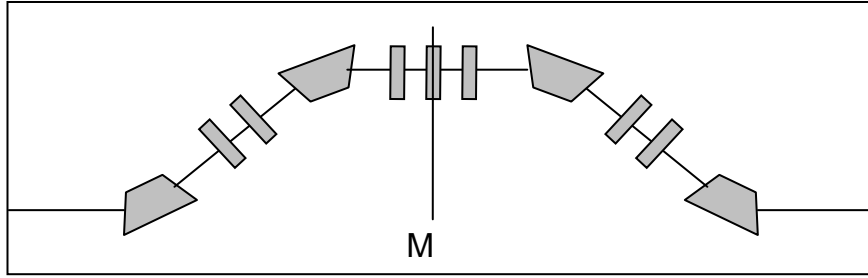


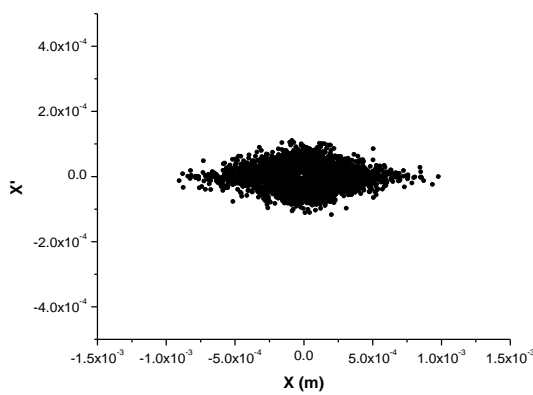
*Fig. 6.8 Geometry of C-chicane optics*

*Table 6.1: Parameters of the chicane optics*

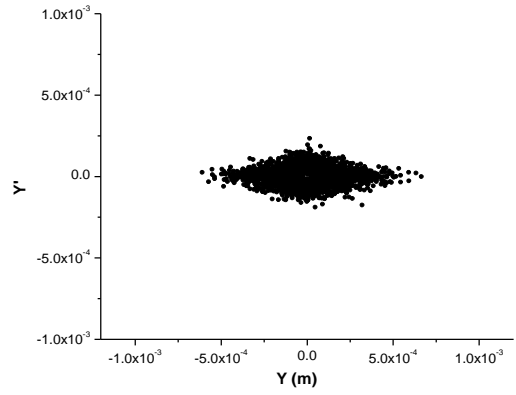
Parameters	Values
Beam energy	300MeV
Horizontal emittance	10nm-rad
Vertical emittance	10nm-rad
Initial $\beta_H$	7.922m
Initial $\beta_V$	3.271m
Initial $\alpha_H$	0.000
Initial $\alpha_V$	0.000

The optics is tuned to  $R_{56}=-0.25$  m and a chirped beam to attain the minimum bunch length is tracked through the optics. The results obtained by tracking the motion of electrons using MAD8 is termed as numerical results. In other case, only at the place of dipole magnets analytical map is used, otherwise MAD8 is used. We refer to these results as the analytical

results. The initial Gaussian distributed beam consisting of 3000 electrons, is shown in transverse plane in Fig. 6.9. Cases of different bunch lengths are considered and thus beam distribution is different in longitudinal plane in each case. In each case, the chirping is done differently for achieving minimum bunch length and in chirping, only linear effects ( $R_{56}$  and  $R_{65}$ ) are considered. The results of transverse emittance show a little difference between analytical and numerical model. However in longitudinal plane, the difference is larger with increasing the initial bunch length as depicted in Fig. 6.10. To observe the effect further, a longer bunch of 80 ps is also tracked and difference becomes even larger (Fig. 6.10C). For a longer bunch length, chirping produces larger momentum spread and due to this, chromatic effect creates larger difference between numerical and analytical results. For high momentum spread, higher order chromatic effects also become important, which are not present in numerical model (MAD8 up to third order tracking). In numerical results, it is clear that the dominant nonlinear effects are seen due to  $T_{566}$  only, while at higher momentum deviation, even more higher order terms causes important effects and effect of  $T_{566}$  up to some extent are cancelled out. In all the results, initial transverse emittance is kept constant and therefore transverse geometric effects on bunch length are almost same. For higher momentum spread, in transverse phase space, almost there is no difference between the two results (Fig. 6.10E and 6.10F). To test the results further, numerical tracking of higher order using code ELEGANT [59] is performed (exact dipole Hamiltonian with integration order of 4). The tracking results reaches closer to analytical results as shown in Fig. 6.10D. In this tracking also, for obtaining analytical results, for the dipole magnets, the analytical map is used, for remaining part ELEGANT is used. This shows that the higher order numerical codes reaches closer to analytical results.

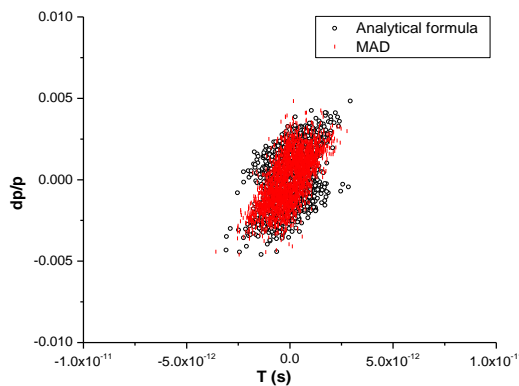


(A) Horizontal phase space

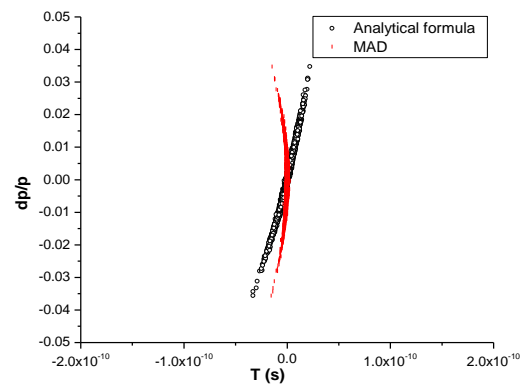


(B) Vertical phase space

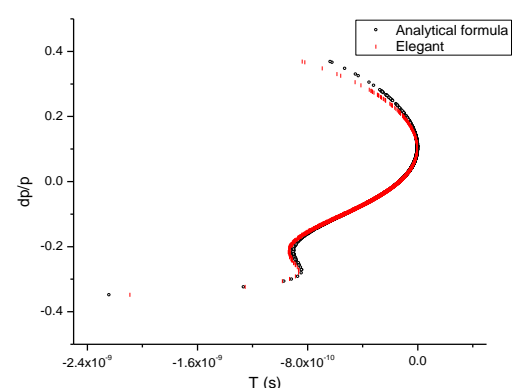
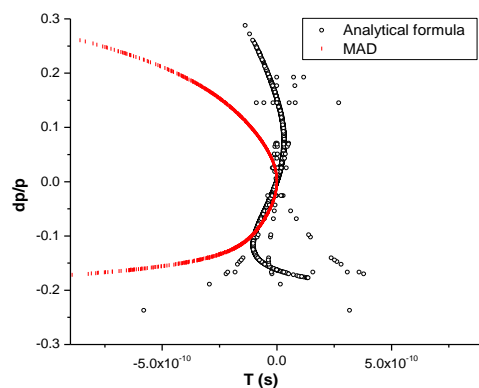
**Fig. 6.9 Initial beam distribution in horizontal and vertical phase space (emittance of 10 nm-rad in both the planes)**



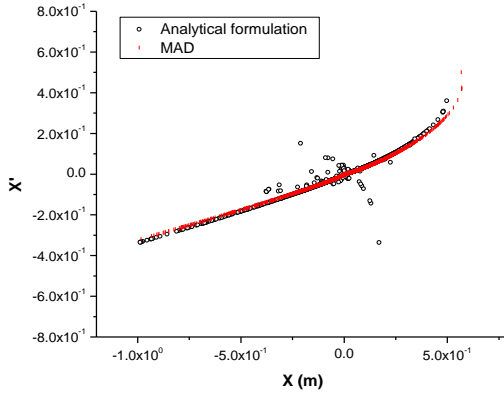
(A) Bunch Length: 1 ps



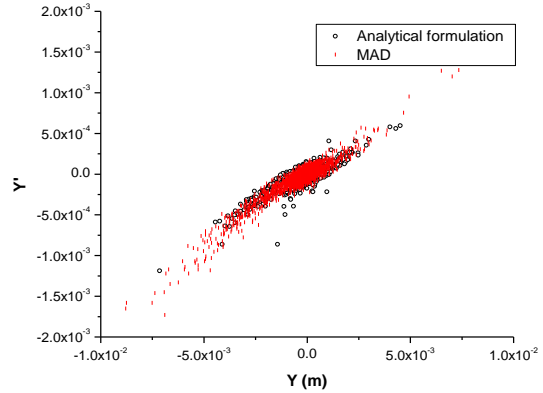
(B) Bunch Length: 8.3 ps



(C) Bunch Length: 80 ps



(D) Bunch Length: 80 ps



(E) Bunch Length: 80 ps

(F) Bunch Length: 80 ps

*Fig. 6.10 Phase space distribution of beam after bunch compressor (analytical and numerical model)*

## 6.4 Analytical map for wedge magnet

Exact analytical map (in hard edge approximation) of a wedge magnet can also be obtained using the geometrical approach similar to that used for a sector type dipole magnet. In general, map of a wedge magnet is obtained considering equivalent sector magnet and edge effects. In geometrical approach also we will use an equivalent sector magnet which has the same design trajectory as that of the wedge magnet as depicted in fig. 6.11 [73].

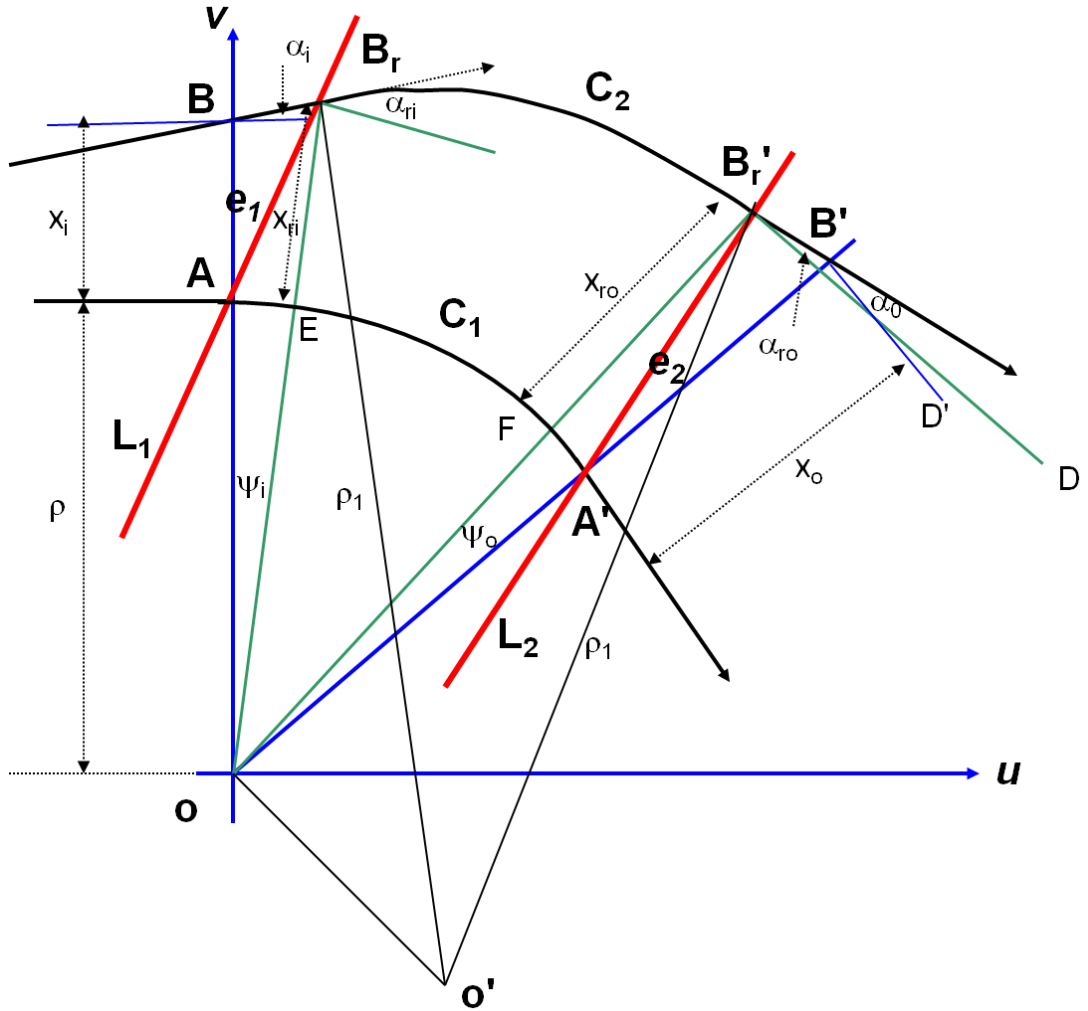


**Fig. 6.11 Geometry of the wedge magnet in fixed  $u$ - $v$  co-ordinate system**

Again we consider fixed  $u$ - $v$  co-ordinate system. Two red lines ( $\mathbf{L}_1$  and  $\mathbf{L}_2$ ) show the entry and exit edge of the wedge magnet. The  $v$ -axis of the co-ordinate system coincides with the entry edge of the equivalent sector magnet. The exit edge of sector magnet is  $\mathbf{OB}'$ , shown in blue colour. Design trajectory  $\mathbf{C}_1$  is a circular arc ( $\mathbf{AA}'$ ) in the median plane. The edge angle of the wedge magnet is  $e_i$ . The trajectory of a deviated particle from the design trajectory is shown by curve  $\mathbf{C}_2$  ( $\mathbf{BB}_r\mathbf{B}'_r\mathbf{B}'$ ). The co-ordinates of this particle at the entrance of the sector magnet are  $x_i$  and  $\alpha_i$  and at the entrance of wedge magnet, these co-ordinates are  $x_{ri}$  and  $\alpha_{ri}$ . At exit, the co-ordinates are  $x_{re}$ ,  $\alpha_{re}$  and  $x_e$ ,  $\alpha_e$  at the edge of wedge magnet and sector magnet respectively. The exit edge of wedge magnet is inclined and makes an angle of  $e_e$  with edge

of the sector magnet. Inside the wedge magnet (from  $x_{ri}$ ,  $\alpha_{ri}$  to  $x_{re}$ ,  $\alpha_{re}$ ), the particle follows a circular path. In this analytical model, there is a difference between  $x_i$  and  $x_{ri}$  as well as between  $x_e$  and  $x_{re}$ . In usual accelerator maps, the edge effects are considered as the thin lens (even in higher order) and under this approximation, this difference vanishes. Therefore, in our analytical computation, for obtaining the co-ordinates at the exit of wedge magnet ( $x_{re}$ ,  $\alpha_{re}$ ), requires two steps, first is to obtain a function which gives  $x_{ri}$ ,  $\alpha_{ri}$  from  $x_i$ ,  $\alpha_i$  and in second step using these  $x_{ri}$ ,  $\alpha_{ri}$ , the  $x_{re}$ ,  $\alpha_{re}$  are observed. The second step is very similar to the procedure followed for the sector magnet.

Let a particle enters the edge at point  $\mathbf{B}_r$ . The distance of this point from the design orbit along the edge is given by

$$L_i = \frac{x_i \cos \alpha_i}{\cos(\alpha_i + e_i)}$$

$$x_{ri} = -\rho_0 + \sqrt{\rho_0^2 + L_i^2 + 2\rho_0 L_i \cos e_i} \quad [6.21]$$

$$\psi_i = \sin^{-1} \left[ \frac{L_i}{x_{ri} + \rho_0} \sin e_i \right]$$

$$\alpha_{ri} = \alpha_i + \psi_i \quad [6.22]$$

Now the deviated particle traces an arc of a circle up to  $\mathbf{B}'_r$  with centre of circle  $\mathbf{O}'$  and radius of  $\rho_1$ . The co-ordinates at the exit edge of the wedge magnet are the common point of circle  $C_2$  and edge  $L_2$ . The co-ordinates of the centre of the circle

$$u_c = (x_{ri} + \rho_0) \sin \psi_i + \rho_0 \sin(\alpha_i - \psi_i) \quad [6.23]$$

$$v_c = (x_{ri} + \rho_0) \cos \psi_i + \rho_0 \cos(\alpha_i - \psi_i) \quad [6.24]$$

The  $x_{re}$  is the distance between  $\mathbf{B}_r'$  and  $\mathbf{F}$ , which is given by

$$x_{re} = -\rho_0 + \sqrt{\rho_0^2 + L_e^2 + 2\rho_0 L_e \cos e_e} \quad [6.25]$$

Here

$$L_e = \sqrt{(u_{Br'} - \rho_0 \sin \theta)^2 + (v_{Br'} - \rho_0 \cos \theta)^2} \quad [6.26]$$

Here  $u_{Br'}$  and  $v_{Br'}$  is the common point between exit edge of magnet and trajectory of the deviated particle and is given by

$$u_{Br'} = \frac{1}{(1+m_e^2)} \left[ \{u_c - m_e(c_e - v_c)\} + \sqrt{\{u_c - m_e(c_e - v_c)\}^2 - (1+m_e^2)(c_e - v_c)^2 + u_c^2 - \rho^2} \right] \quad [6.27]$$

$$v_{Br'} = m_e u_{Br'} + c_e \quad [6.28]$$

Here  $m_e = \cot(\theta - e_e)$  and  $c_e = \rho_0(\cos \theta - m_e \sin \theta)$

The angle of the deviated particle with respect to design orbit at the exit edge is given by

$$\alpha_{re} = \tan^{-1} \left( -\frac{u_{Br'} - u_c}{v_{Br'} - v_c} \right) - \tan^{-1} \left( -\frac{1}{m} \right) \quad [6.29]$$

Thus Eq. 6.25 and 6.29 are the desired transfer function in the median plane.

Then there will be an additional optional step if one wants to obtain again the co-ordinates  $x_e$  and  $\alpha_e$  from the  $x_{re}$  and  $\alpha_{re}$ . This transformation is also provided below.

$$\psi_e = \sin^{-1} \left[ \frac{L_e}{x_{re} + \rho_0} \sin e_e \right]$$

$$\alpha_e = \alpha_{re} - \psi_e \quad [6.30]$$

$$x_e = \frac{(x_{re} + \rho_0) \cos \alpha_e}{\cos \alpha_{re}} - \rho_0 \quad [6.31]$$

The path length of the deviated particle inside the magnet is given by

$$S = \rho_1 \left[ \sin^{-1} \left( \frac{u_{Br'} - u_c}{\rho_1} \right) - \sin^{-1} \left( \frac{u_{Br} - u_c}{\rho_1} \right) \right] \quad [6.32]$$

$$\text{Here } u_{Br} = \frac{1}{(1+m_i^2)} \left[ \{u_c - m_i(\rho_0 - v_c)\} + \sqrt{\{u_c - m_i(\rho_0 - v_c)\}^2 - (1+m_i^2)(\rho_0 - v_c)^2 + u_c^2 - \rho^2} \right]$$

and  $m_i$  is the slope of the entry edge from  $u$ -axis. The difference between  $S$  and  $\rho_0\theta$  gives the path length difference for the deviated particle. If there is some finite initial vertical angle of the particle with median plane, radius of curvature will be increased by  $1/\cos\beta_i$ . The vertical co-ordinates can be obtained similar to sector magnet using  $S$  as follows

$$y_{re} = y_{ri} + S \tan \beta_{ri} \quad [6.33]$$

$$\beta_{re} = \beta_{ri} \quad [6.34]$$

It is easy to see that the transformation from  $x_i, \alpha_i$  to  $x_{ri}, \alpha_{ri}$  (and similarly from  $x_{re}, \alpha_{re}$  to  $x_e, \alpha_e$ ) becomes usual thin (de)focusing lens with strength of  $\tan(e_i)/\rho_0$  on retaining linear terms only. Also the formulae reduce to the sector magnet formulae in case of  $e_i=e_e=0$ .

An example of emittance change after beam transportation through a rectangular magnet is shown in Fig. 6.12 as a function of input horizontal emittance (vertical emittance is kept constant and very small i.e. 1 nm-rad) using analytical expression and MAD. The parameters

of the magnet are the same as that of the sector magnet ( $30.75^\circ$  of bending angle and 0.96 m of bending radius) and assuming a monochromatic beam. As pointed out earlier in the section that analytical expression brings a difference between  $x_{ri}$  and  $x_i$  (similarly  $x_{re}$  and  $x_e$ ), the emittance growth is less than the growth indicated by MAD in the horizontal plane while in vertical plane it is more. In vertical plane due to coupling (higher order) analytical expression changes vertical emittance (although change is very small) due to increase in input horizontal emittance. The difference in bunch length with momentum deviation for a rectangular magnet between the results obtained using analytical expression and MAD is not much significant.

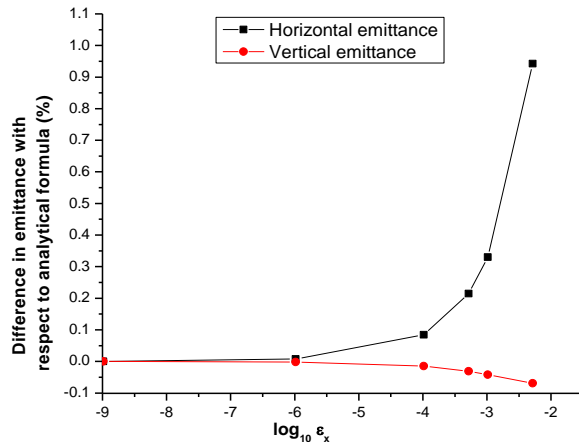


**Fig. 6.12 deviation in emittance from numerical computation using analytical results as a function of initial horizontal emittance**

Although, computer codes are available to simulate the dynamics up to very high order, but we obtained expressions correct up to all order with an alternative, and simpler approach, which can be used to estimate higher order effects very quickly. The study shows that in case of a sector magnet for large momentum spread and shorter bunches, higher order effects in longitudinal plane becomes important. Although in a bunch compressors, in general effects of CSR is much more prominent than this nonlinear effect, nevertheless to know the exact results is also important.

## SUMMARY AND CONCLUSIONS

In this thesis, a general layout for optical design of bunch compressors is presented with a detailed design study of CTF3 Transfer Line-2 (TL-2) bunch compressor. In Chapter 1, necessary background of charged particle beam optics is briefly discussed including types of bunch compressor optics. In Chapter 2, a short introduction to CLIC and CTF3 is presented.

With geometrical and magnetic constraints in view, TL-2 bunch compressor is designed for a very wide tuning range of  $R_{56}$  from -0.30 m to +0.30 m. For ease in the design and operation, this line is divided into three modules. First module matches the optics from extraction point of Combiner Ring to Module-2. Module-2 matches the Module-1 and Module-3. Module-2 also sends the beam vertically up through a vertical achromat required due to the different floor levels. In this module, a long element free clear space is provided to accommodate a tail clipper. Module-3, built by four dipole magnets, forms the tunable  $R_{56}$  arc. For controlling the beta function and to shape the dispersion for obtaining the desired  $R_{56}$ , this module employs nine quadrupoles in set of three triplets. These nine quadrupoles are grouped in five families. After this arc, this module has a quadrupole doublet to match the final required beta function at the exit point of this line. Chapter 3 summarizes all these various aspects of TL-2 design and relevant calculations.

Under the building geometry and magnetic constraints, it is not possible to obtain a symmetric solution for the entire range of tuning in Module-3 i.e.  $R_{56}$  arc is not optically symmetric and thus correction of  $T_{566}$ , which is needed for the entire range is a challenge. The inclusion of sextupole magnets to control  $T_{566}$ , should not deteriorate the emittance in transverse plane (horizontal and vertical) more than 10%. Due to lack of optical symmetry in

this arc, no standard technique for cancellation of aberration of sextupole magnets works. Therefore a new scheme is evolved in which the geometrical aberration is minimized by considering the total kicks imparted to the particles, by sextupole magnets. For this minimization, required initial Twiss parameters at the beginning of line are obtained and these parameters are matched by Module-2. This scheme successfully worked in entire range of tuning and thus optical design has been completed. Chapter 4 describes this scheme and results.

Bunch compressors faces another problem of coherent synchrotron radiation (CSR). When bunch length becomes extremely small, the radiation emitted from an electron bunch on a curved trajectory becomes coherent. Thus a significant magnitude of the field is created. This field can cause tail to head interactions in the bunch and can also excite betatron oscillations around dispersive orbit. Thus transverse emittance and bunch length may deteriorate due to CSR. Although, the bunch length in TL-2 is not extremely short, but for a complete study, we carried out the study of CSR to look into bunch behaviour. The dynamics in presence of CSR is simulated using code ELEGANT. Emittance dilution and lengthening of bunch is seen due to CSR in TL-2. The results are provided in Chapter 5.

On the design presented in this thesis, TL-2 line has been installed in CTF3 at CERN.

In any bunch compressor, where very short bunches have to be produced with a reasonable value of  $R_{56}$ , momentum spread has to be increased in a correlated way by an RF system. For a large momentum spread, the path length should be obtained up to higher orders to estimate bunch length more accurately. Major control on the bunch length is obtained using dipole magnets. Therefore a higher order description of dipole magnet becomes necessary. Although computer codes can compute the bunch length with very high orders, but increasing the order costs the computation time. Available analytical techniques are based on perturbation

methods and increasing one order in calculations demand a complicated mathematics. In this thesis, an analytical map for a hard edge magnet, is obtained, which is correct up to all orders. This provides a quick estimation of the phase space distribution of beam passing through a dipole magnet. There is remarkable difference in the results for a large momentum spread obtained through computation, truncated to second and third order in codes and from analytical map. An example of chicane type bunch compressor for comparison is presented. It is shown that difference is larger in case of a sector type dipole magnet than a rectangular dipole magnet.

## Appendix A

In this appendix, a short introduction to beam matrix approach to describe the propagation of beam parameters through a magnetic optics is presented. The equation for the phase space ellipse can be written as [15]

$$\tilde{\mathbf{X}}^T \boldsymbol{\sigma}^{-1} \tilde{\mathbf{X}} = 1 \quad [\text{A.1}]$$

Here  $\tilde{\mathbf{X}}$  is the following column vector of the co-ordinates

$$\tilde{\mathbf{X}} = \begin{bmatrix} x \\ x' \\ y \\ y' \\ \Delta t \\ \delta \end{bmatrix}$$

The volume of the 6-D ellipse defined by Eq. A.1 is given by

$$V = \frac{\pi^3}{6} \sqrt{\det \boldsymbol{\sigma}}$$

For horizontal plane ( $x, x'$ ), Eq. A.1 becomes

$$\sigma_{22}x^2 - (\sigma_{12} + \sigma_{21})xx' + \sigma_{11}x'^2 = \det \boldsymbol{\sigma}$$

Comparing this equation with ellipse equation, showing Courant-Synder invariant, gives

$$\boldsymbol{\sigma} = \varepsilon^2 \begin{bmatrix} \beta & -\alpha \\ -\alpha & \gamma \end{bmatrix} \quad [\text{A.2}]$$

This is known as beam matrix. The different elements of this beam matrix are related with RMS parameters of the beam as follows

$$\sigma_{11} = \langle x^2 \rangle$$

$$\sigma_{22} = \langle x'^2 \rangle$$

$$\sigma_{12} = \sigma_{21} = \langle xx' \rangle$$

Determinant of the beam matrix gives the square of the beam emittance in the considered plane i.e.

$$\varepsilon^2 = \sigma_{11}\sigma_{22} - \sigma_{12}^2 = \langle x^2 \rangle \langle x'^2 \rangle - \langle xx' \rangle^2$$

Which is the statistical definition of the beam emittance.

One of the important aspects of the beam matrix is the evolution of this matrix through a magnetic optics and it is given by

$$\boldsymbol{\sigma}_{out} = \mathbf{R} \boldsymbol{\sigma}_{in} \mathbf{R}^T \quad [A.3]$$

Here  $\mathbf{R}$  is the transfer matrix of the considered optics (or element). This equation directly gives the evolution of the beam from one point to other in a given optics.

Similar to the transverse plane, the beam matrix can be defined explicitly for the longitudinal plane also [9]. For this plane

$$\sigma_{55} = \langle z^2 \rangle = \beta_l \epsilon_l$$

$$\sigma_{66} = \langle \delta^2 \rangle = \gamma_l \epsilon_l$$

$$\sigma_{56} = \langle z\delta \rangle = \alpha_l \epsilon_l$$

Here subscript ' $l$ ' refers to the longitudinal plane. In case of  $R_{66} = I$  (i.e. no change in central beam energy), symplectic transformation of beam matrix as defined in Eq. A.3 is also possible in longitudinal plane and this provides the evolution of longitudinal Twiss parameters through the optics. This gives propagation of the  $\beta_l$  as follows

$$\beta_{l,out} = \beta_{l,in}(1 + R_{56}R_{65})^2 - 2\alpha_{l,in}R_{56}(1 + R_{56}R_{65}) + \gamma_{l,in}R_{56}^2$$

This expression gives that in case of  $\lim R_{56} \rightarrow 0$  and  $\lim R_{56}R_{65} \rightarrow -1$ , the longitudinal  $\beta \rightarrow 0$  i.e. very short bunch length. But these settings requires very small  $R_{56}$  and very large  $R_{65}$  (i.e. RF voltage and momentum spread reaches towards infinity). The same fact is discussed in Section 1.8.1 (Eq. 1.55).

## Appendix B

In this appendix, derivations of expressions of  $R_{56}$  for different optics used in Chapter 1 and Chapter 3 are provided. First, an expression of the  $R_{56}$  for a chicane with quadrupole magnets (Chapter 1) is obtained. In next section, the  $R_{56}$  for the S-arc optics with two different bending magnets and three families of quadrupole magnets (Chapter 3) is obtained.

### B 1. Approximate value of $R_{56}$ for a chicane optics with quadrupole magnets

In a chicane optics, the rectangular magnets are placed with their pole faces parallel to each other. The beam in the first magnet of the chicane optics enters at the right angle with the pole face. In the linear map, presented in Eq. 1.12, the orientation of the rectangular magnet is considered in which beam enters at an angle of  $\pi/2 - \theta$  with the pole face. Now here in this section, we provide a difference between path lengths of an off-momentum trajectory and the design trajectory for a rectangular magnet as placed in a chicane optics. The expressions are derived using geometry of the magnets under consideration, instead of using transfer matrices. The orientation of the rectangular magnet in this optics is shown in Fig. B.1.

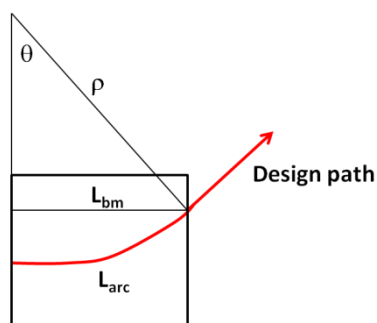


*Fig. B.1 Rectangular magnet as used in chicane geometry*

Using simple geometry, we can get

$$L_{arc} = \rho\theta$$

and

$$L_{bm} = \rho \sin \theta \quad [B.1]$$

These two equations provide

$$L_{arc} = L_{bm} \frac{\theta}{\sin \theta} \quad [B.2]$$

If we obtain change in  $L_{arc}$  with the momentum deviation, this gives change in path length due to momentum offset for the magnet.

$L_{arc}$  depends on  $\theta$  (Eq. B.2) and  $\theta$  depends on bending radius  $\rho$  (Eq. B.1). Therefore, the deviation in  $L_{arc}$  with momentum is given by [74]

$$\frac{dL_{arc}}{dp/p} = p \frac{dL_{arc}}{d\theta} \frac{d\theta}{d\rho} \frac{d\rho}{dp} \quad [B.3]$$

First two differentials  $ds/d\theta$  and  $d\theta/d\rho$  can be obtained using Eq. B.1 and B.2 as follows

$$\cos \theta \frac{d\theta}{d\rho} = -\frac{L_{bm}}{\rho^2} = -\frac{\sin \theta}{\rho}$$

$$\frac{ds}{d\theta} = L_{bm} \left( \frac{\sin \theta - \theta \cos \theta}{\sin^2 \theta} \right)$$

In a magnetic field,  $p=eB\rho$ . Using this relation, we get  $\frac{d\rho}{dp} = \frac{\rho}{p}$ . Using all these differential relations in Eq B.3, we get [74, 75]

$$\frac{dL_{arc}}{d\delta} = -\frac{L_{bm}}{\sin \theta} (\tan \theta - \theta) \quad [B.4]$$

Up to second order in bending angle, this expression becomes

$$\frac{dL_{arc}}{d\delta} \approx -\frac{L_{bm}}{3}\theta^2 \quad [B.5]$$

Before proceeding further to obtain the  $R_{56}$  of the complete optics, it is worth clarifying the basic difference between the two approaches (i.e. geometrical and matrix based), employed to obtain the  $R_{56}$  of an optics. In this thesis, different optics for bunch compressors are analyzed analytically using geometrical approach as it is used in deriving Eq. B.5 [74]. The another approach, based on transfer matrices is introduced in Chapter 1 and is also used by the computer code MAD8, which is utilized for optimization and simulations for TL-2. In transfer matrix approach, a dipole magnet (sector, rectangular or wedge) is specified in terms of a sector magnet with thin lenses at its edges to account for the edge angle or angles of the entry and exit. In geometrical approach, the path length actually traversed by an electron within a dipole magnet is considered. In this case, the path length change is the actual difference between the path length of an off-momentum trajectory and the design trajectory. Though with these two approaches, calculated change in path length due to momentum offset in the individual magnets and drift spaces may be different but for the complete optics,  $R_{56}$  values are equal in both the cases. In Fig. B.2, the difference between these two approaches are shown for the first two magnets of a chicane optics.

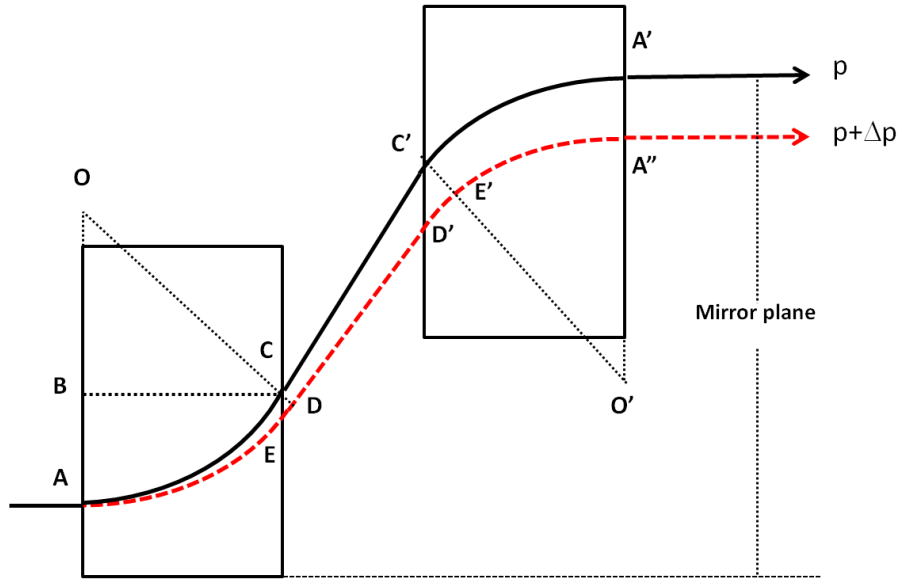


**Fig B.2 First half geometry of a chicane optics**

Here, curve **ACC'A'** (black solid curve) is the design trajectory of an on-momentum electron. Curve **AEDD'E'A''** (red dotted) is the trajectory of an off-momentum particle ( $p+\Delta p$ ). Equivalent sector magnets, used to define the local co-ordinate system, are also shown with apex **O** and **O'**. In matrix approach, the path length of an off-momentum trajectory is calculated in first dipole magnet from **A** to **D** and in the second magnet from **E'** to **A''**, while in geometrical approach, we calculate the path length from **A** to **E** in the first magnet and from **D'** to **A''** in the second magnet. The path length for the off-momentum trajectory (**AD**) in matrix approach is longer in the first magnet as compared to the path length of the design trajectory (**AC**) and it is (**E'A''**) much shorter in the second magnet as compared to the design trajectory **C'A'**, which gives smaller positive and larger negative  $R_{56}$  in the first and second magnet, respectively. In geometrical approach, the path lengths of the off momentum trajectories (**AE** and **D'A''**) are equal in both the magnets and are shorter than the path length of the design trajectories (**AC** and **C'A'**, which are equal to each other). The path length in drift space in geometrical approach is calculated from **E** to **D'**, while when matrix are used, the path length in drift is from **D** to **E'**. In matrix approach, a slight change in path length of

an off-momentum trajectory in the drift space due to angle with respect to design trajectory is taken into account through the dispersion dependence of  $R_{56}$ . Needless to mention that in the geometrical approach, the path length difference in drift space is calculated using the geometry in that section (for example Eq. B.10).

Overall result for complete optics are the same by both the approaches [74]. In matrix approach, edges are approximated as a thin lens, while in geometrical approach, no such approximation is involved. In following sections for analyzing different optics, we adopted the geometrical approach.

In case of the optics of a chicane with quadrupole magnets, there is change in angles of an off-momentum trajectory at the entrance and exit of the second dipole magnets and therefore, difference between path lengths of an off-momentum trajectory and the design trajectory in the first and second dipole magnets become different. The change in angle with respect to design trajectory due to momentum offset ( $\delta$ ) in first order is the derivative of dispersion i.e.  $\Delta\theta/\delta = D'$ . Using geometrical approach, change in path length with respect to the path length of the design trajectory due to momentum offset i.e.  $R_{56}$  (we will refer to this change in path length due to momentum offset inside the magnet body as  $R_{56}$ , but in strict sense it is different from the  $R_{56}$  which is defined in the matrix approach as discussed above) for the magnet in such case is given by

$$R_{56} \approx \frac{D'_{in} L_{bm}}{2} \theta - \frac{L_{bm}}{3} \theta^2 \quad [B.6]$$

Here  $D'$  is used at the place of  $\Delta\theta/\delta$ . The optics of chicane with quadrupole magnets is depicted in Fig. 1.12. We consider an off-momentum trajectory with an offset  $\delta$  in this optics,

which coincides with the design trajectory before entering the optics. The lateral displacement of this off-momentum trajectory up to the first quadrupole magnet is given by

$$X_{q1\delta} = L_{bm} \tan\left(\frac{\theta}{2(1+\delta)}\right) + L_{1q} \tan\left(\frac{\theta}{1+\delta}\right)$$

Up to second order in angle and first order in  $\delta$ , this becomes

$$X_{q1\delta} = \left(L_{1q} + \frac{L_{bm}}{2}\right)\theta - \left(L_{1q} + \frac{L_{bm}}{2}\right)\theta\delta$$

The deviation of this trajectory from the design trajectory at this location becomes

$$\Delta X_{q1} = -\left(L_{1q} + \frac{L_{bm}}{2}\right)\theta\delta$$

Therefore, the kick of quadrupole (strength  $K_1$ ) on this trajectory is given by

$$\theta_{q1} = K_1 \Delta x_{q1} (1 + \delta)^{-1}$$

In above expression, for focusing quadrupole magnet  $K_1$  will be negative. Using  $\Delta X_{q1}$  in above expression, finally we get in first order of  $\delta$

$$\theta_{q1} = -K_1 \left(L_{1q} + \frac{L_{bm}}{2}\right)\theta\delta \quad [B.7]$$

Due to quadrupole kick, the angle made by off-momentum trajectory at the entrance of the second dipole magnet with respect to the design trajectory is given by

$$\Delta\theta_{bm2} = -\theta\delta - K_1 \left(L_{1q} + \frac{L_{bm}}{2}\right)\theta\delta \quad [B.8]$$

Dividing  $\Delta\theta_{bm2}$  by momentum offset  $\delta$  gives the derivative of dispersion ( $D'$ ) at the entrance to the second dipole magnet. Using this  $D'$  in Eq. B.6, contribution in  $R_{56}$  from the second dipole magnet can be obtained as follows

$$R_{56, \text{second dipole}} = -\frac{L_{bm}}{2}\theta^2 - K_1 \frac{L_{bm}}{2} \left( L_{1q} + \frac{L_{bm}}{2} \right) \theta^2 - \frac{L_{bm}}{3} \theta^2 \quad [\text{B.9}]$$

In optics without quadrupole magnets, only last term of above equation is there. The first two terms are produced due to quadrupole magnet.

The path length of an off-momentum trajectory in the first drift space (first dipole exit to the first quadrupole magnet) is given by

$$L_{d1\delta} = \frac{L_{1q}}{\cos\left(\frac{\theta}{1+\delta}\right)} \approx L_{1q} + \frac{L_{1q}\theta^2}{2} - L_{1q}\theta^2\delta$$

This gives the change in path length due to momentum offset as follows

$$\frac{\Delta L_{d1}}{\delta} = -L_{1q}\theta^2 \quad [\text{B.10}]$$

After quadrupole kick, the total angle for an off-momentum trajectory becomes  $\frac{\theta}{1+\delta} + \theta_{q1}$ .

The angle  $\theta_{q1}$  depends on  $\delta$  (Eq. B.9) and in path length calculation, angle appears in quadratic form (Eq. B.10). Therefore, this angle  $\theta_{q1}$  alone changes the path length in second order in momentum deviation. In computing  $R_{56}$ , the change in first order is only considered and this change is ignored, however a cross term of  $\theta_{q1}$  with bending angle  $\theta$  is a first order term in momentum offset. Thus, using Eq. B.7, the change in path length for off momentum particle in second drift space is

$$\frac{\Delta L_{d2}}{\delta} = -L_{q2}\theta^2 - K_1 \left( L_{1q} + \frac{L_{bm}}{2} \right) \theta^2$$

With these two expressions, the difference between path length of the design and off-momentum trajectory in drift spaces can be found and is given as

$$\frac{\Delta L_d}{\delta} \approx -L_{12}\theta^2 - K_1 L_{q2} \left( L_{1q} + \frac{L_{bm}}{2} \right) \theta^2 \quad [\text{B.11}]$$

This change in path length in drift space contains an additional term as compared to that of the optics without quadrupole magnet. Adding  $R_{56}$  contribution from the first dipole magnet ( $D' = 0$ ) to contributions from Eq. B.9 and Eq. B.11, provides  $R_{56}$  for the half optics of a chicane and due to symmetry, total  $R_{56}$  will be twice of this. the  $R_{56}$  of complete optics is thus can be given by

$$R_{56} = -2 \left( L_{12} + \frac{2L_{bm}}{3} \right) \theta^2 - L_{bm} \theta^2 - 2K_1 \left( L_{1q} + \frac{L_{bm}}{2} \right) \left( L_{q2} + \frac{L_{bm}}{2} \right) \theta^2$$

It shows that a focusing quadrupole magnet (negative value of  $K_1$ ) adds a positive value to  $R_{56}$ . The second term has its origin in the difference in angular deviation in off-momentum trajectory at the entrance of the second dipole magnet as compared to optics without quadrupole magnet. Without quadrupole magnets, this term also vanishes. This expression can be written as

$$R_{56} = R_{56,\text{chicane}} - L_{bm} \theta^2 - 2K_1 \left( L_{1q} + \frac{L_{bm}}{2} \right) \left( L_{q2} + \frac{L_{bm}}{2} \right) \theta^2 \quad [\text{B.12}]$$

Here  $R_{56,\text{chicane}}$  is the  $R_{56}$  of the optics without quadrupole magnets. The quadrupole magnet can thus be used to tune the  $R_{56}$  of this optics.

## B.2 Approximate value of $R_{56}$ for an S-arc

The  $R_{56}$  for a rectangular magnet (pole face orientation as used in Eq. 1.12) is obtained by putting the integration of the dispersion inside the magnet (Eq. 1.16) in Eq. 1.21. The

resulting  $R_{56}$  is (here again  $R_{56}$  is the "geometrical change in path length due to momentum offset inside the magnet body only" and therefore is different from the usual matrix element  $R_{56}$ , see pages 166-167 for details)

$$R_{56} = D'_{in}\rho(1 - \cos\theta) + \rho(\theta - \sin\theta) \quad [B.13]$$

Now expanding above expression up to second order in bending angle  $\theta$  is given by

$$R_{56} \approx \frac{D'_{in}L_{bm}\theta}{2} + \frac{L_{bm}\theta^2}{6} \quad [B.14]$$

Here  $L_{bm}$  is the magnet length and this length has a simple geometrical relation with bending angle and radius and is given below

$$\rho = \frac{L_{bm}}{2\sin\left(\frac{\theta}{2}\right)}$$

In a rectangular magnet, the path length does not depend on the deviation of an off-momentum trajectory from the design trajectory, instead it depends on the angle of an off-momentum trajectory with the design trajectory. Therefore, in  $R_{56}$  only  $D'$  contributes, not the  $D$ . Knowing derivative of the dispersion at the entrance of different dipole magnets in each optics, Eq. B.14 can provide  $R_{56}$ . The optics of the S-arc, discussed in Chapter 3, employs dipole magnets in this orientation. The tuning arc of TL-2 is a variation in this type of optics. Layout of this optics is shown in Fig. 3.6. Length and angle for the first and fourth dipole magnet are equal and are  $L_{bm1}$  and  $\theta_1$ , respectively. Similarly, the length and angle for the second and third dipole magnet are  $L_{bm2}$  and  $\theta_2$ , respectively. Third dipole magnet bends beam opposite to second dipole magnet and fourth dipole magnet bends the beam opposite to first dipole magnet, resulting in a net zero bending. The kick angle on an off momentum trajectory due to first quadrupole magnet (in first order of  $\delta$ ) is

$$\theta_{q1} = \frac{K_1 \Delta X_{q1}}{1 + \delta} \approx -K_1 \left( L_{1q} + \frac{L_{bm1}}{2} \right) \theta_1 \delta \quad [\text{B.15}]$$

Due to this quadrupole kick, at the location of the second quadrupole magnet, deviation in off-momentum trajectory from the design trajectory is given by

$$\Delta X_{q2} \approx - \left\{ L_{1q} + L_{qq1} + \frac{L_{bm1}}{2} + K_1 L_{qq1} \left( L_{1q} + \frac{L_{bm1}}{2} \right) \right\} \theta_1 \delta \quad [\text{B.16}]$$

$L_{qq1}$  is the distance between the first two quadrupole magnets. Using this expression of the above displacement, kick angle on this trajectory imparted by second quadrupole magnet can be obtained

$$\theta_{q2} = \frac{K_2 \Delta X_{q2}}{1 + \delta} \approx -K_2 \left\{ L_{1q} + L_{qq1} + \frac{L_{bm1}}{2} + K_1 L_{qq1} \left( L_{1q} + \frac{L_{bm1}}{2} \right) \right\} \theta_1 \delta \quad [\text{B.17}]$$

Using these two quadrupole kicks, the angle of an off-momentum trajectory at the entrance of the second dipole magnet from the horizontal axis (black dotted line in Fig. 3.6) is given by

$$\theta_{bm2\delta} = \theta_1 - [1 + K_1 A + K_2 (A + L_{qq1} \{1 + K_1 A\})] \theta_1 \delta \quad [\text{B.18}]$$

Here

$$A = L_{1q} + \frac{L_{bm1}}{2}$$

The design trajectory has an angle of  $\theta_1$  with the horizontal axis at the entrance of the second dipole magnet. The difference in angles made by design trajectory and an off-momentum trajectory provides the derivative of the dispersion at the entrance to the second dipole magnet. This is given by

$$D' = [1 + K_1 A + K_2(A + L_{qq1}\{1 + K_1 A\})]\theta_1 \quad [\text{B.19}]$$

Using this expression, the  $R_{56}$  contribution from the second dipole magnet is given by

$$R_{56,BM2} = \frac{1}{6}L_{bm2}\theta_2^2 - \frac{L_{bm2}}{2}[1 + K_1 A + K_2(A + L_{qq1}\{1 + K_1 A\})]\theta_1\theta_2 \quad [\text{B.20}]$$

From the first dipole exit to the entrance of the second dipole magnet, the difference in path length of an off-momentum trajectory from the design trajectory is given by

$$\frac{\Delta L_{12}}{\delta} = -L_{12}\theta_1^2 - K_1 A(L_{qq1} + L_{q2})\theta_1^2 - K_2 L_{q2}(A + L_{qq1})\theta_1^2 - K_1 K_2 A L_{qq1} L_{q2} \theta_1^2 \quad [\text{B.21}]$$

Here  $L_{q2}$  is the distance from the second quadrupole magnet to the entrance of the second dipole magnet. Similarly the change in path length due to momentum offset from the exit of second dipole magnet to the third quadrupole magnet can be obtained as following

$$\begin{aligned} \frac{\Delta L_{2q}}{\delta} = & -L_{2q}(\theta_1 + \theta_2)^2 - K_1 A L_{2q}(\theta_1 + \theta_2)\theta_1 - K_2 L_{2q}(A + L_{qq1})(\theta_1 + \theta_2)\theta_1 \\ & - K_1 K_2 A L_{qq1} L_{2q}(\theta_1 + \theta_2)\theta_1 \end{aligned} \quad [\text{B.22}]$$

The change in path length for an off-momentum trajectory as compared to the design trajectory from the third quadrupole magnet to the mid-point of this quadrupole doublet can be calculated using the kick imparted by the third quadrupole magnet. This kick can be derived similar to the kicks, as derived for the first two quadrupole magnets. At the location of the third quadrupole magnet, deviation in off-momentum trajectory from the design trajectory is given by

$$\begin{aligned}\Delta X_{q3} = & - \left( \frac{L_{bm1}}{2} + L_{12} + L_{bm2} + L_{2q} \right) \theta_1 \delta - \left( \frac{L_{bm2}}{2} + L_{2q} \right) \theta_2 \delta \\ & + (L_{qq1} + L_{q2} + L_{bm2} + L_{2q}) \theta_{q1} + (L_{q2} + L_{bm2} + L_{2q}) \theta_{q2}\end{aligned}\quad [\text{B.23}]$$

Here  $L_{2q}$  is the distance from the exit of the second dipole magnet to third quadrupole magnet. Using above expression of the displacement and Eq. B.15 and B.17, kick angle on this trajectory imparted by the third quadrupole magnet can be obtained as following

$$\begin{aligned}\theta_{q3} = & -K_3[(A + B + C + L_{qq1})\theta_1 + B\theta_2]\delta - K_1 K_3 A(B + C + L_{qq1})\theta_1 \delta \\ & - K_2 K_3 (B + C)(A + L_{qq1})\theta_1 \delta - K_1 K_2 K_3 A L_{qq1} \theta_1 \delta\end{aligned}\quad [\text{B.24}]$$

Here  $B = \frac{L_{bm2}}{2} + L_{2q}$  and  $C = \frac{L_{bm2}}{2} + L_{q2}$ .

The  $R_{56}$  contribution from the third quadrupole magnet to the mid-point of the quadrupole doublet formed by Q3 is given by

$$\begin{aligned}\frac{\Delta L_{qq2}}{\delta} = & -L_{qq2}(\theta_1 + \theta_2)^2 - K_1 A L_{qq2}(\theta_1 + \theta_2)\theta_1 \\ & - K_2 L_{qq2}(A + L_{qq1})(\theta_1 + \theta_2)\theta_1 \\ & - K_3[(A + B + C + L_{qq1})\theta_1 + B\theta_2](\theta_1 + \theta_2) \\ & - K_1 K_2 A L_{qq1} L_{qq2}(\theta_1 + \theta_2)\theta_1 \\ & - K_1 K_3 A(B + C + L_{qq1})(\theta_1 + \theta_2)\theta_1 \\ & - K_2 K_3 (B + C)(A + L_{qq1})(\theta_1 + \theta_2)\theta_1 \\ & - K_1 K_2 K_3 A L_{qq1}(\theta_1 + \theta_2)\theta_1\end{aligned}\quad [\text{B.25}]$$

Here  $L_{qq2}$  is the distance between the third quadrupole magnet and symmetry point of the optics. Adding all the contributions of  $R_{56}$  from Eq. B.20, B.21, B.22 and B.25 to the contribution from the first dipole magnet, provides  $R_{56}$  for half of the arc. Twice of this gives

$R_{56}$  of the arc. By introducing three new variables i.e.  $\Theta = \theta_1 + \theta_2$ ,  $\Phi = \Theta\theta_1$  and  $D = A + L_{qq1}$ , the  $R_{56}$  of the arc is given by

$$R_{56} = P_0 - \sum_{i=1}^3 K_i P_i - \sum_{i,j=1; i \neq j}^3 K_i K_j P_{ij} \quad [B.25]$$

Here

$$\begin{aligned} P_0 &= -\frac{1}{3}(L_{bm1} + L_{bm2})\theta_1^2 - 2L_{12}\theta_1^2 - L_{bm2}\theta_1\theta_2 - 2(L_{qq2} + L_{2q})\Theta^2 \\ P_1 &= 2A(L_{qq1} + L_{q2})\theta_1^2 + 2A(L_{qq2} + L_{2q})\Phi + AL_{bm2}\theta_1\theta_2 \\ P_2 &= DL_{bm2}\theta_1\theta_2 + 2D(L_{qq2} + L_{2q})\Phi \\ P_3 &= 2[(B + C + D)\theta_1 + B\theta_2]\Theta \\ P_{12} &= P_{21} = AL_{qq1}\left(\frac{1}{2}\theta_1\theta_2 + L_{qq2}\Phi\right) + AL_{qq1}L_{q2}(\theta_1^2 + \Phi) \\ P_{13} &= P_{31} = A(B + C + L_{qq1})\Phi \\ P_{23} &= P_{32} = D(B + C)\Phi \end{aligned} \quad [B.26]$$

This is Eq. 3.1. In TL-2 tuning arc, one defocusing quadrupole magnet in the first and last straight section also adds an additional degree of freedom and helps in obtaining a desired value of dispersion at the location of sextupole magnet to correct the  $T_{566}$  within the available sextupole strength. One more defocusing quadrupole magnet at the mirror location provides a control over vertical beta function without affecting the value of  $R_{56}$ , as the dispersion is zero at this location.

## Appendix C

In this appendix, a brief discussion on dispersion and  $T_{566}$  is presented. The co-ordinate  $x$  and  $x'$  of a particle after passing through an optics in linear approximation is mapped with its initial co-ordinates as following

$$x = R_{11}x_{in} + R_{12}x'_{in} + R_{16}\delta \quad [C.1]$$

$$x' = R_{21}x_{in} + R_{22}x'_{in} + R_{26}\delta \quad [C.2]$$

For obtaining the propagation of dispersion (i.e.  $D(s)$ ), consider an off-momentum trajectory through the optics, i.e.  $x=D\delta$ ,  $x'=D'\delta$  in above equations. We get

$$D = R_{11}D_{in} + R_{12}D'_{in} + R_{16} \quad [C.3]$$

$$D' = R_{21}D_{in} + R_{22}D'_{in} + R_{26} \quad [C.4]$$

Above equations describe the propagation of dispersion through an optics, when initial dispersion and its derivative are  $D_{in}$  and  $D'_{in}$  respectively. If at the entrance of an optics, dispersion and its derivative, both are zero, above relations yield propagation of dispersion and its derivative through the optics as following

$$D = R_{16} \text{ and } D' = R_{26}$$

Longitudinal dispersion  $R_{56}$  is given by Eq. 1.21, which can be expressed in the following form using Eq. C.1

$$R_{56} = D_{in} \int \frac{R_{11}}{\rho} ds + D'_{in} \int \frac{R_{12}}{\rho} ds + \int \frac{R_{16}}{\rho} ds \quad [C.5]$$

For zero initial dispersion and its derivative,  $R_{56}$  becomes

$$R_{56} = \int \frac{R_{16}}{\rho} ds \quad [C.6]$$

Similarly, we can obtain the propagation of second order dispersion through an optics and its relation with  $T_{566}$ . Assuming only horizontal dispersion, up to second order,  $x$  and  $x'$  is given by

$$\begin{aligned} x = & R_{11}x_{in} + R_{12}x'_{in} + R_{16}\delta + T_{111}x_{in}^2 + (T_{112} + T_{121})x_{in}x'_{in} + T_{122}x'^2_{in} \\ & + (T_{116} + T_{161})x_{in}\delta + (T_{126} + T_{162})x'_{in}\delta + T_{166}\delta^2 \end{aligned} \quad [C.7]$$

$$\begin{aligned} x' = & R_{21}x_{in} + R_{22}x'_{in} + R_{16}\delta + T_{211}x_{in}^2 + (T_{112} + T_{121})x_{in}x'_{in} + T_{222}x'^2_{in} \\ & + (T_{216} + T_{261})x_{in}\delta + (T_{226} + T_{262})x'_{in}\delta + T_{266}\delta^2 \end{aligned} \quad [C.8]$$

Non-listed matrix elements in above equations are zero in an optics consisting of drift spaces, dipole magnets and quadrupole magnets. However  $T_{144}$  is non-zero for a dipole magnet, which gives  $x$  as a function of  $y_{in}^2$ , but we consider only horizontal dispersion and this terms does not give contribution in horizontal dispersion propagation. Up to second order, displacement and angle of an off-momentum trajectory are given by  $x = D\delta + D_{(2)}\delta^2$  and  $x' = D'\delta + D'_{(2)}\delta^2$ . Here  $D_{(2)}$  and  $D'_{(2)}$  are second order dispersion and its derivative, respectively. Using these relations in Eq. C.7 and C.8, propagation of second order dispersion and its derivative in an optics can be obtained as follows

$$\begin{aligned} D_{(2)} = & R_{11}D_{(2)in} + R_{12}D'_{(2)in} + T_{111}D_{in}^2 + (T_{112} + T_{121})D_{in}D'_{in} + T_{122}D'^2_{in} \\ & + (T_{116} + T_{161})D_{in} + (T_{126} + T_{162})D'_{in} + T_{166} \end{aligned} \quad [C.9]$$

$$\begin{aligned} D'_{(2)} = & R_{21}D_{(2)in} + R_{22}D'_{(2)in} + T_{211}D_{in}^2 + (T_{212} + T_{221})D_{in}D'_{in} + T_{222}D'^2_{in} \\ & + (T_{216} + T_{261})D_{in} + (T_{226} + T_{262})D'_{in} + T_{266} \end{aligned} \quad [C.10]$$

In case of vanishing initial dispersion and its derivative, second order dispersion and its derivative propagate as  $D_{(2)}=T_{166}$  and  $D'_{(2)}=T_{266}$ .

Second order change in path length due to momentum offset is quantified by the second order map element  $T_{566}$ , which is related to second order dispersion. The change in path length is given by Eq. 4.2, re-written here as

$$\Delta s = \left( \frac{x}{\rho} + \frac{x^2}{2\rho^2} + \frac{x'^2}{2} \right) ds$$

Due to momentum offset (up to second order), this change in path length becomes

$$\Delta s = \left( \frac{D\delta + D_{(2)}\delta^2}{\rho} + \frac{D^2\delta^2}{2\rho^2} + \frac{D'^2\delta^2}{2} \right) ds$$

From this, we get  $T_{566}$  as following

$$T_{566} = \int \left[ \frac{D_{(2)}}{\rho} + \frac{1}{2} \left( \frac{D^2}{\rho^2} + D'^2 \right) \right] ds \quad [C.11]$$

Using explicit expressions of  $D$ ,  $D'$  and  $D_{(2)}$  from Eq. C.3, C.4 and C.9, value of  $T_{566}$  as a function of map elements can be obtained as follows

$$\begin{aligned}
T_{566} = & D_{(2)0} \int \frac{R_{11}}{\rho} ds + D'_{(2)0} \int \frac{R_{12}}{\rho} ds \\
& + D_0 \int \left\{ \frac{R_{11}R_{16}}{\rho^2} + R_{21}R_{26} + \frac{T_{116} + T_{161}}{\rho} \right\} ds \\
& + D'_0 \int \left\{ \frac{R_{12}R_{16}}{\rho^2} + R_{22}R_{26} + \frac{T_{126} + T_{162}}{\rho} \right\} ds \\
& + D_0^2 \int \left\{ \frac{R_{11}^2}{2\rho^2} + \frac{R_{21}^2}{2} + \frac{T_{111}}{\rho} \right\} ds \\
& + D_0 D'_0 \int \left\{ \frac{R_{11}R_{12}}{\rho^2} + R_{21}R_{22} + \frac{T_{112} + T_{121}}{\rho} \right\} ds \\
& + D'_0^2 \int \left\{ \frac{R_{12}^2}{2\rho^2} + \frac{R_{22}^2}{2} + \frac{T_{122}}{\rho} \right\} ds + \int \left\{ \frac{R_{16}^2}{2\rho^2} + \frac{R_{26}^2}{2} + \frac{T_{166}}{\rho} \right\} ds
\end{aligned} \tag{C.12]$$

In case of zero initial dispersion and derivative, which is the case at the entrance for an achromat optics,  $T_{566}$  becomes

$$T_{566} = \int \left\{ \frac{R_{16}^2}{2\rho^2} + \frac{R_{26}^2}{2} + \frac{T_{166}}{\rho} \right\} ds \tag{C.11]$$

This is Eq. 4.3.

## REFERENCES

- [1] K. Aulenbacher *et al*, "Bunch compressor performances at the CLIC test facility", proceedings of EPAC 1996, Barcelona, Spain
- [2] F. Stulle *et al*, "A bunch compressor for the CLIC main beam", Proceedings of LINAC 2006, Tennessee, USA
- [3] T. E. d' Amico *et al*, "The CLIC main linac bunch compressor", Proceedings of EPAC 1998, Stockholm, Sweden
- [4] Kellen Peterson, "Bunch compression in the International Linear Collider", <http://www.classe.cornell.edu/Public/REU/2005REU/petersen.pdf>
- [5] Eun-San Kim, "Design of short bunch compressors for the International Linear Collider", Proceedings of EPAC 2006, Edinburgh, Scotland
- [6] R. Akre *et al*, "Commissioning of the LCLS Linac and bunch compressors", SLAC PUB-13373, 2008
- [7] W. Decking *et al*, "Bunch compressor for the TESLA Linear Collider", TESLA-2000-40, 2000
- [8] Heinz-Dieter Nuhn, "Technological Challenges to X-ray FELs", Nuclear Instruments and Methods in Physics Research-A, 445, Issues 1-3, 2000
- [9] Andy Wolski, "A short introduction to bunch compressors for linear colliders", Notes for USPAS course on linear colliders, Santa Barbara, June 2003

- [10] P. Piot, "State-of-art Electron Bunch Compression", Proceedings of LINAC-2004, Lubeck, Germany
- [11] Eun-San Kim, "Bunch compressors", ILC Accelerator School 2006
- [12] J. A. Thorpe, "*Elementary Topics in Differential Geometry*", Springer, 1979
- [13] S. Y. Lee, "*Accelerator Physics*", World Scientific, 1999
- [14] E. D. Courant and H. S. Snyder, "Theory of alternating gradient synchrotron", Annals of Physics, 281, 2000
- [15] Helmut Wiedemann, "*Particle Accelerator Physics*", Springer, 3<sup>rd</sup> Ed, 2007
- [16] M. Sands, "The Physics of Electron Storage Ring", SLAC-121, 1979
- [17] Philip J. Bryant, Kjell Johnsen, "*The Principles of Circular Accelerators and Storage Rings*", Cambridge University Press, 1993
- [18] K. Steffen in Proceedings of CERN Accelerator School, General Accelerator Physics, Vol-1, 1984, Edited by P. J. Bryant and S. Turner
- [19] D. A. Edwards and L. C. Teng, "Parameterization of linear coupled motion in periodic system", Proceedings of PAC 1973, San Francisco, CA, USA
- [20] Hans Grote and F. Christoph Iselin, "The MAD Program: User's reference manual", CERN/SL/90-13 (AP), 1996
- [21] F. Christoph Iselin, "The MAD Program: Physical Methods Manual", CERN/SL/92 (AP), 1994
- [22] F. C. Iselin, "Lie transformations and transport equations for combined functions dipole magnets", Particle Accelerators, 17, 1985

- [23] K. L. Brown, "A first and second order matrix theory for the design of beam transport systems and charged particle spectrometers", SLAC Report-75, 1982
- [24] Stanley Humphries Jr., "*Charged Particle Beams*", John Wiley and Sons, 2002
- [25] R. J. England *et al*, "Sextupole correction of the longitudinal transport of relativistic beams in dispersionless transition section", Phys. Rev. Special Topics – Accelerators and Beams, 8, 012801, 2005
- [26] J. B. Flanz, "Symmetry corrected second order achromat", Proceedings of PAC-1989, Chicago, IL, USA
- [27] K. L. Brown, "A second order magnetic optical achromat", Proceedings of PAC-1979, San Francisco, CA, USA
- [28] T. O. Raubenheimer *et al*, "Chicane and wiggler based bunch compressors for future Linear Collider", SLAC-PUB-6119, 1993.
- [29] Hywel L. Owen and Peter H. Williams, "A Modular path length corrector for Recirculating Linacs", Nuclear Instruments and Methods in Physics Research-A, 662, 2012
- [30] Frank Stulle, "A Bunch Compressor for small Emittances and high peak Currents at the VUV Free-Electron Laser", PhD Thesis, University of Hamburg, 2004
- [31] R. Joel England, "First and Second Order optics in the ORION Dogleg", ORION workshop 2003
- [32] J. D. Jackson, "*Classical Electrodynamics*", John Wiley and Sons, Inc. New York
- [33] H. Braun *et al*, "CLIC 2008 Parameters", CLIC Note-764, October, 2008

- [34] Rainer Pitthan, "Comparison of Discrete Klystron produced RF to Two-Beam Produced RF for Large Accelerator System", SLAC-PUB-8570, August 2000
- [35] CLIC Study Team, "Proposals for future CLIC studies and a new CLIC Test Facility (CTF3)", CLIC note 402, July 1999
- [36] R. Corsini, "First Full Beam Loading Operation with the CTF3 Linac", CLIC Note 604, July 2004
- [37] Philippe Royer, "Bunch Frequency Multiplication by RF Injection into an Isochronous Ring", PhD Thesis, University De Lausanne, 2003
- [38] "Bunch compression in CTF3", CTF3 WG Meeting, March 2000, [http://clic-meeting.web.cern.ch/clic-meeting/CTF3\\_Techn\\_Mtgs/2000/May/presentations/corsini.pdf](http://clic-meeting.web.cern.ch/clic-meeting/CTF3_Techn_Mtgs/2000/May/presentations/corsini.pdf)
- [39] H. H. Braun *et al*, "Results from the CLIC test facility", CLIC Note 310, June 1996
- [40] R. Bossart *et al*, "CLIC Test Facility Developments and Results", Proceedings of PAC, Dallas, USA, 1995
- [41] "CLIC Test facilities and the Route to CLIC", <http://clic-study.web.cern.ch/clic-study/report/5TestFac.html>
- [42] Roger Ruber, "CLIC Feasibility Demonstration at CTF3", Proceeding of LINAC 2010, Japan
- [43] Amalendu Sharma *et al*, "Optics design for Transfer Line-2 for CTF3", CTF3 Note 091, May 2008
- [44] Jorge Nocedal and Stephen J. Wright, "*Numerical Optimization*", Springer, 2000

- [45] T. D. Amico and G. Guignard, "Analysis of a Symmetric Triplet and its Application to Ring Insertion", CERN/PS 97-25 (LP), 1997
- [46] Abdurrahim *et al*, "Optimization Strategy of Transfer Line-2 for CTF3", Proceedings of InPAC, Indore, India, 2009
- [47] Robert Joel England, "Longitudinal Shaping of Relativistic Bunches of Electrons Generated by an RF Photoinjector", PhD Thesis, University of California, Los Angeles, 2007
- [48] Yipeng Sun, "Yipeng Sun, "Second-order achromat design based on FODO cell", Phys. Rev. Special Topics – Accelerators and Beams, 14, 060703, 2011
- [49] Joel R. Thompson, "Bunch Compression for a Short-Pulse Mode in Cornell's ERL", Phd Thesis, Cornell University, 2009
- [50] Amalendu Sharma *et al*, "Optics design and second order longitudinal dispersion minimization in a bunch compressor transfer line for CTF3", Nuclear Instruments and Methods in Physics Research-A, 602, Issue 2, 2009
- [51] J. Schwinger, "On radiation by electrons in betatron", transcribed by M. A. Furman, LBNL-39088, 1998
- [52] Albert Hofmann, "*The Physics of Synchrotron Radiation*", Cambridge University Press, New York, 2004
- [53] T. Nakazato *et al*, "Spectrum of coherent synchrotron radiation", PAC-1991, San Francisco, USA
- [54] Bolko Beutner, "Measurement and Analysis of Coherent Synchrotron Radiation Effects at FLASH", PhD Thesis, University of Hamburg, 2007

- [55] E. L. Saldin *et al*, "On the coherent radiation of an electron bunch moving in an arc of a circle", Nuclear Instruments and Methods in Physics Research-A, 398, 1997
- [56] G. V. Stupakov, "Effect of centrifugal transverse wakefield for microbunch in bend", SLAC PUB 8028, March 2006
- [57] R. Li, "Cancellation effects in CSR induced bunch transverse dynamics in bends", EPAC-2002, Paris, France
- [58] M. Borland, "Elegant: A Flexible SDDS-Compliant Code for Accelerator Simulation", Advanced Photon Source LS-287, September 2000, Version 25.1.0 (2012)
- [59] M. Borland, "A Simple Method for Simulation of Coherent Synchrotron Radiation in a Tracking Code", Proc. of ICAP-2000, September, 2000, Darmstadt, Germany
- [60] Borland, "Simple method for particle tracking with coherent synchrotron radiation", Phys. Rev. Special Topics – Accelerators and Beams, 4, 070701, 2001
- [61] Amalendu Sharma *et al*, "CSR studies of Transfer Line-2 Bunch Compressor at CTF3, CERN", Proceedings of InPAC 2013, Kolkata, India
- [62] David C. Carey, "Minimization of Aberrations in Beam Line Design", Proceedings of PAC-1973, San Francisco, CA, USA, 1973
- [63] H. Wollnik, "Second order transfer matrices of real magnetic and electrostatic sector fields", Nuclear Instruments and Methods in Physics Research 52, 1967
- [64] David C. Carey, "Third order combined function bending magnets", Proceedings of PAC-1989, Chicago, IL, USA, 1989

- [65] Leonid Sagalovsky, "Beam transport optics of dipole fringe field in the framework of third-order matrix theory", Nuclear Instruments and Methods in Physics Research-A 298, 1990
- [66] V. V. Andreev, I. P. Yudin, "Third-Order Bending Magnet Optics for Cartesian Coordinates", Proceedings of PAC-1993, Washington DC, USA, 1993
- [67] Etienne Forest, "Geometric Integration for Particle Accelerators", J. Phys. A: Math. Gen. 39, 2006
- [68] Martin Berz, *Modern map methods in Particle Beam Physics*, Academic press, 1999
- [69] P. K. Skowronski *et al*, "Advances in MAD-X using PTC", LHC Project Report 1016, 2007
- [70] M. Berz and K. Makino, "Cosy infinity, version 8.1, Users Guide and Reference Manual", Michigan State University, May 2001
- [71] F. Schmidt, "Six Track, User's reference manual", CERN/SL/94-56 (AP), 2012
- [72] H. Wollnik, *"Optics of charged particles"*, Academic Press, 1987
- [73] Amalendu Sharma *et al*, "Analytical expressions of transfer functions for a hard edge dipole magnet using a basic geometrical approach", Phys. Rev. Special Topics – Accelerators and Beams, 16, 014001, 2013
- [74] P. Castro, "Beam trajectory calculations in bunch compressors of TTF2", DESY Technical Note 2003-01, 2003
- [75] F. Chautard and L. Rinolfi, "Bunch Compressor for the CLIC Test Facility", CERN PS/94-30 (LP), 1994